Omics to Multi-Omics:

New Implications for Serum Bile Acid Profiles by Mass Spectrometry-Based Biomarker Discovery

A Dissertation Submitted to

the Graduate School of Life and Environmental Sciences,

the University of Tsukuba

in Partial Fulfillment of the Requirements

for the Degree of Doctor of Philosophy

(Doctoral Program in Life Sciences and Bioengineering)

Takashi SHIMADA

Abbreviations

2-D PAGE	2-dimensional polyacrylamide gel electrophoresis
9-AA	9-aminoacridine hemihydrates
A2m	alpha-2-macroglobulin
ACTH	adrenocorticotrophic hormone
Alad	delta-aminolevulinic acid dehydratase
Aldo	fructose-bisphosphate aldolase
ALT	alanine aminotransferase
ANOVA	one-way analysis of variance
Apo	apolipoprotein
AST	aspartate aminotransferase
BAL	bile acid CoA ligase
BAS	bile acid CoA synthetase
BAT	bile acid CoA:amino acid N-acyl-transferase
CBB	coomassie brilliant blue
CCl_4	carbon tetrachloride
Ces	carboxylesterase
CHAPS	3-((3-cholamidopropyl)dimethylammonium)-1-propanesulfonate
CHCA	α-cyano-4-hydroxycinnamic acid
CHIP	chemical inkjet printer
CoA	coenzyme A
CSV	comma separated values
CV	central vein

CYP7A1	cholesterol 7α-hydroxylase
CYP7B1	oxysterol 7α-hydroxylase
CYP8B1	sterol 12α-hydroxylase
CYP27A1	mitochondrial sterol 27-hydroxylase
DTT	dithiothreitol
ELISA	enzyme-linked immunosorbent assay
ER	endoplasmic reticulum
Fah	fumarylacetoacetase
Fbp	fructose-1
Fgb	fibrinogen
FXR	farnesoid X receptor
G6Pase	glucose-6-phosphatase
GCA	glycocholic acid
GCDCA	glycochenodeoxycholic acid
GLCA	glycolithocholic acid
GO	gene ontology
GOA	gene ontology annotation
GPCR	G-protein coupled receptors
Gpd	glycerol-3-phosphate dehydrogenase
Gsn	gelsolin
HAI	histology activity index
HE	hematoxylin & eosin
Hsp	heat shock protein
HUPO	human proteome organization

IAA	iodoacetamide
ICR	Institute of Cancer Research
i.p.	intraperitoneal injection
Idh	isocitrate dehydrogenase
IEF	isoelectric focusing
IMS	imaging mass spectrometry
ITO	indium-tin oxide
LC	liquid chromatography
MALDI	matrix-assisted laser desorption/ionization
Mbl	mannose-binding protein C
MOWSE	MOlecular Weight Search
Mr	mobility shift
MRM	multiple reaction monitoring
N-AG	N-acetyl glucosamine
NCBI	National Center for Biotechnology Information
NPA	N-1-naphthylphthalamic acid
NR	nuclear receptors
nr	non-redundant
OBO	open biological ontologies
OBP	odorant binding protein
PE	phosphatidylethanolamine
PEPCK	phosphoenol pyruvate carboxykinase
PHx	partial hepatectomy
pI	isoelectric point

PMF	peptide mass fingerprinting
PSA	prostate specific antigen
Psm	proteasome subunit
PV	portal vein
QIT	quadrupole ion trap
Rbp	plasma retinol-binding protein
Saa	serum amyloid A
SDS	sodium dodecyl sulfate
SHP	small heterodimer partner
SPE	solid-phase extraction
SSP	protein spot number
STAR D1	steroidogenic acute regulatory protein D1
SULT2B1b	hydroxycholesterol sulfotransferase 2B1b
TAMCA	tauro-α-muricholic acid
TCA	taurocholic acid
TCDCA	taurochenodeoxycholic acid
TFA	trifluoroacetic acid
TGR5	G protein-coupled T cell-surface receptor
THCA	taurohyocholic acid
TLCA	taurolithocholic acid
TOF MS	time-of-flight mass spectrometry
Tris	tris(hydroxymethyl)aminomethane
UDP	uridine diphosphate
UniProt	Universal Protein Resource

Contents

Chapter I:

Preface

Bile acid chemistry

Bile acids were isolated from bile in the 19th century, and the field of bile acid chemistry preceded the development of classical biochemistry.[1] Bile acids are amphipathic (hydrophilic and hydrophobic face) end products of cholesterol metabolism that facilitate lipids or vitamins absorption in the intestine. Bile acids are synthesized in the liver as primary bile acids from oxidation of cholesterol by cytochrome P-450 enzyme family, and are conjugated with either glycine or taurine by amidation.[2] Normal conjugated form of glycine and taurine are existed 3:1 ratio in human bile, but dominant bile acid classes are dependent on each animal species. Bile acids are released into the proximal intestine, and reabsorbed in the distal intestine via the portal vein, an enterohepatic circulation system. And a part of bile acids are modified by bacteria to termed secondary bile acids. The complexity of bile acid nomenclature can be explained by the evolution of multiple biochemical pathways that serve to convert cholesterol.[3]

Pathway of bile acid biosynthesis

There are two major bile acid biosynthetic pathways in the liver, the neutral and alternative pathway.[4] The neutral pathways are initiated by cholesterol 7α-hydroxylase (CYP7A1), the rate-limiting step. Sterol 12α-hydroxylase (CYP8B1) determines the ratio of cholic acid to chenodeoxycholic acid. The neutral bile acid biosynthetic pathway consists of least 16 enzymatic steps leading to the formation of cholic acid and chenodeoxycholic acid. The alternative pathways are initiated by mitochondrial sterol 27-hydroxylase (CYP27A1), the rate-limiting step appears to be transport of cholesterol to the inner mitochondrial membrane. In humans, the neutral pathway is the major pathway of synthesis under normal physiological conditions. While CYP7A1 is

expressed only in hepatocytes, mitochondrial CYP27A1 is expressed in many different tissues, a potential role in feedback regulation of cholesterol. 25α-hydroxycholesterol and its sulfated form in alternative pathways may play potential regulatory oxysterol and metabolite. STAR D1, steroidogenic acute regulatory protein D1; SULT2B1b, hydroxycholesterol sulfotransferase 2B1b; CYP7B1, oxysterol 7α-hydroxylase; BAL, bile acid CoA ligase; BAT, bile acid CoA:amino acid *N* -acyltransferase.

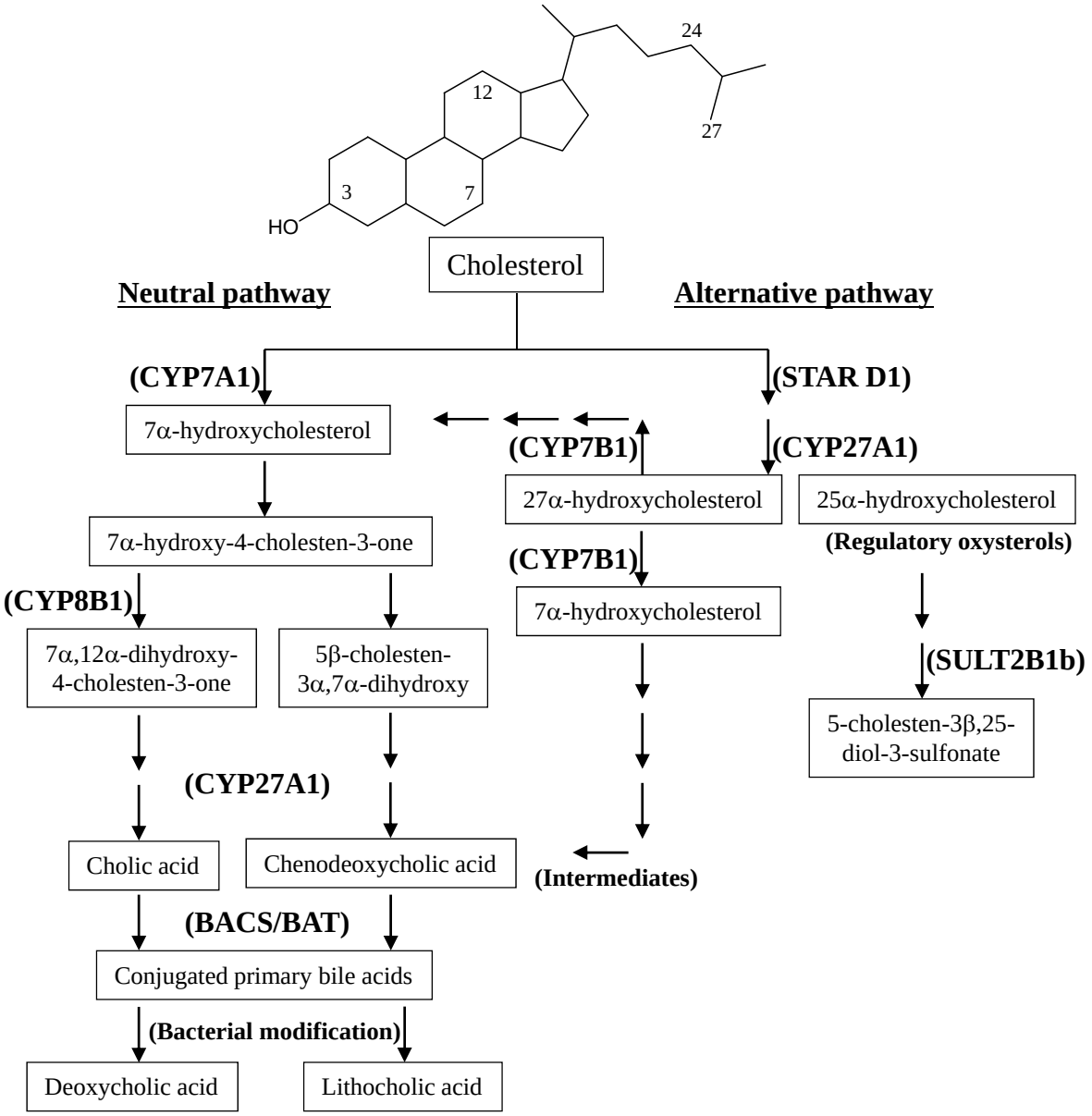
24
12
27
3
7
HO
Cholesterol
Neutral pathway
Alternative pathway
(CYP7A1)
(STAR D1)
7α-hydroxycholesterol
(CYP7B1)
(CYP27A1)
27α-hydroxycholesterol
25α-hydroxycholesterol
(Regulatory oxysterols)
7α-hydroxy-4-cholesten-3-one
(CYP7B1)
(CYP8B1)
7α-hydroxycholesterol
7α,12α-dihydroxy-4-cholesten-3-one
5β-cholesten-3α,7α-dihydroxy
(SULT2B1b)
5-cholesten-3β,25-diol-3-sulfonate
(CYP27A1)
Cholic acid
Chenodeoxycholic acid
(Intermediates)
(BACS/BAT)
Conjugated primary bile acids
(Bacterial modification)
Deoxycholic acid
Lithocholic acid

Bile acids turn into hormones

Recently, bile acids emerged as complex metabolic integrators and versatile signaling molecules endowed with systemic endocrine functions.[5-6] Bile acids have many physiological functions such as regulation of gene expression involved in cholesterol, glucose, and their own homeostasis. Bile acids are ligands for G-protein coupled receptors (GPCR) such as TGR5 and modulate several nuclear hormone receptors including farnesoid X receptor (FXR).[7-8] Through activation of these versatile signaling molecules, bile acids have been shown to regulate not only their own synthesis and enterohepatic circulation, but also triglyceride, cholesterol, energy, and glucose homeostasis. These bile acid controlled signaling pathways have become the source of promising novel drug targets to treat common metabolic and hepatic diseases such as obesity, type 2 diabetes, hypertriglyceridaemia, atherosclerosis and non-alcoholic steatohepatitis. And some of bile acid related drugs and FXR antagonists are in clinical or preclinical phase. Moreover, physiological impact of bile acid signaling extends beyond the strict control of metabolism, as important roles of bile acids have already been identified in regulation of cell proliferation and of inflammation.[5]

Chapter II:

New proteomic data annotation method for quantitative proteome

Serum proteome for biomarker development

Good biomarkers are measurable from non-invasive test, and indicators of a biological state, disease risk or stage, early disease detection and classification of disease type or organ. And, in the future, biomarker is an indicator for personalized therapy or a target of drug. Because biomarkers in clinical diagnosis are usually development of a blood test, blood is a logical body fluid for biomarker discovery. Human plasma is high complexity and large dynamic concentration range of proteins up to 12 orders identified by the HUPO plasma proteome project.[9] Plasma proteins can be categorized in three groups: classical plasma protein in the range of mg/ml to μg/ml, tissue leakage product of around ng/ml and interleukins/cytokines of under ng/ml to pg/ml. The concentration of prostate specific antigen (PSA), best known plasma biomarker, is about 2 ng/ml and prostate cancer risk is indicated above 4 ng/ml, so sensitivity of biomarker discovery should be exactly quantitative detection of plasma protein in the low range of ng/ml.

In recent years, the biomarker development by proteomics has been activated.[10] The biomarker discovery promising comprehensive analysis has advanced greatly accompanying the rapid advance of mass spectrometric technology and bioinformatics. Proteomic approach enables global protein identification, and can be obtained systematic data. While such technologies provide a greater understanding of large-scale and complex biological event, it has necessitated effective data annotation method and simple user interface to link to distinctive biological process. Therefore, the functional classification of proteins is critical for proteomic studies aimed at discovering disease biomarkers.

The process of new biomarker development can be mainly divided into three aspects (Table 1).[11] First, screening step, proteins by differential analysis are identified and classified as biomarker candidate. Second, verification step, biomarker candidate was quantified and verified by western blotting or immunohistochemistry by the specific antibody. And third validation step, surviving biomarker candidate are validated by high-throughput quantification assay for establishment of sensitivity and specificity, usually enzyme-linked immunosorbent assay (ELISA). And remaining candidate will be next large-scale clinical or cohort study. By advance of MS technology, MS-based validation method such as quantitative multiple reaction monitoring (MRM) is being established as next generation's biomarker validation system.

However, such biomarker strategy is faced on several essential issues. The proof of concept on candidate biomarker is very difficult to demonstrate. For example, sensitivity and specificity between preexisting biomarkers and novel biomarker or combination of biomarkers, correlation between pathobiology and expression change of target molecules, evidence of leakage from specific disease tissue or organ by serum proteome, possible diagnosis platform as circulating biomarkers or autoantibodies, validation of detectable biomarker from serum by tissue proteome, good animal model for biomarker development, high-cost performance of antibody dependent validation method, these issues are the essential for omics study. And large dataset confuse researchers how to select their candidate molecules or to judge important biological significance.

Gene ontology-based statistical data annotation

In the proteomic field, effective data annotation of large-scale dataset is one of the essential issues. Data analysis of the large protein dataset is a very important downstream task to understand the biological significance of the output proteins. This annotation can become it informative or invalid depending on data processing.[12] The quality of large-scale dataset derived from proteomic studies is one of the most important concepts that directly influence the success of the following functional analysis. In the complexity of the data-mining situations involved in biological studies, there is no good systematic way at present. But a good dataset may exhibit the following characteristics:[13]

1. Appropriate protein extraction, tryptic digestion and peptide recovery for each analytical platform
2. Reproducible and quantitative dataset of possible confirmation by another experimental method
3. Accurate protein identification by mass spectrometric method (peptide mass fingerprinting, MS/MS analysis and precise criteria of database search results or verification of protein physicochemical property)
4. Contain many important proteins in the dataset as expected for objective research field
5. Statistically quantitative cutoff with appropriate number of dataset (100 to 2000 data, not low or high)
6. Time-dependent quantitative dataset
7. Biologically over-representation by up- or down-regulated protein expression

It is very important to understand not only what a kind of targeted biomarker, biomarker for response to therapy or prediction of disease risk, post-translational modifications as biomarker, but also what biological function, mechanism of disease or pathway. So, I focused on functional analysis of proteomic dataset and developed a new data mining method based on gene ontology. In this data annotation concept, I will propose one of the essential solutions for serum proteomic research.

The gene ontology database can be freely accessed from the Gene Ontology website (GO, www.geneontology.org), Gene ontology annotation (GOA) and Open biological ontologies (OBO).[14] The GO term and ontology component of OBO was divided into three categories; "molecular_function", "cellular_component", and "biological_process". I first prepared the data set consisting of a pair of UniProt ID, GO ID, term and component. Each UniProt ID and spot quantity can be highlighted to correspond to multiple GO IDs. GO analysis was performed and GO terms categorized in the "biological_process" component with $p < 0.05$ as significant terms by χ^2 test and Fisher's exact test in serial time points.

In figure 1, schematic flow of the gene ontology based proteomic data annotation method. This annotation method provides several strategies to show how and when the proteins of interest are distributed among gene ontology terms by statistically over-represented biological process. And this makes the overall biological picture assembled on the basis of the proteomic dataset.

Tables

Table 1. Novel biomarker development process.

Phase	Process	Sample	No. of analyte	No. of sample
SCREEN Discovery of biomarker candidate	Candidate identification by proteomics (unbiased) (semi-quantitative)	Plasma, serum Cell line Animal model	1000s	10s
VERIFY Verification and quantification	Specific antibody assay MS-based quantitation (targeted) (quantitative)	Plasma, serum	10s	100s
VALIDATE Clinical assay Sensitivity and specificity	High-throughput immunoassay (targeted) (quantitative)	Plasma, Serum (population)	5-10	1000s

Figure captions

Figure 1. Scheme for gene ontology based data annotation.

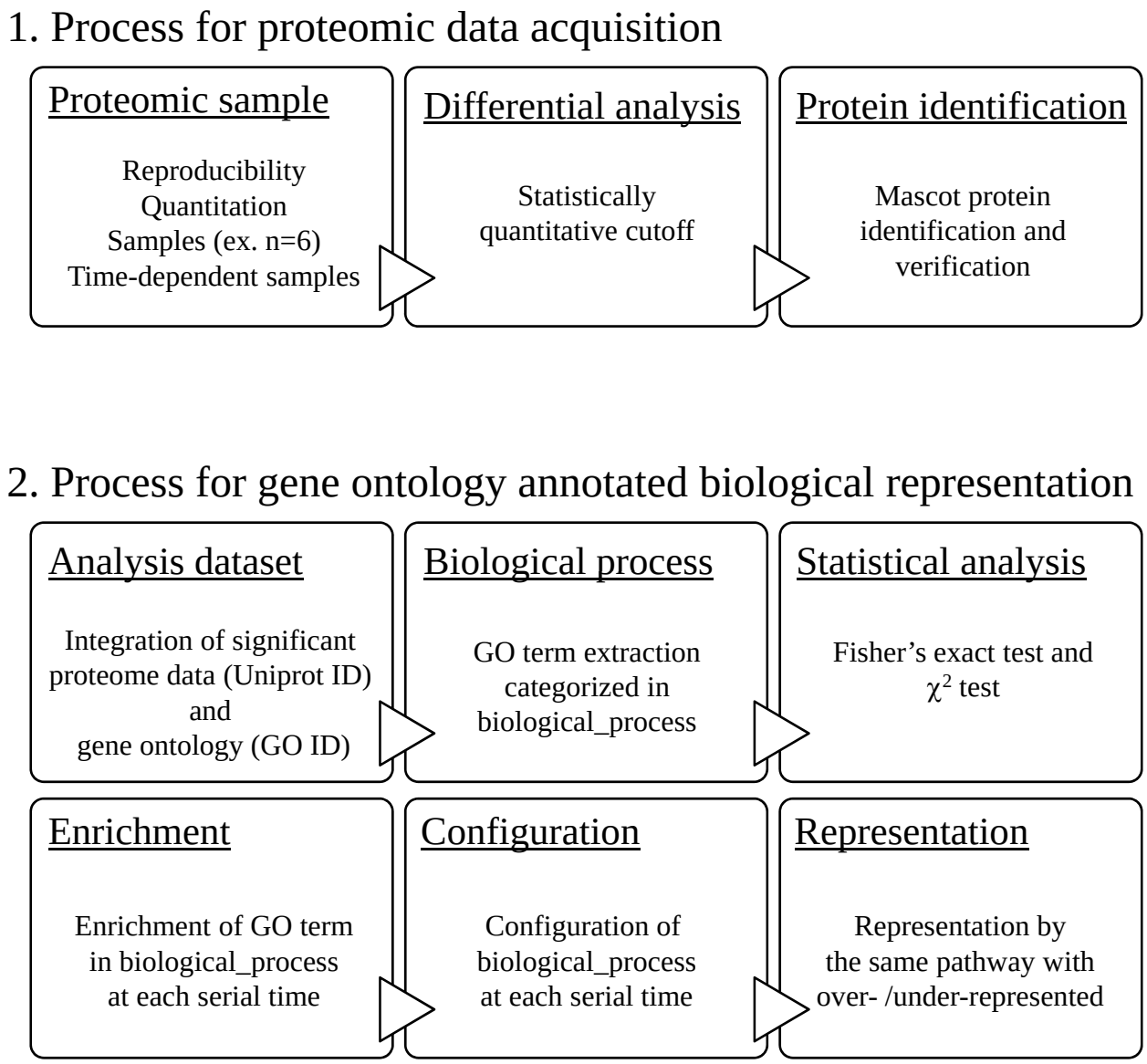

Chapter III:

New approach for biomarker discovery from the multi-omics:

Potential implications for monitoring serum bile acid profiles in circulation with serum proteome for carbon tetrachloride-induced liver injury/regeneration model in mice.

Summary

Bile acids have recently emerged as versatile signaling molecules, and their signaling pathway is a promising target for the treatment of metabolic diseases. Here, I developed a highly sensitive and high-throughput quantification method for six taurine- and glycine-conjugated bile acids using matrix assisted laser desorption/ionization time-of-flight mass spectrometry after solid-phase extraction (SPE-MALDI-TOF MS). In a carbon tetrachloride (CCl_4)-induced liver injury/regeneration model in mice, serum bile acid profiles were monitored, and the same samples were separated by two-dimensional polyacrylamide gel electrophoresis (2-D PAGE), and protein spots that significantly changed in quantity in a serial time points were identified by MALDI-TOF MS. Serum taurocholic acid (TCA) concentration was significantly elevated earlier than the increase of serum aspartate aminotransferase (AST)/alanine aminotransferase (ALT) activity, a potentially sensitive marker for minimal hepatic damage. Furthermore, TCA peaked at 20 h after treatment when massive serum proteins appeared in circulation. It should be noted that direct MALDI-imaging mass spectrometry (IMS) has succeeded in showing a hepatic lobular distribution change of TCA, predominantly seen in zone 1 area whereas necrotic changes were dominant in zone 3 area. The in-depth analysis of bile acid profiles in circulation with hepatic lobular distribution is a strong basis to understand the serum proteome in CCl_4-induced liver injury model.

Introduction

Bile acids are amphiphilic end products of cholesterol catabolism that facilitate lipid absorption in the intestine. Bile acids are synthesized in the liver, released into the proximal intestine, and reabsorbed in the distal intestine via the portal vein, a process termed enterohepatic circulation.[1] Serum bile acid levels therefore vary during the day following a rhythm of the ingestion of meals. Based on these observations, systemic bile acids are well positioned to inform the peripheral tissues that a meal has been ingested and that energy will become available.[3, 15-16] Recently, bile acids emerged as versatile signaling molecules endowed with systemic endocrine functions. Bile acids are ligands for G-protein coupled receptors (GPCR) such as TGR5 and modulate several nuclear hormone receptors including farnesoid X receptor (FXR).[7, 17] Through activation of these versatile signaling molecules, bile acids have been shown to regulate not only their own synthesis and enterohepatic circulation, but also triglyceride, cholesterol, energy, and glucose homeostasis. These bile acid controlled signaling pathways have become the source of promising novel drug targets to treat common metabolic and hepatic diseases.[5]

Many of the proteins in serum are synthesized in the liver and the abundance and structures of these proteins change in response to liver diseases. It is expected to facilitate the understanding of liver biological processes and their dysregulations in diseased status using the mapping of the liver proteome content.[18-19] In addition, the discovery of novel biological markers for the early detection of liver disease as well as therapy's efficacy or side effects is urgently needed.[20-21] Especially, liver regeneration is an important process. Although many regulatory events and their temporal distribution

during liver regeneration have been identified to date, the study on single pathways and signaling factors has thus far been insufficient to fully delineate the metabolomic complexity of the proliferative response after liver injury.[22] Several attempts have been undertaken to obtain a more global picture of the cellular processes that occur during liver regeneration. Animal models are available, which include a liver regeneration model induced by partial hepatectomy (PHx) and carbon tetrachloride (CCl_4).[23-26]

Even with the current proteomic technologies with wide quantitative range, complexity of serum protein expression often requires multiple platforms.[9, 27] In addition, a big debate in the clinical proteomics field is which type of sample, blood or tissue, should be used to discover serologic biomarkers. Proteomic studies using blood still have not resolved the question of whether plasma or serum can serve as a window into the state of patients' disease, and there is currently no scientific evidence that a linear relationship exists between protein changes in diseased tissue and protein changes in blood. Recent advances in high-throughput proteomics have made it possible to profile the global compositions of entire tissues, organelles, or interactomes at specific time points or under particular developmental or disease states. While such methods provide researchers with a greater understanding of large-scale, complex biological changes to overcome greater dynamic range such as serum proteome, it has necessitated an increasing reliance on standardized annotation to link results to known biological activities. Therefore, the functional classification of identified proteins is critical for proteomic studies aimed at discovering disease biomarkers.

Consistent with these notions, here I try to cross-validate bile acid homeostasis and serum proteome. Historically, bile acid analysis has been hindered by difficulties in separating many structurally similar compounds and isomers in a highly complex matrix.

Lately, LC-MS has been shown to be a sensitive and quantitative method of analysis for identification of major bile acids in urine and plasma.[28] I have developed and shown here a modified bile acid-targeted profiling method by solid phase extraction-based sample pretreatment and subsequent MALDI-TOF MS analysis,[29] giving superior specificity and a high-throughput analysis. I applied this method to the systemic analysis of the CCl_4-induced acute liver injury/regeneration model resulting in comprehensive profiling of both serum proteome and serum bile acid metabolome. In addition, the serum bile acid profiles were also validated by direct imaging mass spectrometry on liver histology.[30-31] This in-depth analysis of the bile acid profiles and corresponding serum proteomes provides a strong basis for investigations of liver pathobiology that employ mouse models of acute liver injury/regeneration in an effort to better understand, diagnose, treat, and prevent human liver diseases.

Materials and methods

Chemicals

Transaminase C-II test kit (L-Type GOT/J2 aspartate aminotransferase kit, L-Type GPT/J2 alanine aminotransferase kit) and mass spectrometry grade recrystallized α-cyano-4-hydroxycinnamic acid was purchased from Wako Pure Chemical (Osaka, Japan). Glycocholic acid (GCA), glycochenodeoxycholic acid (GCDCA), glycolithocholic acid (GLCA), taurocholic acid (TCA), taurochenodeoxycholic acid (TCDCA), and taurolithocholic acid (TLCA) were from Steraloids (Newport, RI) as sodium salts. 9-Aminoacridine hemihydrate (9-AA) was from Acros Organics (Geel, Belgium). N-1-Naphthylphthalamic acid (NPA) was from Fluka (Buchs SG, Switzerland). Empore 96-well disk plates C18-SD were from 3M (St. Paul, MN). Indium-tin oxide (ITO) coated glass slides (8-12 Ω/sq) were from Sigma-Aldrich (St. Louis, MO). Modified trypsin sequencing grade was from Promega (Madison, WI).

Animal study

This study was approved by the Ethics Committee of Kyoto Prefectural University of Medicine (Document number M21-164). Five-week-old male ICR mice (body weight 23-25 g, CLEA, Japan) were maintained on a fixed artificial light cycle (12 h of light and 12 h of dark) with free access to water. CCl_4 was mixed with mineral oil at a dose of 1 mg/kg body weight and injected intra-peritoneally. Serum samples were collected at serial time points of 0, 1, 3, 6, 12, 20, and 48 h after CCl_4 administration from orbital venous plexus. Seven and six mice were fed for CCl_4 i.p.

and mineral oil i.p. control, respectively. Samples were kept frozen at -80 °C until use. At each time point, livers were removed and kept frozen until further analysis. Serum AST/ALT activity was measured with transaminase C-II test kit. Frozen tissue samples were sliced with a thickness of 10 μm using a cryostat microtome (Leica, Germany). Histological images were obtained by a simple optic density method and hematoxylin and eosin and Oil Red O staining. Imaging was obtained by microscope (TE300-EF, NIKON, Japan).

Bile acid quantification

Bile acid standard concentration was 4-1000 μg/mL for glycine conjugate (GCA, GCDCA, GLCA) and 0.3-160 μg/mL for taurine conjugate (TCA, TCDCA, TLCA) in ethanol, and 100 μL of standard solution was mixed in 1.8 mL of deionized water. Bile acid solution was purified using Empore 96-well disk plates C18-SD and eluted with 150 μL of methanol. A serum sample of about 50 μL was also dissolved in 1.8 mL of water and 100 μL of ethanol was added. Eluate was mixed in an equal volume of 28 μg/mL N-1-naphthylphthalamic acid (NPA) and 10 mg/mL 9-aminoacridine (9-AA) in methanol and spotted on a MALDI target plate. MS data of bile acids was obtained by automated data acquisition and internal calibration with deprotonated signals from NPA (m/z 290.08) and 9-AA (m/z 193.08) in the same well using an AXIMA CFRplus MALDI-TOF MS (Shimadzu, Japan). Peak intensity was calculated by peak area integration and was normalized by NPA signal in same spectrum. Peak intensity was averaged from four measurements. Calibration curve was generated from the normalized intensity of each bile acid standard concentration, and the concentration was converted to each approximation curve of glycine- or taurine-conjugated standard.

Proteomic procedures

Serum proteins were separated by two-dimensional polyacrylamide gel electrophoresis (2-D PAGE). The procedures for proteomic analysis were carried out as described previously.[32] Briefly, serum protein concentration was determined by Bradford reagent (Sigma-Aldrich), and 300 μg of protein was dissolved in isoelectric focusing (IEF) buffer (6 M urea, 2 M thiourea, 3% CHAPS, 1% Triton X-100 and 1% DeStreak reagent) by gentle vortexing for 30 min at room temperature. A 13 cm DryStrip gel of nonlinear pH 3-10 gradient was used for IEF using an IEF Cell (BioRad, Hercules, CA). After IEF, the DryStrip gel was equilibrated in sample buffer (6 M urea, 2% SDS, 20% glycerol, 2% DTT, and 375 mM Tris-HCl, pH 8.8) for 20 min, and a 10-16% polyacrylamide gradient gel was used for the SDS-PAGE. Protein spots were visualized with high-sensitivity CBB G-250 solution, and gel images were acquired using a GS-800 calibrated imaging densitometer (BioRad). Protein spot analysis was performed by PDQuest, version 7.2, 2-D analysis software (BioRad). Protein spots were excised and digested in-gel with trypsin after reductive alkylation with DTT and following iodoacetamide. After incubation at 37 °C overnight, tryptic peptides were desalted with ZipTip μC18 (Millipore, Billerica MA). Recrystallized α-cyano-4-hydroxycinnamic acid (10 mg/mL in 0.1% trifluoroacetic acid and 50% acetonitrile) was used as MALDI matrix.

Protein identification was performed by peptide mass fingerprinting (PMF). Peptide masses were analyzed using an AXIMA CFRplus MALDI-TOF MS. The acquisition mass range was 650-4000 Da. The equipment was first externally calibrated by protonated mass signals of a five peptide mixture, bradykinin fragment 1-7

(monoisotopic m/z 757.40), angiotensin II (m/z 1046.54), P14R synthetic peptide (m/z 1533.86), ACTH fragment 18-39 (m/z 2465.20), and insulin oxidized B chain (m/z 3494.65). Each data point was internally calibrated by protonated signals from tryptic autolysis fragments (m/z 842.51 and m/z 2211.10). The raw spectrum data was opened by Mascot Distiller, version 2.2.0, peak picking software (Matrix Science, London) and processed by default parameters. Protein was identified against UniProt (June 10, 2008; 389 046 Mus musculus sequence entries) and NCBInr (September 7, 2008; 7 020 262 non-redundant mammalian sequence entries) database on Mascot Server, version 2.2, up to one missed cleavage, peptide tolerance of 0.2 Da, fixed modifications of cystein carbamydomethylation, and variable modifications of methionine oxidation. MOWSE scores above 54 for UniProt and 71 for NCBInr were considered significant ($p < 0.05$).

Use of gene ontology in serum proteome

Identified proteins were further annotated using gene ontology to perform functional analysis. The GO database can be freely accessed from the Gene Ontology website (www.geneontology.org), Gene ontology annotation (GOA) and Open biological ontologies (OBO).[14] The GO term and ontology component of OBO was divided into three categories; “molecular_function”, “cellular_component”, and “biological_process”. I first prepared the data set consisting of a pair of UniProt ID, GO ID, term and component. I used in this data set the gene_ontology_edit. obo (Feb. 26, 2009) and the gene_association.mgi (Feb.26, 2009). In case proteins did not fit to Mus musculus, gene_association.rgd and gene_association.goa_human were used. Each UniProt ID and spot quantity can be highlighted to correspond to multiple GO IDs.

Statistical analyses

Differentially expressed protein spots on 2D gels corresponding to CCl_4 administration were selected widely by comparison with average of seven CCl_4-treated samples against six control samples using PDQuest. Each volume of selected spot was refined by the one-way analysis of variance (ANOVA) test using GeneSpring GX, ver.10, gene expression analysis software (Agilent, Santa Clara, CA). From the two-step-criteria, about 250 protein spots of statistically significant change and serial time points were selected as the candidates for further analysis. GO analysis was performed using GeneSpring, and GO terms categorized in the "biological_process" component with $p < 0.05$ as significant terms by $\chi 2$ test and Fisher's exact test[13] in serial time points.

Imaging mass spectrometry (IMS)

Frozen liver tissues were sliced with a thickness of 10 μm, and the section was attached onto ITO coated glass slides. Using a chemical inkjet printer CHIP-1000 (Shimadzu), a mixed solution with 10 mg/mL 9-AA and 6 μg/mL NPA in 10% 2-propanol and 80% methanol was printed over the tissue section at a spatial interval of 200 μm as 50 iterations at 300 pL per iteration. MS data was obtained using an AXIMA Performance MALDI-TOF MS (Shimadzu). Automated data acquisition was performed for each matrix deposit. Deprotonated signals of 9-AA and angiotensin II (m/z 1044.52) were used for external calibration. An electrical image of each section on the target plate was scanned using CHIP-1000. The obtained mass spectra were converted, for selected m/z value, into comma-separated values (CSV) associating signal intensity with XY coordinate. The ion image highlighted the signal intensity obtained from a specific

molecule. Peak intensity was normalized by NPA standard in the same spectrum. These specific ion images for compounds of interest were displayed by plotting the spacial dimensions of X and Y versus the signal amplitude.

Results

Assessment of CCl_4-induced liver injury / regeneration model

The serum biochemical markers for CCl_4-induced liver injury/regeneration model were measured at 0, 1, 3, 6, 12, and 20 h after administration (Figure 1a, b). Conventional serum AST/ALT activity indicated that an acute liver injury could be diagnosed 6-12 h after CCl_4 administration when both activity markers were markedly increased.

Because ideal attributes of biomarkers for liver damage include organ specificity for liver, histological analysis is essential. According to the previous study, I scored histopathology of the liver from "0" to "V" in order of increasing damage and regeneration; 0, no observed necrosis; I, a few degenerating parenchymal cells; II, minimal necrosis; III, extensive necrosis in which central veins were surrounded by several layers of dead or degenerating cells; IV, massive necrosis of extensive liver areas; V, regenerative stage.[33] I observed for time 0 h, 0; 1 h, 0-I; 3 h, I-II; 6 h, III; 12 h, IV; 24 h, IV-V; and 48 h, V. These observations were based on our histopathology shown in Figure 2a, b.

Quantification of serum bile acid

Quantitative analysis by MALDI-TOF MS has been demonstrated for compounds of biological interest. In the previous study, the bile acids were separated from urine by SPE cartridges and quantitative analysis by MALDI-TOF MS.[29] I demonstrated quantification of bile acids at biologically relevant concentrations directly from serum with minimal sample preparation. Dynamic range of bile acid concentration in serum by

our method was 4-1000 μg/mL for glycine conjugates and 0.3-160 μg/mL for taurine conjugates (Supporting Information).

Concentrations of six cholic acid conjugates, TCA, TCDCA, TLCA, GCA, GCDCA, and GLCA, in murine serum were determined (Figure 3a-f). TCA concentration was markedly elevated as liver injury progressed, significantly from 3 h, reaching a maximum at 20 h after administration. After 48 h, it remained at a higher level than that of the normal control. Serum TCDCA concentration was also elevated significantly from 6 h and reached a maximum at 20 h, as I have shown in the TCA profile. However, the amplitude of its change is much smaller, about 1/50. Serum TCA and TCDCA of control mice did not show any increase during the experiments. Secondary bile acid, TLCA and GLCA, did not show any significant change. With these observations, taurine-conjugated primary bile acids TCA and TCDCA could be defined as biomarkers for acute liver injury.

In Table 1, I showed serum concentration ratio of [TCA]/[TCDCA], which is adjusted by control mouse value in each time point. As liver injury progresses, the ratio increased up to 16.6 at 3 h and reached as high as 71.0 at 12 h, and then decreased to 24.4 at 48 h. It is notable that such an elevation of serum [TCA]/[TCDCA] was sustained more than 2 days.

Serum proteome

More than one hundred densitometric features were reproducibly detected on each 2-D PAGE for each mice serum (Supporting Information). Serum proteins as quantified by differential 2-D PAGE seemed remarkably stable in the absence of liver injury since so few changes were observed from 0 to 1 h. However, during the time of high toxicity

with a known liver injury dose of CCl_4 as determined by histopathology and AST/ALT activity (Figure 1), differential proteomic analysis showed the greatest number of serum protein changes (Table 2 and Supplementary Table, Supporting Information).

According to our proteomic data, alterations in serum bile acid metabolites and serum proteins are well correlated. From 6 to 12 h after CCl_4 administration, the change rate of bile acids and increase number of serum proteins were most prominent and reached maxima at 6-12 h. In earlier time points before 6 h, 12 up-regulated and 3 down-regulated proteins belonging to above criteria are as follows: up-regulated at 1 h, OBP2A; up-regulated at 1-3 h, Hspa5, Fgb, Saa2, Psma2, and Aldoa; up-regulated at 3-6 h, Fbp1, Saa2, Ald, Gpd1, Idh1, and Fah; down-regulated at 1-3 h, Gsn; down-regulated at 3-6 h, Fgb and Psma2 (Table 2 and Supplementary Table, Supporting Information).

Applying GO into serum proteomics

All identified proteins were translated into GO terms as described in OBO, and the results are shown in Figure 4. Apparently, I can discriminate time-dependent histological events of this hepatotoxicity model according to GO statistical analysis. For acute phase, several proteins have started to become up-regulated and a few proteins were down-regulated, mostly belonging to acute response. As for blood regulation and actin regulation, some were up-regulated and some were down-regulated.

The most prominent changes in serum proteins were observed between 6 and 12 h after CCl_4 treatment. I can call it a fulminant liver injury stage. More than 150 proteins belonging to amino acid metabolism were over-represented in serum. And at this time point only, proteins concerned with regulation of programmed cell death appeared in

serum. Although proteins of amino acid metabolism continued to be over-represented until 20 h, proteins of oxidative reduction, protein metabolism, and carbohydrate biosynthesis were underrepresented. From 20 h, some proteins concerned with regeneration, regulation of immune system processes, organic acid metabolism, and lipoprotein metabolic processes were overrepresented.

Imaging mass spectrometric analysis

Direct MS/MS fragment pattern analysis from liver section was performed to demonstrate that mass signals of m/z 514 and m/z 498 were derived from TCA and TCDCA, respectively (Figure 5a, b and Supporting Information). The ion images constructed from these signals on normal control and pathological liver tissue sections are shown in Figure 6a-d. In 6 and 20 h after CCl_4 administration, the ion images for m/z 514 were strongly elevated diffusely all over the liver section. As a control, there are few signals in normal control liver. Of note, the peak from TCA was noticeable in accordance with portal vein structure in the normal control liver (Figure 6, circled). Hepatic lobular structure that TCA could be detected was around portal vein, not central vein (Figure 6). While TCA and TCDCA were successfully detected on liver sections, peaks from TLCA, GCA, GCDCA, and GLCA were not detected (data not shown). In 3 h IMS data (white arrow in [TCA, 3 h]), ectopic TCA signals were observed not related to hepatic lobular structure, which might be blood contamination in dissection. Furthermore, I tried to perform semi-quantitative analysis of TCA and TCDCA directly from liver section (Supporting Information). TCA and TCDCA profiles on tissue were similar to serum one except for at 12 h, because ionization suppression occurred by large amount of signals such as phosphatidylethanolamine.

With all these findings of imaging mass analysis, I may say that TCA in the acute phase of CCl_4-induced liver injury is well correlated with the serum profile of TCA as well and that the TCA profile could be a surrogate biomarker of liver injury.

Discussion

In this study, I demonstrated that serum bile acid profile can be a diagnostic marker for liver injury/regeneration in the CCl_4-induced mouse model. This is indicated by a novel and informative biomarker strategy integrating time and space distribution of bile acids in circulation. To our knowledge, this is the first study to apply imaging mass spectrometry to cross-validate serum biomarkers directly on the diseased tissue. Importantly, simultaneous measurement of changes in multiple serum proteins and bile acid metabolites made it possible to explore connections between proteomic and metabolomic changes in acute, fulminant, and recovery course of hepatotoxicity. One of the remarkable findings of this investigation is the significant elevation in serum TCA in acute to fulminant liver injury above the physiological level. Previous studies showed that CCl_4 toxicity can be assessed by serum AST/ALT activity at 6-24 h (AST) or 6-36 h (ALT) in a time-dependent manner,[23-24] which is also reproduced in our study. As serum concentrations of TCA become elevated from 3 h after CCl_4 administration, profiling serum bile acids is more sensitive than a classical AST/ALT activity.

CCl_4-induced hepatotoxicity is characterized by increased oxidative stress leading to increased lipid peroxidation.[34] In the present study, expressions of some proteins were up- or down-regulated in the acute phase, meaning that these are empirical serum protein biomarkers for acute hepatotoxicity of CCl_4. For example, in 1-3 h after CCl_4 administration, serum gelsolin was significantly down-regulated. Because other critical situations exist that cause circulating gelsolin to decrease in plasma by forming actin-gelsolin complexes, gelsolin is not a hepatotoxicity-specific marker.[35] Serum amyloid A-2 is also up-regulated in the acute phase in the present model, but it is a

well-known responder to various tissue injuries.[36] Interestingly, odorant binding protein Ia, which appeared in serum in a very acute time course, is not implicated in acute response, so it can be a novel protein biomarker candidate.[37] Fibrinogen beta chain was up-regulated from 1 to 3 h in serum with a subsequent decrease before 6 h. This clearly shows how blood coagulation contributes to the pathogenesis of CCl_4-induced liver injury. There are some decreased proteins in a recovery phase; mannose binding protein C and plasma retinol binding protein[38] can be recognized as protein markers for the recovery phase of this hepatotoxicity model.

Assuming that these proteins are candidates for serum biomarkers of acute liver injury, they must be interpreted in a systemic background.[15] For example, the relation between liver gene expression profiles and CCl_4 hepatotoxicity has been well studied in toxicogenomics. In this study, I applied GO statistical analysis in serum proteomics in making a whole map to understand proteome-wide alterations in serum in response to CCl_4. Serum proteomics with GO annotation can further give us information about histological events of liver from acute to regenerative phases. Based on gene expression in the CCl_4-administered rats, maximal toxic time was estimated to be 6 h from the analysis of hierarchical clustering.[23] It is interesting to note that up-regulated genes peaks at 6 h after CCl_4 administration and soon returned to normal levels within 12 h. With our proteomic data, massive protein alteration started from 6 h to end in 12 h, mostly classified into amino acid metabolism, apoptosis, and regeneration. This is fairly understandable because proteins of amino acid metabolism are tightly linked to a proper liver function of the periportal area. In addition, histopathology has shown that CCl_4 induces necrosis and apoptosis around the central veins. This is clearly reflected in the heat map chart of GO over-representation. Before this massive change, I can pick up

some acute reactant proteins, as well as proteins concerned with apoptosis. Most importantly, GO analysis on serum proteomics clearly demarcated that regeneration started from 12 h after CCl_4 exposure.

The heterogeneity of liver histochemistry is related to the blood supply; cells located in the upstream or periportal zone differ from those in the downstream or perivenous zone in their equipment with key enzymes, translocators, receptors, and subcellular structures and therefore have different functional capacities. This is the basis of the model of metabolic zonation, according to which glucose release from glycogen and via gluconeogenesis, amino acid utilization and ammonia detoxification, TCDCA can be detected on the tissue sections from 3 h after CCl_4 administration. It is important to note that liver 12 h after CCl_4 administration is full of many different molecular species such as phospholipids (Supporting Information). In normal control liver, I can observe vascular-shaped regions of TCA protective metabolism, bile formation, and the synthesis of certain plasma proteins such as albumin and fibrinogen occur mainly in the periportal area, whereas glucose utilization, xenobiotic metabolism, and the formation of other plasma proteins such as R1-antitrypsin or R-fetoprotein occur predominantly in the perivenous zone.[39] Recent developments in MALDI-MS have enabled direct detection of lipids as intact molecular species present within cellular membranes.[31] Abundant lipid related signals are produced from the direct analysis of tissue sections when sequential spectra are acquired across a tissue surface that has been coated with a MALDI matrix. As I expected, peaks responsible for TCA and much less with elevation (Figure 6, circled). This can be a portal vein, reflecting enterohepatic circulation of TCA. In later time course, zonal distributions of TCA become much prominent. At 3 h after CCl_4 treatment, a bile flow from portal vein is clearly demarcated from surrounding

lobular organization as shown in Figure 6.[40-41] At 6 h later, TCA distribution patterns spread all over the liver, and this continues to 20 h after CCl_4 treatment.

Bile acid metabolism plays a critical role for the elimination of excess cholesterol in the liver.[1, 3] This pathway is achieved via transcriptional regulation of cholesterol 7a-hydroxylase (CYP7A1), the limiting enzyme of bile acid biosynthesis.[4] Upon bile acid stimulation, a member of nuclear receptors (NRs), FXR, potently activates transcription of the small heterodimer partner, SHP, which is an atypical orphan NR lacking a DNA binding domain.[5, 42] On its activation by bile acids, FXR regulates bile acid synthesis, conjugation, and transport, as well as various aspects of lipid and glucose metabolism. This means that in the regenerative phase of the CCl_4-induced liver injury model, bile acids can contribute to successive gene expression of the hepatocytes, which is concerned with feedback regulation of bile acids itself. Recently, in vitro and in vivo data showed that bile acids modulate gluconeogenesis by regulating the expression of the rate-controlling enzyme phosphoenol pyruvate carboxykinase (PEPCK), as well as of glucose-6-phosphatase (G6Pase) and fructose-1,6- bisphosphatase (FBP1).[43] Our proteomics data have suggested that the FXR driven proteins via SHP were down-regulated in the recovery phase of the present model, such as FBP1 and ApoA1.[5]

Before translating these observations into human study, I must think about species-specific differences of bile acid metabolism. For example, previous research has shown that the effect of bile duct ligation on the total bile acid synthesis appears to be different between rats and hamsters.[44] Amidation of bile acids in the liver requires the sequential action of two separate enzymes, bile acid CoA synthetase (BAS) and bile acid CoA:amino acid N-acyl-transferase (BAT).[45] In the first reaction, BAS catalyzes the formation of bile acid CoA thioesters. In the second reaction, BAT catalyzes the

reaction between the bile acid CoA thioester and either taurine or glycine. In case of mouse, mBAT uses taurine but not glycine as a substrate for the conjugation of bile acids, which was totally proven by the present study. However, rat and human synthesize both taurine- and glycine-conjugated bile acids.[2] Besides their well established roles in dietary lipid absorption and cholesterol homeostasis, it has recently emerged that bile acids are also signaling molecules, with systemic endocrine functions. It must be important to monitor bile acid profiles in terms of systemic approaches for metabolic perturbed situations such as diabetes and hypertriglycemia before and after preclinical drug development. It is extremely important to monitor serum bile acid profiles in the clinical trials of novel drug development in the category of FXR agonists, modulators, bile acid pool modulators, and TGR5 agonists.[5] In addition, targeted metabolomics applied to analyze the role of genetic variants on bile acid profiles in a large human population will be a very powerful approach in the future.

In conclusion, the present study demonstrated that bile acid profiling would be a promising biomarker that may help to evaluate therapeutic risks, efficacy, and drug actions during the drug development process, as well as applying to clinical and epidemiological study.

Tables

Table 1. Adjusted serum TCA/TCDCA concentration ratio.

Adjusted ratio of serum TCA to TCDCA concentration of CCl_4 treated mice compared with control mice was calculated as [TCA_CCl_4] - [TCA_control]/[TCDCA_CCl_4] - [TCDCA_control].

Time	0hr	1hr	3hr	6hr	12hr	20hr	48hr
Ratio	0.6	5.6	16.6	31.0	71.0	50.3	24.4

Table 2. Scoring histopathology of CCl_4-induced liver injury/regeneration model with corresponding serum proteomic data.

At 0, 1, 3, 6, 12, 20, and 48 h after CCl_4 treatment, images of liver histology based on a simple optic density method are indicated. Scoring (zone) represents scoring of necroinflammatory activity of this model according to histology activity index (HAI) of the Scheuer System,[33] which is modified as follows. Grades 0 to 4 represent 0) no or minimal change, 1 = inflammation but no necrosis, 2 = mild or focal necrosis, 3 = moderate necrosis or severe focal cell damage, 4 = severe necrosis or damage including bridging necrosis. Serum proteome indicates the up- and down-regulated protein ID or number of identified protein.

Time	Histology	Scoring (Zone)			Serum proteome	
hrs	Simple optic density	1	2	3	Up-regulated	Down-regulated
0	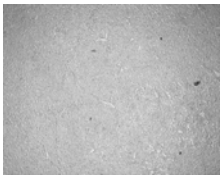	0	0	0	--	--
1	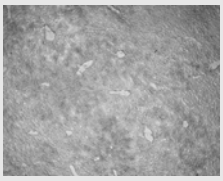	0	0	0	OBP2A	--
3	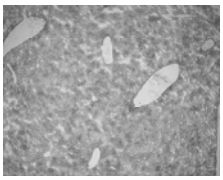	1	0	1	Hspa5 Fgb Saa2 Psma2 Aldoa	Gsn
6	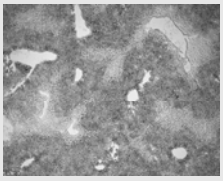	3	1	1	Fbp1 Saa2 Alad Gpd1 Idh1 Fah	Fgb Psma2
12	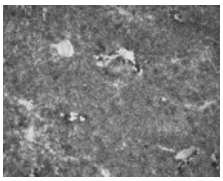	4	3	2	151	--
20	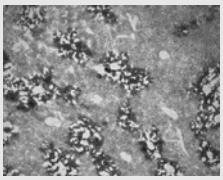	4	4	3	132	Mbl2 Rbp4
48		0	1	3	Apoa4 Rbp4 A2m Ces3 APOB	185

Figure captions

Figure 1. Asparatate and alanine aminotransferase activity in mouse serum.

Time-dependent enzymatic (a) AST and (b) ALT activity of CCl_4-administrated serum (solid) and control (dotted) is demonstrated using a transaminase test kit. Single and doubled asterisk indicate $p < 0.05$ and $p < 0.01$, respectively.

Figure 2. Histopathological image of mouse liver section.

Histological images were obtained at each serial time point of 0, 1, 3, 6, 12, 24, and 48 h after CCl_4 administration by (a) HE staining image and (b) Oil Red O staining. Typical histopathological observations of CCl_4-induced liver injury/regeneration model are obtained. From image of 0 h, normal hepatic lobular structure was observed, and shape of hepatocyte was slightly changed in 1 h. Hepatocyte ballooning and inflammation was observed in 3 h, and mild necrosis around portal vein was occurred in 6 h. Fatty degeneration or necrosis was advanced at 6-12 h, and massive necrosis and cell damage occurred in 20 h. In 20 h, some hepatocyte regeneration seemed to begin around the portal vein. In 48 h, hepatic lobular regeneration was observed from the portal vein, but necrosis or fatty degeneration remained around the central vein.

Figure 3. Time-dependent quantitative profile of serum bile acids.

Serum samples were measured at 0, 1, 3, 6, 12, 20, and 48 h after CCl_4 administration: (a) TCA in CCl_4 (solid) and control (dotted); (b) TCDCA in CCl_4 and control; (c) TLCA in CCl_4 and control, (d) GCA in CCl_4 and control; (e) GCDCA in CCl_4 and control; f) GLCA in CCl_4 and control. Y-axis of taurine conjugate was the range of 0-20 μg/mL

except for TCA, and glycine conjugate was 0-120 μg/mL, which is 1/8 of each dynamic range. A t test was carried out for each time point vs the previous time point. Single and doubled asterisk indicate $p < 0.05$ and $p < 0.01$, respectively.

Figure 4. Gene ontology based biological process representation.

Over-represented GO terms with $p < 0.05$ of "biological_process" in a serial time points are shown with two-color heat map chart: color scale indicates significant GO terms associated with over-represented proteins (yellow) and under-represented proteins (blue), and no-signal is indicated by black. The major biological process is indicated in the left column of Process. Proteins used in this analysis are shown in the supplementary table, Supporting Information.

Figure 5. Direct MS/MS analysis from liver section of TCA and TCDCA.

MS/MS spectrogram of (a) TCA and (b) TCDCA were obtained by AXIMA Resonance MALDI-quadrupole ion trap-TOF MS (Shimadzu). The lower spectrogram shows TCA and TCDCA standard, and the upper one shows TCA and TCDCA signal directly from liver section at 6 h. The distinct fragment ion derived from taurine (m/z 124) is shown in each MS/MS signal. A dehydration fragment ion from steroid basic structure is also observed.

Figure 6. Imaging mass spectrometric analysis of TCA and TCDCA on liver section.

TCA and TCDCA distribution image was obtained from liver frozen section at (a) 0, (b) 3, (c) 6, and (d) 20 h after CCl_4 administration. Each image is marked as follows: [TCA]

TCA distribution; [TCDCA] TCDCA distribution; [HE] HE staining image of serial section of IMS; [HE circled] HE image around circled area of TCA signal elevation; [IMS image] acquired section image of IMS. Circled area indicates around portal vein, and white arrow in [TCA, 3 h] of (b) is ectopic TCA signals. Scale bar indicates 2 mm. PV = portal vein; CV = central vein.

Figure 1

a)

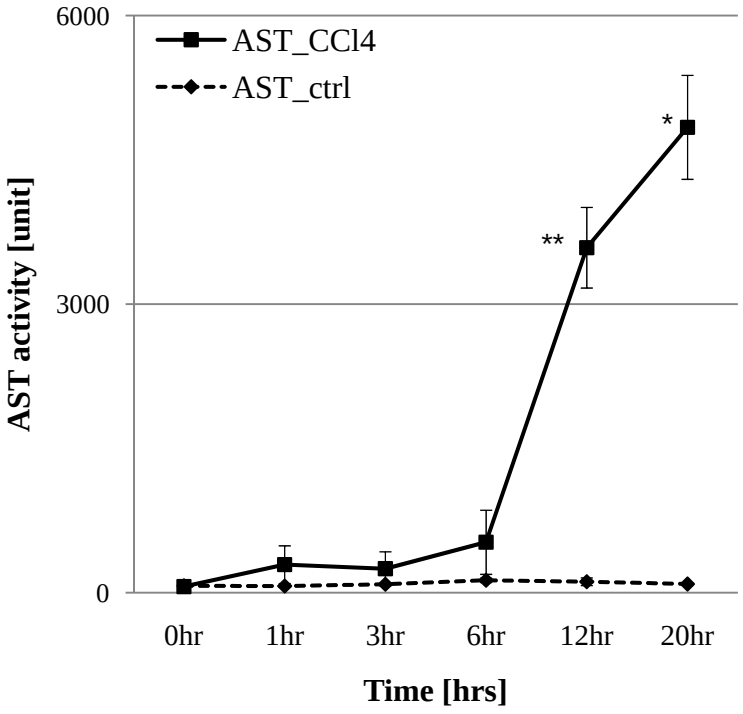
6000
3000
0
AST_CCl4
AST_ctrl
*
**
AST activity [unit]
0hr
1hr
3hr
6hr
12hr
20hr
Time [hrs]

b)

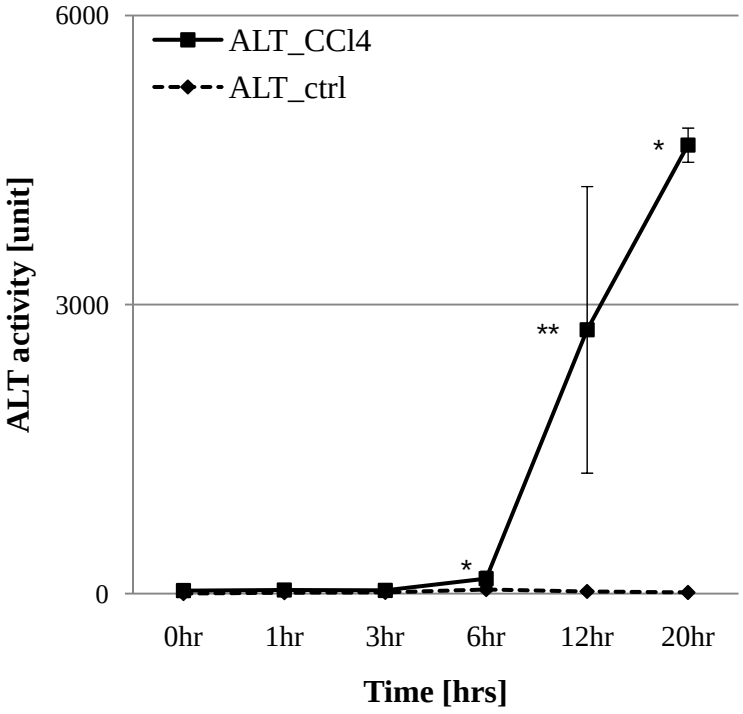
6000
3000
0
ALT_CCl4
ALT_ctrl
*
**
*
ALT activity [unit]
0hr
1hr
3hr
6hr
12hr
20hr
Time [hrs]

Figure 2

a)

0 hr

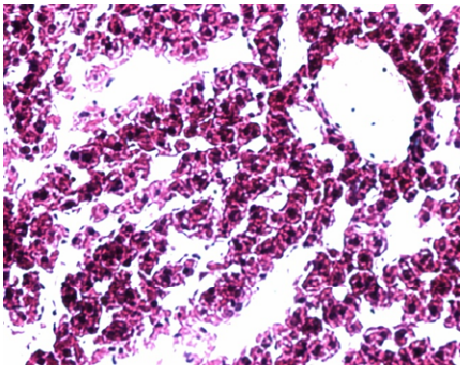

12 hr

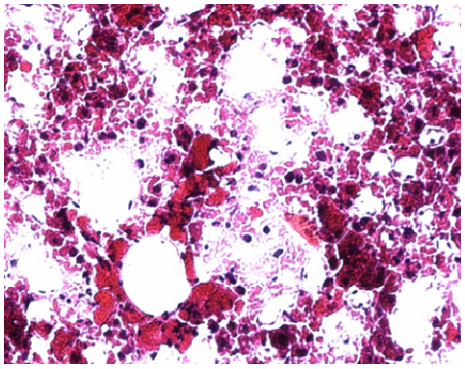

1 hr

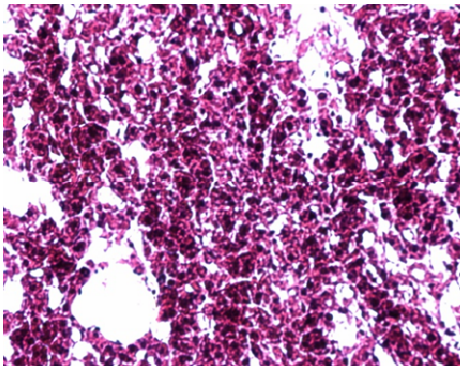

20 hr

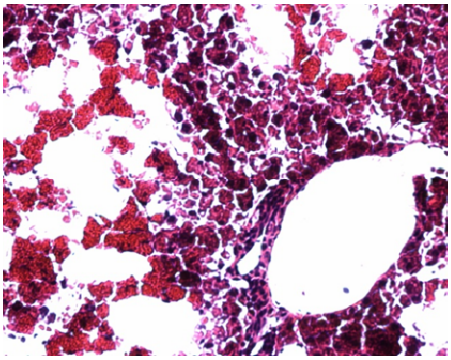

3 hr

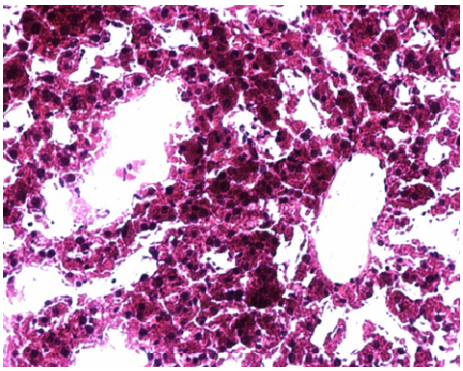

48 hr

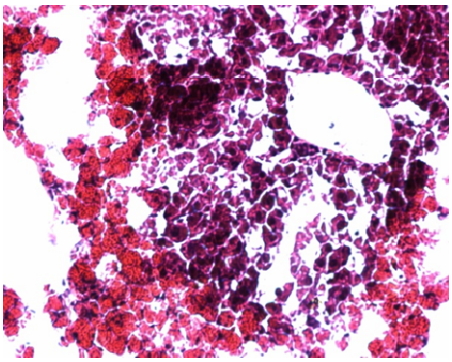

6 hr

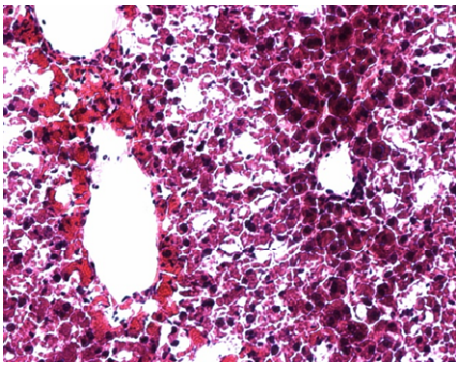

Figure 2

b)

0 hr

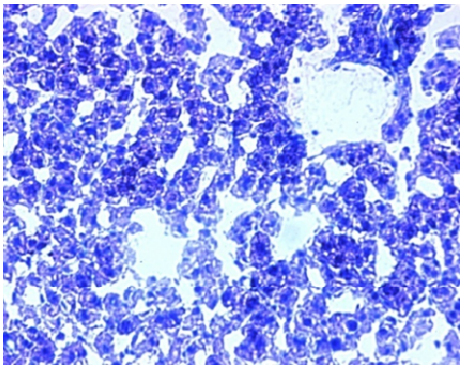

12 hr

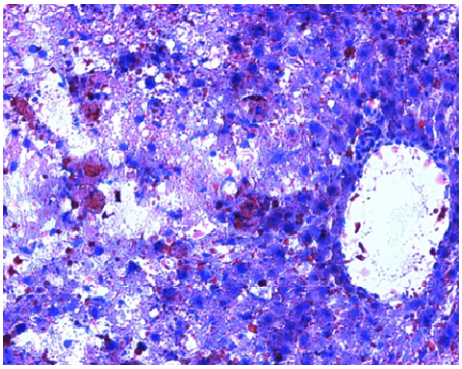

1 hr

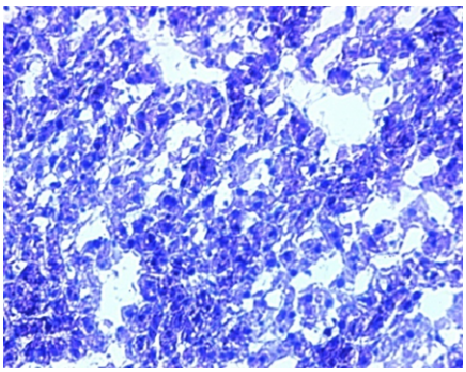

20 hr

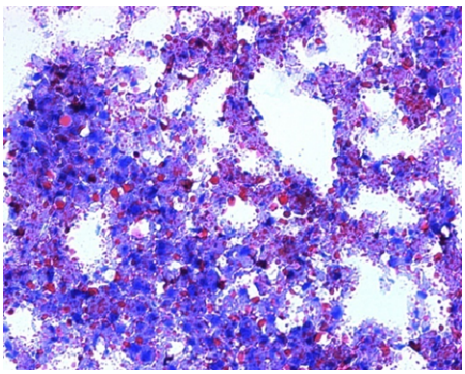

3 hr

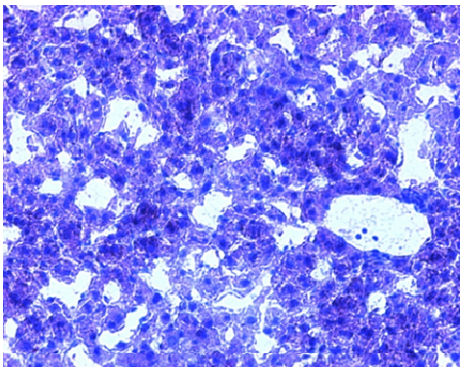

48 hr

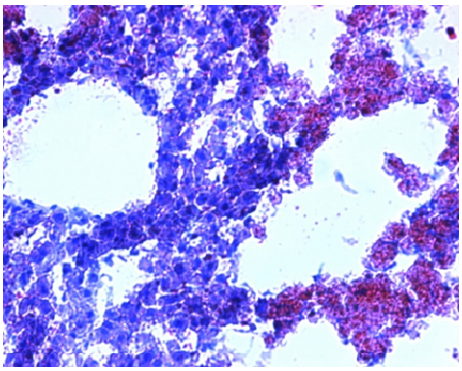

6 hr

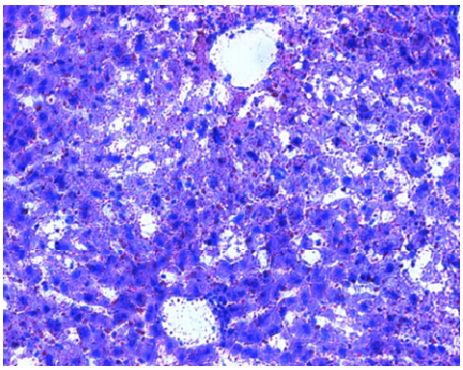

Figure 3

a)

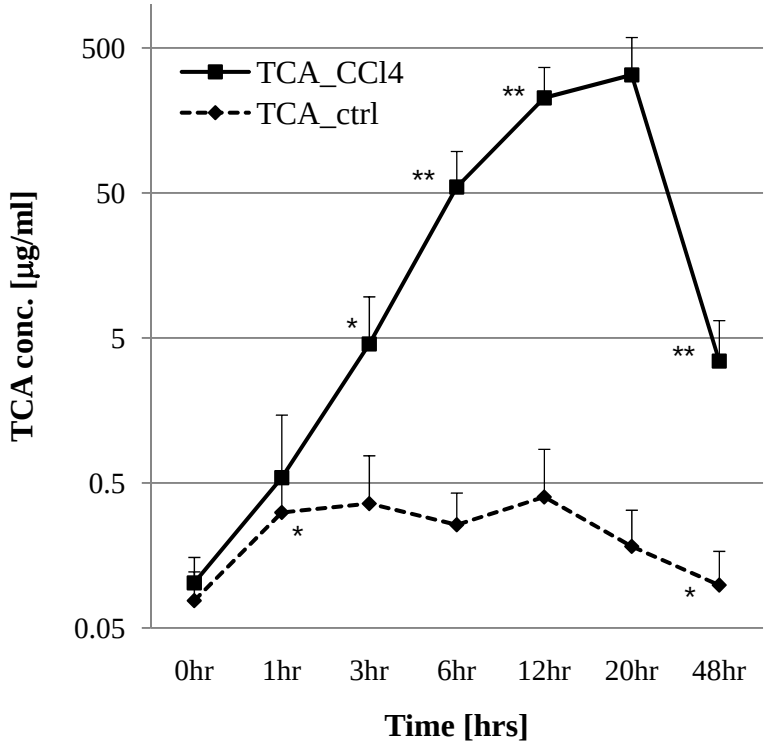
500
50
5
0.5
0.05
TCA_CCl4
TCA_ctrl
TCA conc. [µg/ml]
0hr
1hr
3hr
6hr
12hr
20hr
48hr
Time [hrs]

b)

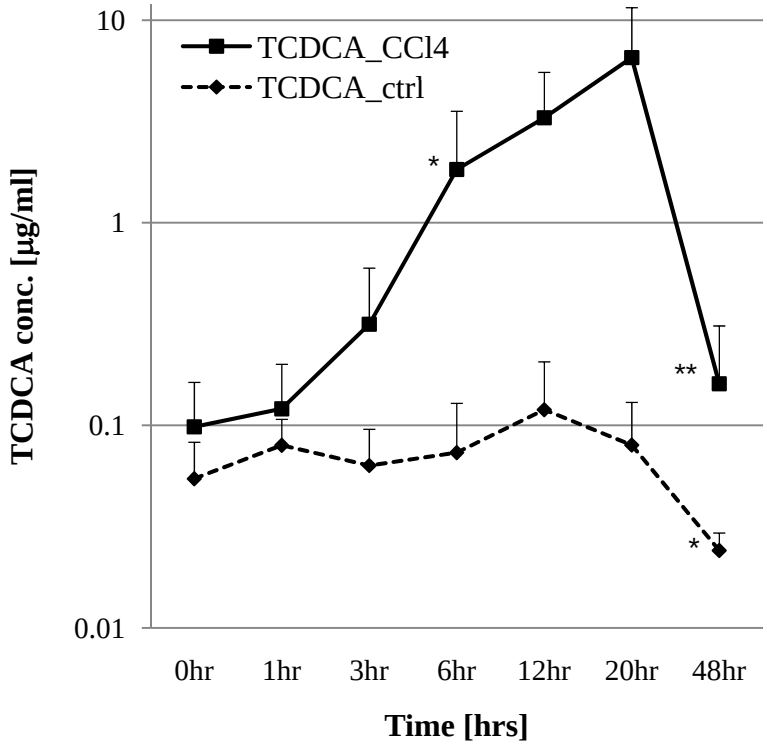
10
1
0.1
0.01
TCDCA_CCl4
TCDCA_ctrl
TCDCA conc. [µg/ml]
0hr
1hr
3hr
6hr
12hr
20hr
48hr
Time [hrs]

Figure 3

c)

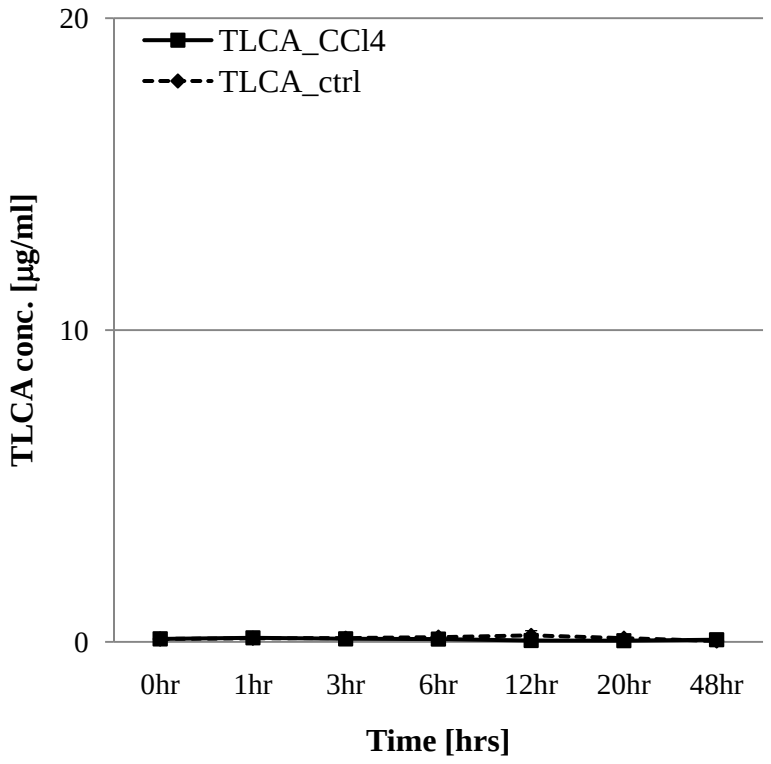
20
10
0
TLCA_CCl4
TLCA_ctrl
TLCA conc. [µg/ml]
0hr
1hr
3hr
6hr
12hr
20hr
48hr
Time [hrs]

d)

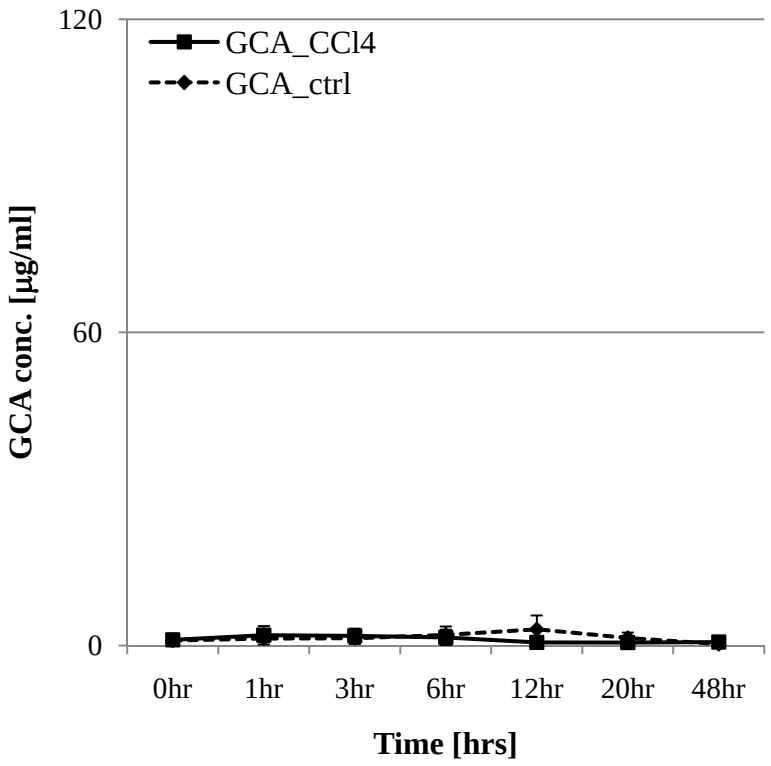
120
60
0
GCA_CCl4
GCA_ctrl
GCA conc. [µg/ml]
0hr
1hr
3hr
6hr
12hr
20hr
48hr
Time [hrs]

Figure 3

e)

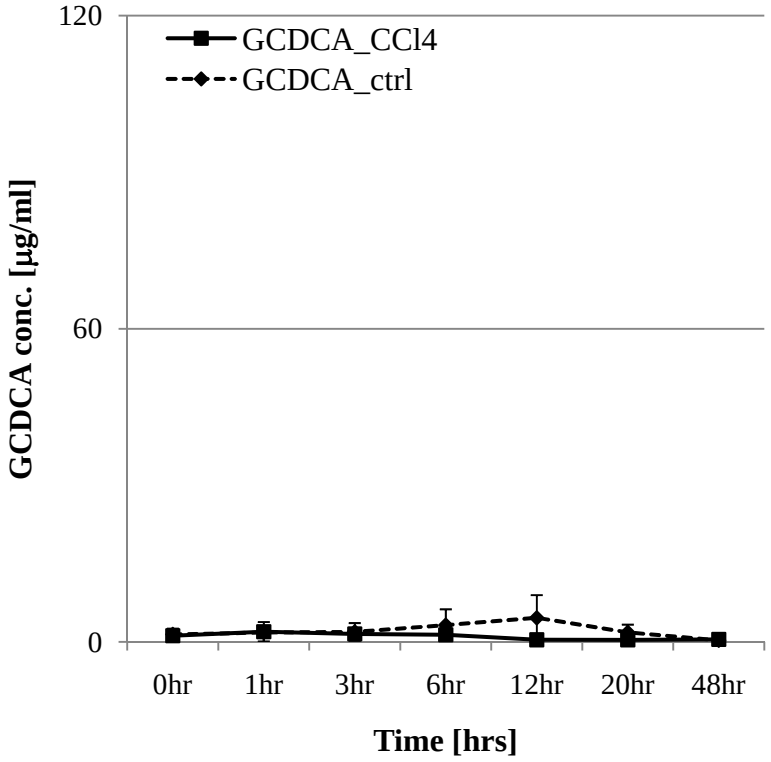
120
60
0
GCDCA_CCl4
GCDCA_ctrl
GCDCA conc. [µg/ml]
0hr
1hr
3hr
6hr
12hr
20hr
48hr
Time [hrs]

f)

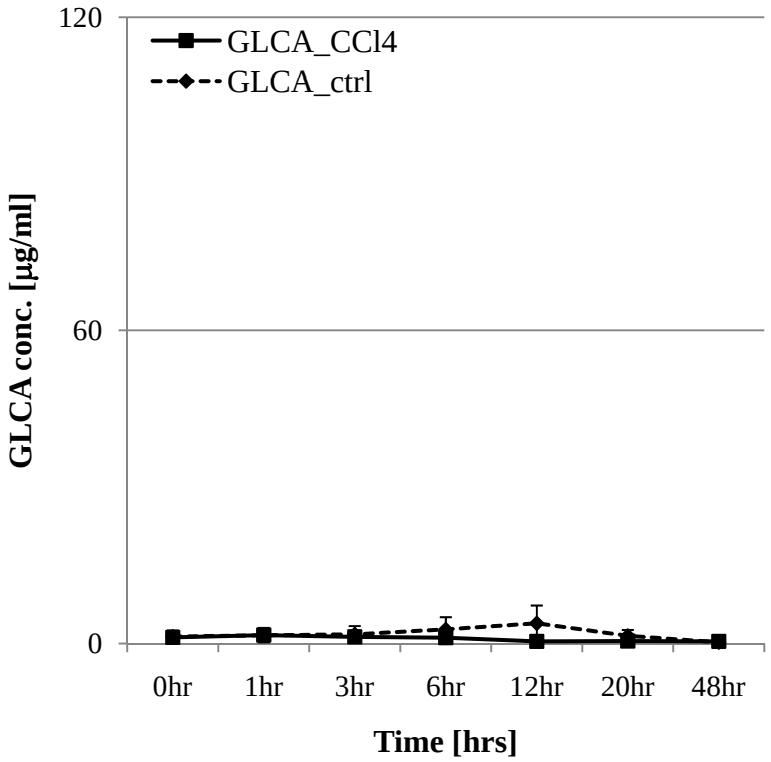
120
60
0
GLCA_CCl4
GLCA_ctrl
GLCA conc. [µg/ml]
0hr
1hr
3hr
6hr
12hr
20hr
48hr
Time [hrs]

Figure 4

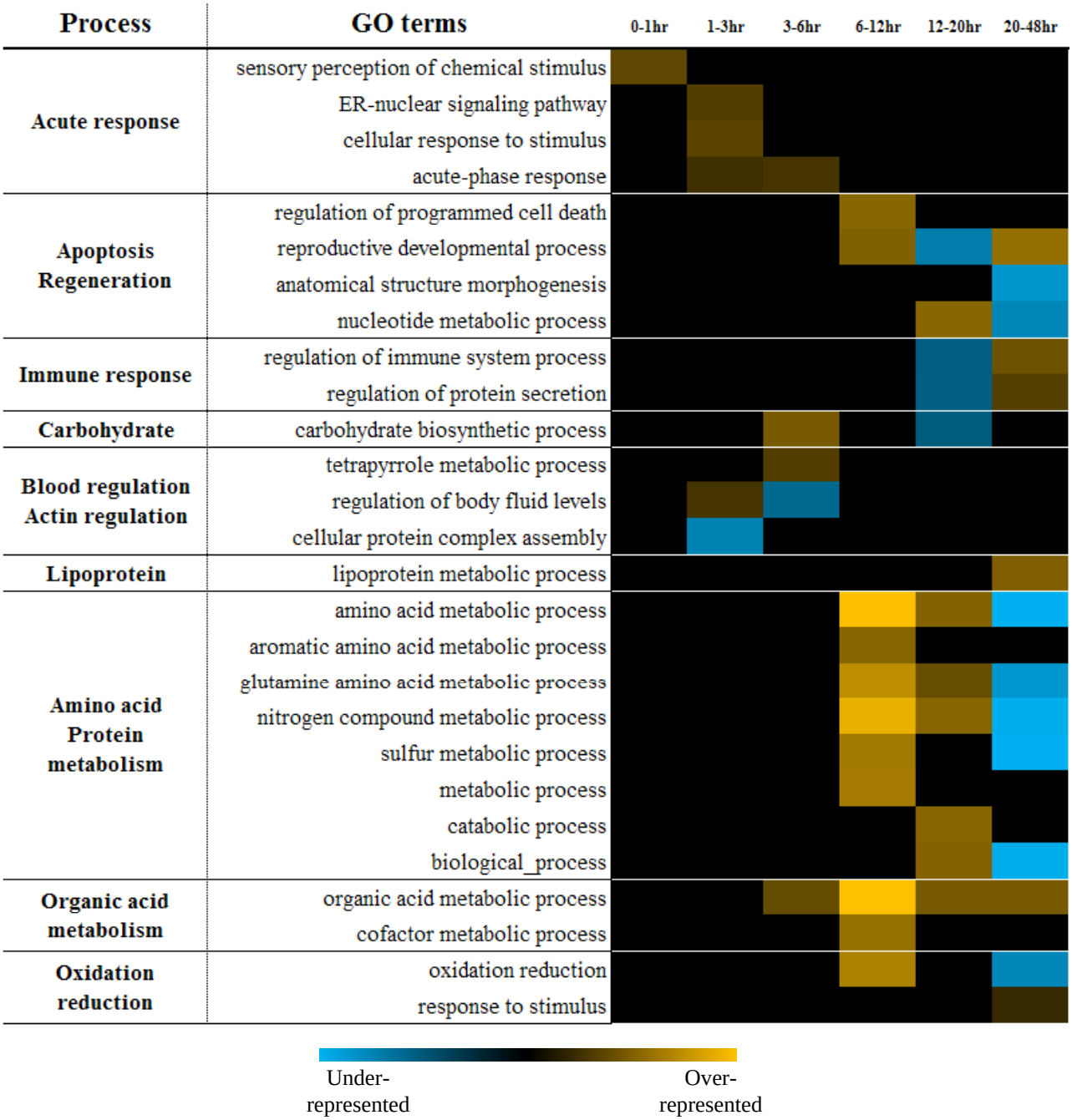
Process
GO terms
0-1hr
1-3hr
3-6hr
6-12hr
12-20hr
20-48hr
Acute response
sensory perception of chemical stimulus
ER-nuclear signaling pathway
cellular response to stimulus
acute-phase response
Apoptosis
Regeneration
regulation of programmed cell death
reproductive developmental process
anatomical structure morphogenesis
nucleotide metabolic process
Immune response
regulation of immune system process
regulation of protein secretion
Carbohydrate
carbohydrate biosynthetic process
Blood regulation
Actin regulation
tetrapyrrole metabolic process
regulation of body fluid levels
cellular protein complex assembly
Lipoprotein
lipoprotein metabolic process
Amino acid
Protein
metabolism
amino acid metabolic process
aromatic amino acid metabolic process
glutamine amino acid metabolic process
nitrogen compound metabolic process
sulfur metabolic process
metabolic process
catabolic process
biological_process
Organic acid
metabolism
organic acid metabolic process
cofactor metabolic process
Oxidation
reduction
oxidation reduction
response to stimulus
Under-
represented
Over-
represented

Figure 5

a)

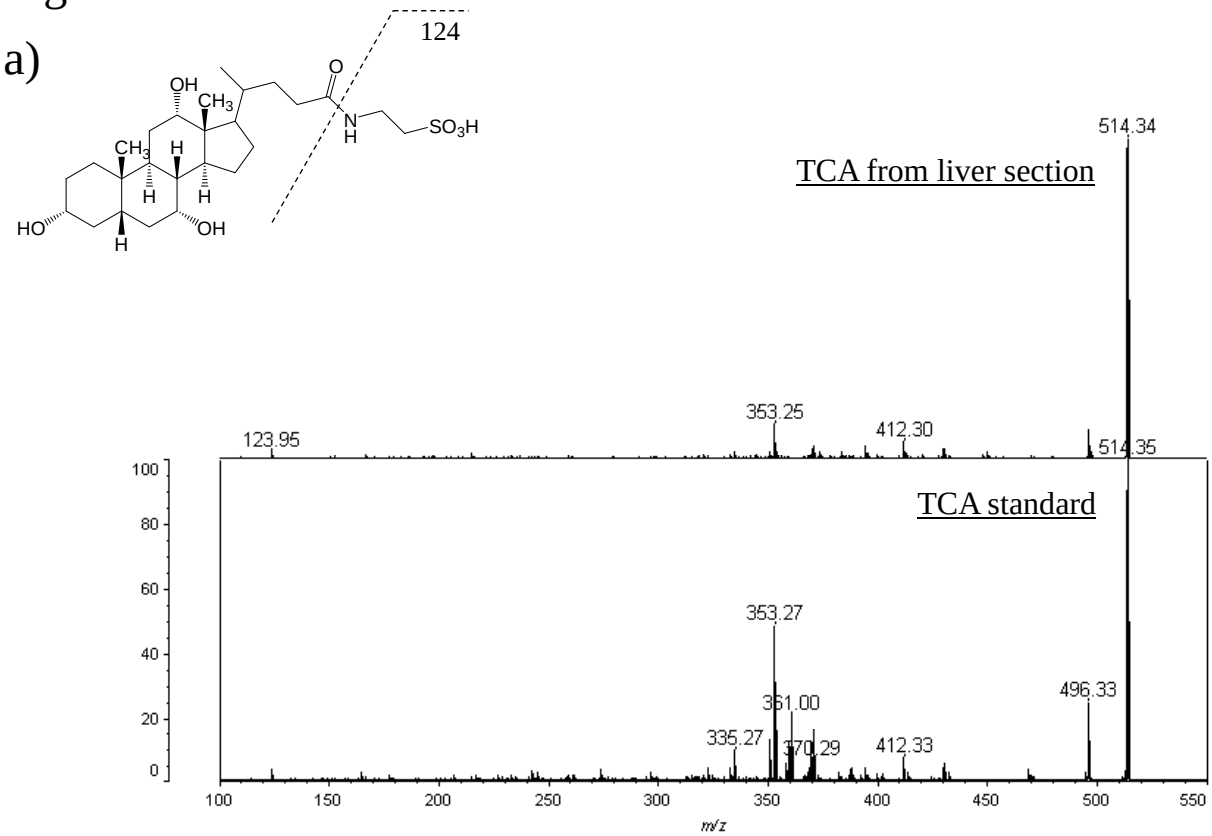
124
TCA from liver section
514.34
353.25
412.30
123.95
514.35
TCA standard
353.27
361.00
496.33
335.27
370.29
412.33
m/z

b)

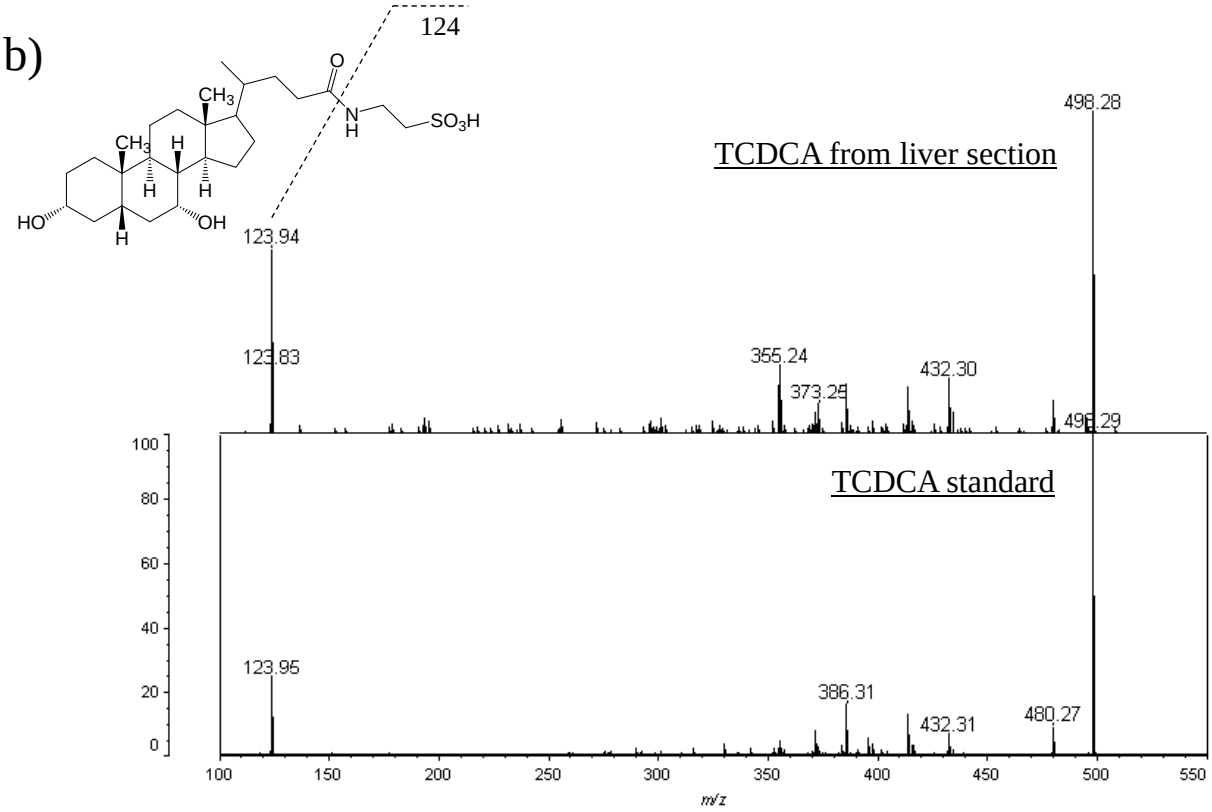
124
TCDCA from liver section
498.28
123.94
123.83
355.24
373.25
432.30
TCDCA standard
123.95
386.31
432.31
480.27
m/z

Figure 6

a)

[TCA, 0 h]

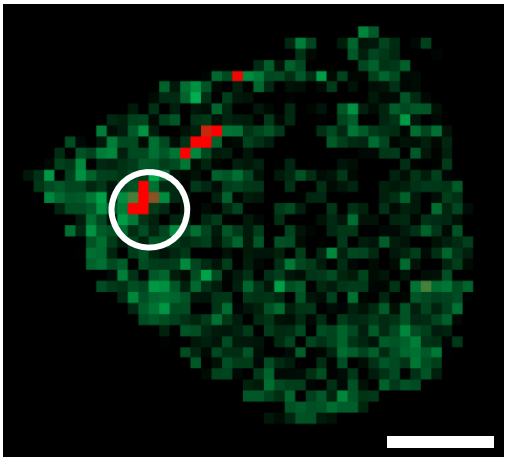

[TCDCA, 0 h]

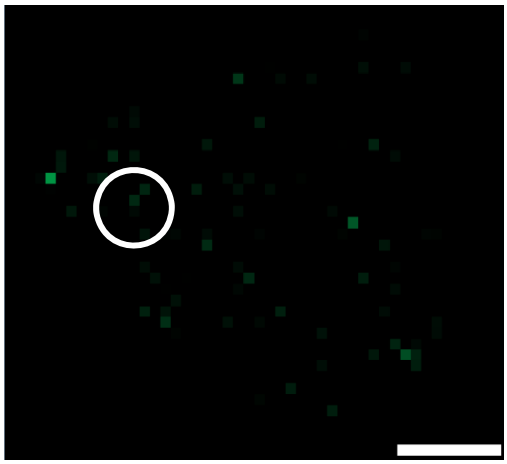

[HE, 0 h]

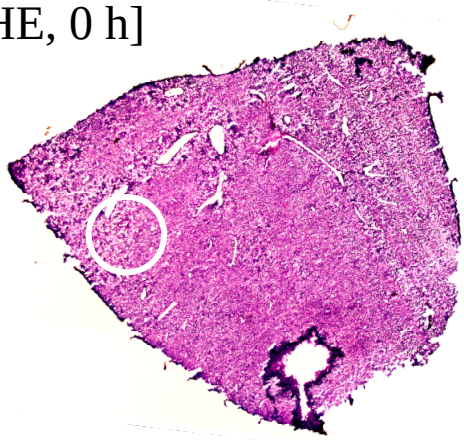

[HE, 0 h, circled]

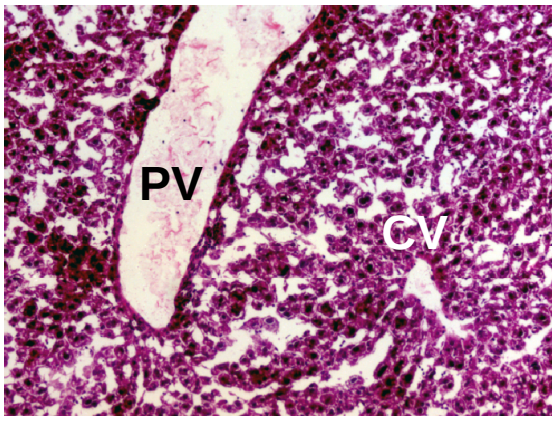

[IMS image, 0 h]

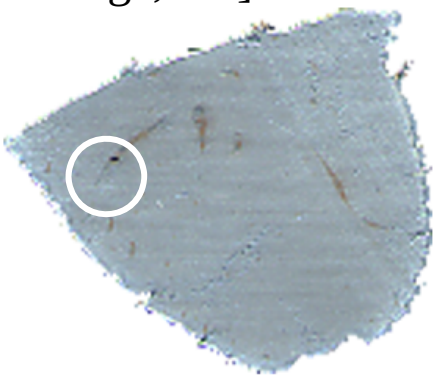

Figure 6

b)

[TCA, 3 h]

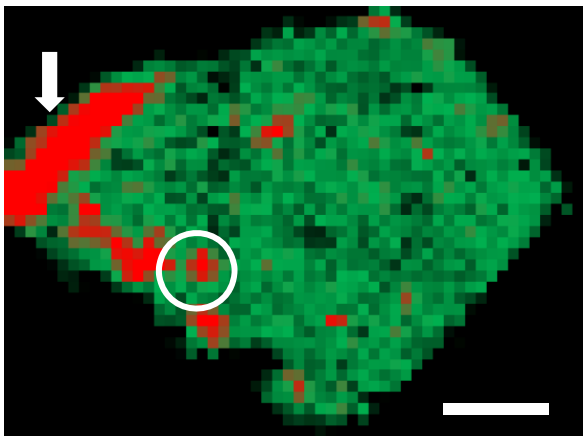

[TCDCA, 3 h]

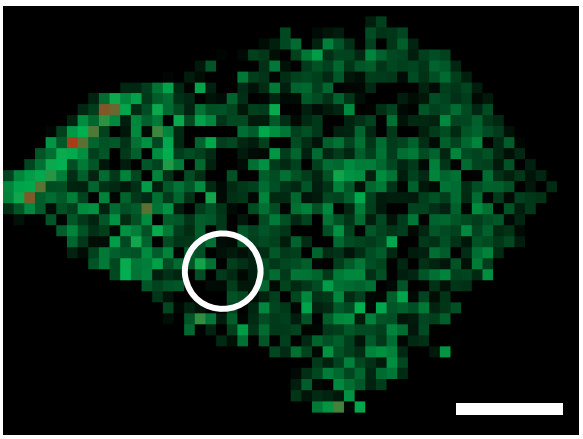

[HE, 3 h]

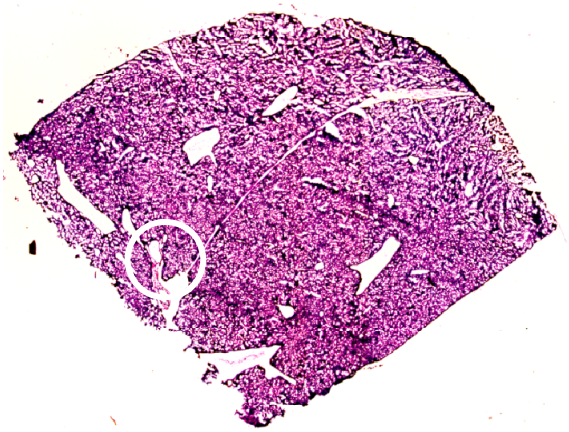

[HE, 3 h, circled]

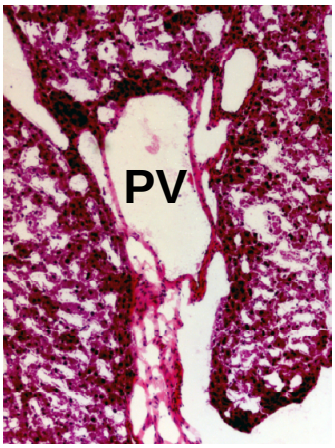

[IMS image, 3 h]

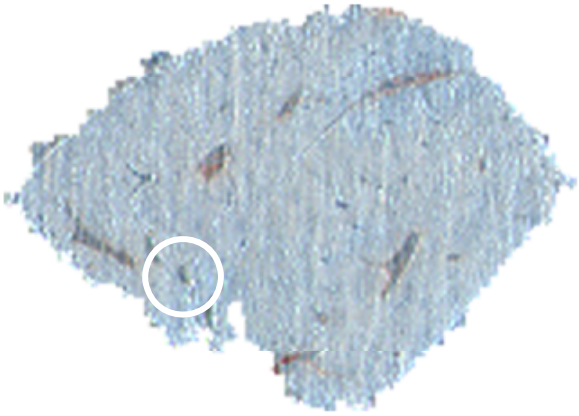

Figure 6

c)

[TCA, 6 h]

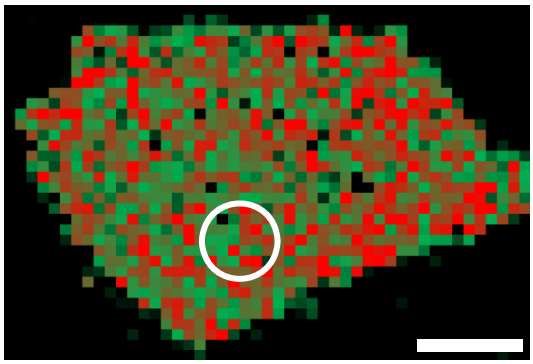

[TCDCA, 6 h]

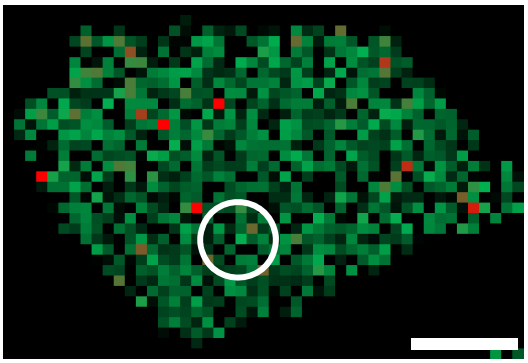

[HE, 6 h]

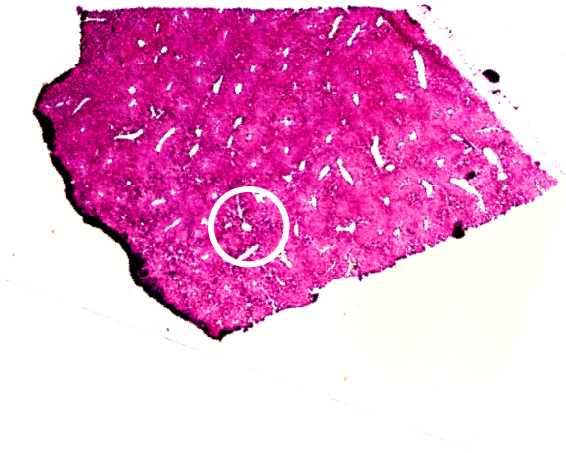

[HE, 6 h, circled]

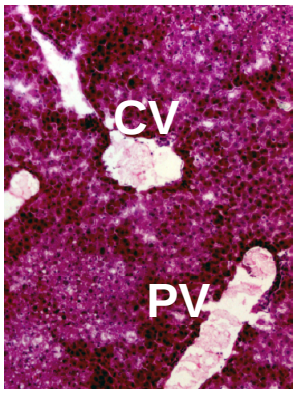

[IMS image, 6h]

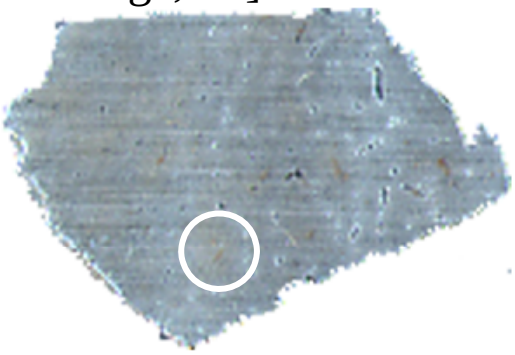

Figure 6

d) [TCA, 20 h] [TCDCA, 20 h]

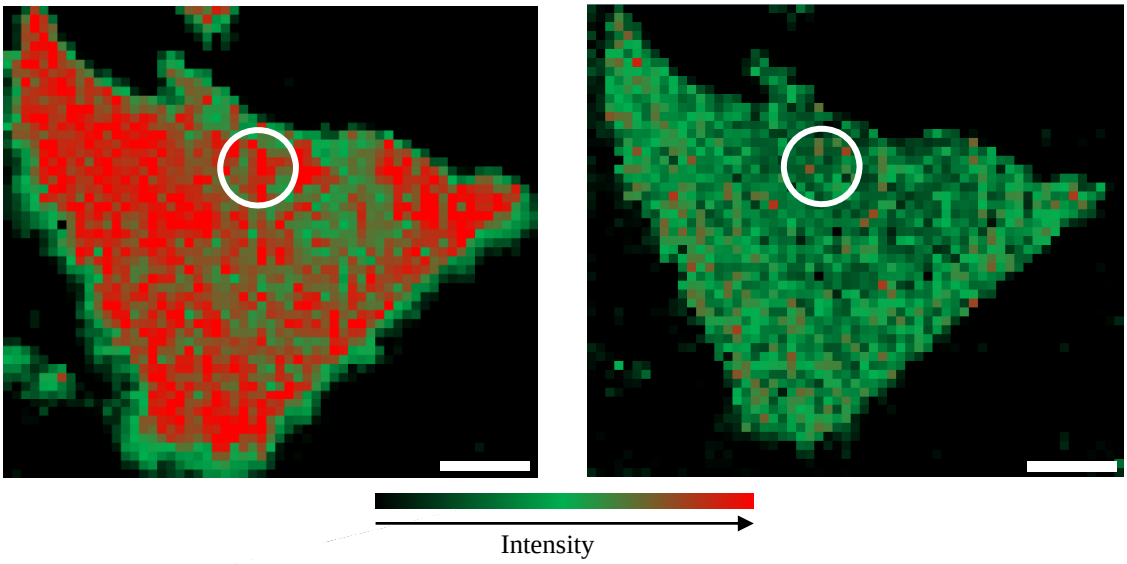

[HE, 20 h] [HE, 20 h, circled]

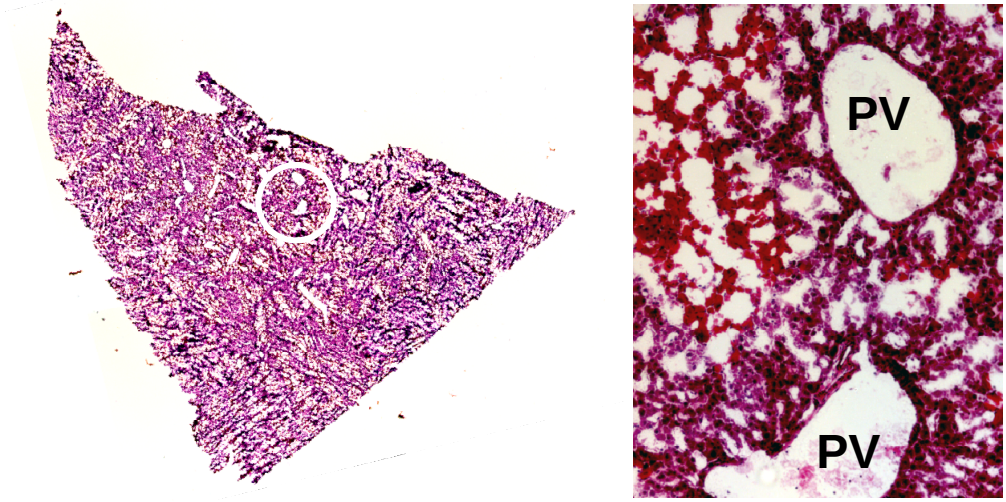

[IMS image, 20 h]

Supporting information

Supplementary figure 1. Chemical structure of bile acids and other reagents for MS.

Six bile acid standard of a) GCA (glycocholic acid, MW = 465.62), b) GCDCA (glycochenodeoxycholic acid, MW = 449.62), c) GLCA (glycolithocholic acid, MW = 433.62), d) TCA (taurocholic acid, MW = 515.70), e) TCDCA (taurochenodeoxycholic acid, MW = 499.70) and f) TLCA (taurolithocholic acid, MW = 483.71) are shown. g) NPA (N-1-naphthylphthalamic acid, MW = 291.30) is used as internal standard of SPE-MALDI-TOF MS analysis. h) 9-AA (9-aminoacridine, MW = 194.23) is as MALDI matrix for bile acid detection.

Supplementary figure 2. Calibration curve of six bile acids.

Bile acid calibration curve are shown. Upper panel is of GCA (solid), GCDCA (dotted), GLCA (wide dotted), and lower of TCA (solid), TCDCA (dotted) and TLCA (wide dotted). Each bile acid calibration curve is on secondary function with $R^2 > 0.99$, possibly because of correlation with abundance of sample and ionizing acceleration by local heat generation by laser irradiation:

GCA; $Y = 0.1141\ X^{0.5216}$ ($R^2 = 0.998$),

GCDCA; $Y = 0.1162\ X^{0.4957}$ ($R^2 = 0.996$),

GLCA; $Y = 0.1118\ X^{0.492}$ ($R^2 = 0.992$),

TCA; $Y = 0.8405\ X^{0.6713}$ ($R^2 = 0.998$),

TCDCA; $Y = 0.8564\ X^{0.6676}$ ($R^2 = 0.999$),

TLCA; $Y = 0.7646\ X^{0.6776}$ ($R^2 = 0.997$).

Supplementary figure 3. Representative SPE-MALDI-TOF MS spectra from serum bile acids.

Raw MS spectra of serum bile acid profile are shown in this figure from 0 to 48 h after a) CCl_4 i.p. and b) mineral oil i.p. control. Significant change of MS signal from TCA (m/z 514.3) and small change of TCDCA was obtained in CCl_4 i.p. group, but no change was observed in control. MS signal of m/z 290.1 was from internal standard of NPA.

Supplementary figure 4. Representative images of time-dependent serum proteome on CBB G250-stained 2D-PAGE gel.

Collected serum at each time point was developed on 1st dimensional IEF of pH 3-10 and 2nd dimensional 10-16% SDS-PAGE. All gels were visualized by high-sensitive CBB G-250 staining solution. a) Control group (6 samples) and b) CCl_4 administration group (7 samples).

Supplementary figure 5. Pattern analysis of structural isomers of TCA by MS/MS.

From the bottom, TCA, Taurohyocholic acid (THCA) and Tauro-α-muricholic acid (TAMCA) were indicated. Structural isomers of TCA, Taurohyocholic acid and Tauro-α-muricholic acid, were analyzed by MS/MS fragment assignment using AXIMA QIT. MS/MS fragment peaks were indicated the individual patterns of each molecule by the vicinal hydroxyl group direction. Major and secondary fragment peak pattern suggested that MS/MS peaks on liver tissue were possible to TCA, not to other structural isomers.

Supplementary figure 6. MS spectra of TCA and other metabolite profile on liver section.

Major MS spectra of TCA, UDP-N-acetyl glucosamine (UDP-N-AG) and phosphatidylethanolamine (PEs) were obtained from liver section at 0, 6, 12 and 20 h. At 12 h, ionization suppression effect occurred by large amount of signals such as m/z 762 possibly from PEs, for example appeared on surface of the liver reflecting massive necrosis.

Supplementary figure 7. Time-dependent semi-quantitative profile of bile acids on liver section for challenging quantitative analysis on imaging mass spectrometry.

In order to evaluate the peak intensity for six bile acids at each time point, direct measurement was performed for eight matrix deposits onto each liver section. Matrix solution was micro dispensed using CHIP-1000 as described in manuscript. Eight deposit areas of m/z 514 and m/z 498 with 25% trim-mean were normalized by a peak area of NPA in same spectrum. TCA and TCDCA profile on liver section were shown at 0, 1, 3, 6, 12, 20, 48 h after CCl_4 administration.

* Significant change from previous time point of each group ($p < 0.05$)

Supplementary figure 1

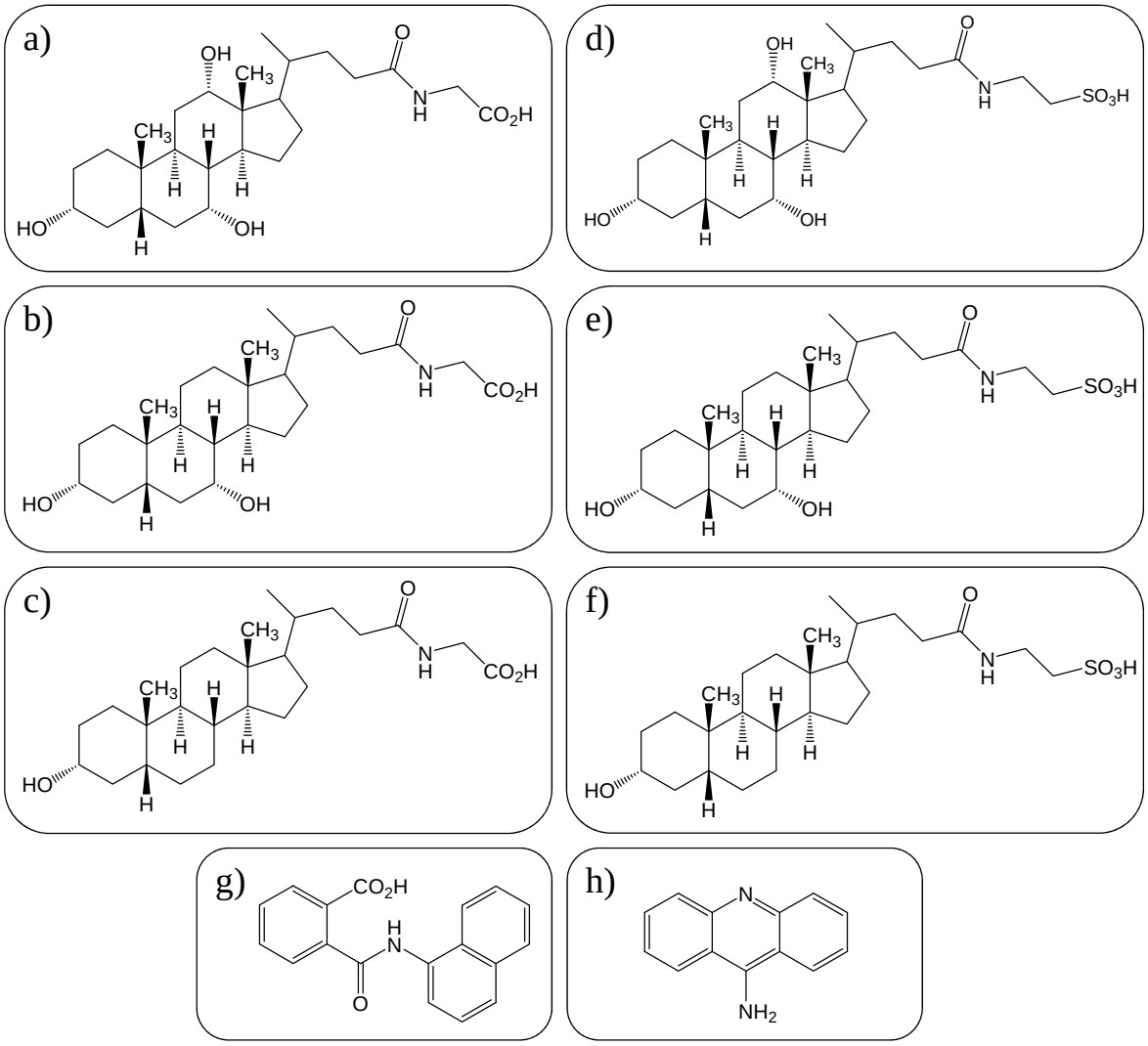

Supplementary figure 2

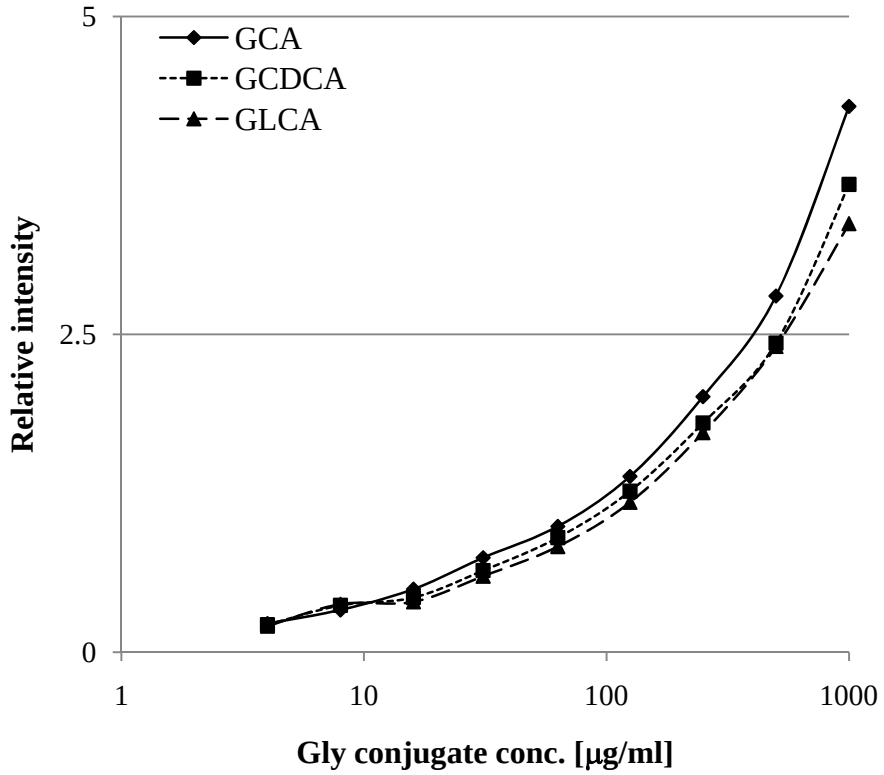

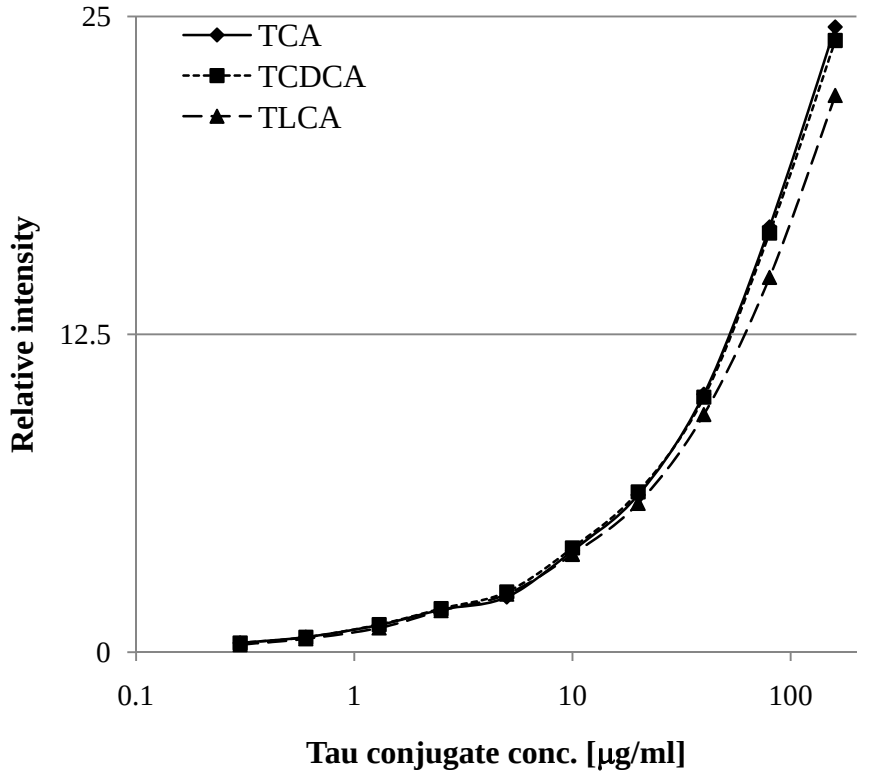

Supplementary figure 3

a)

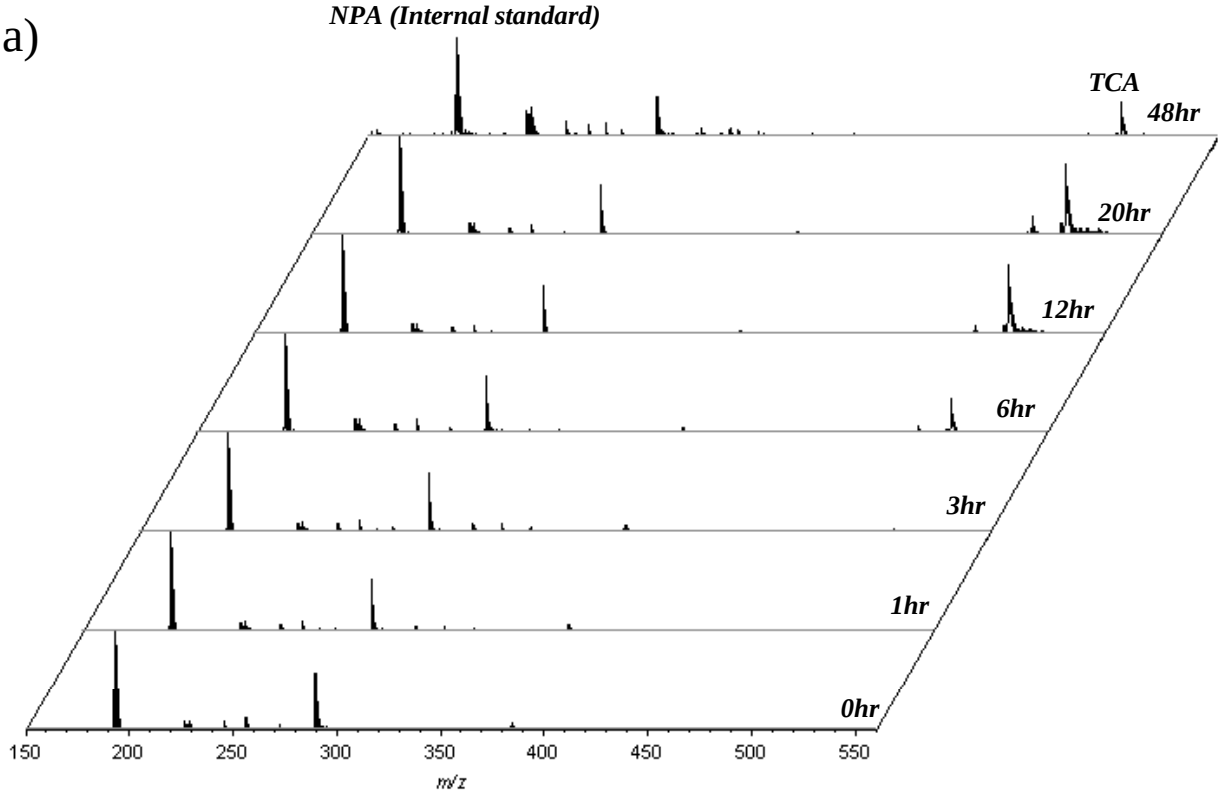

b)

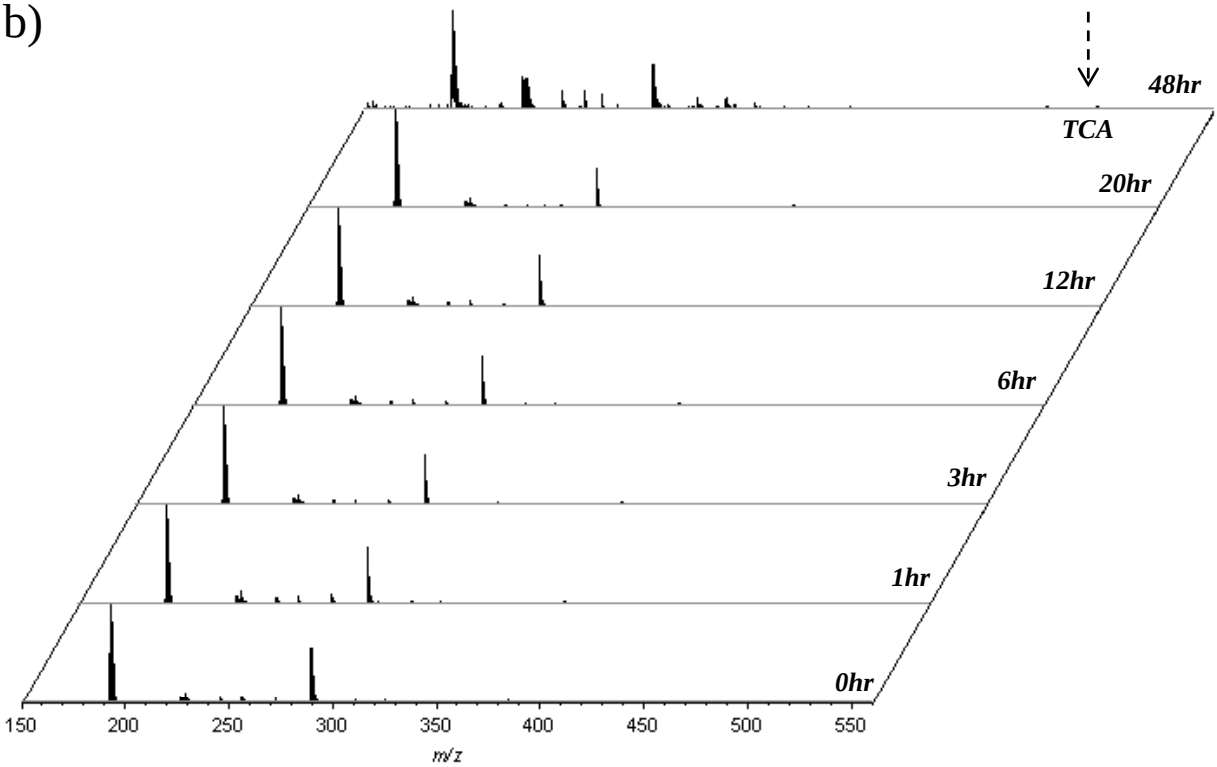

Supplementary figure 4

a)

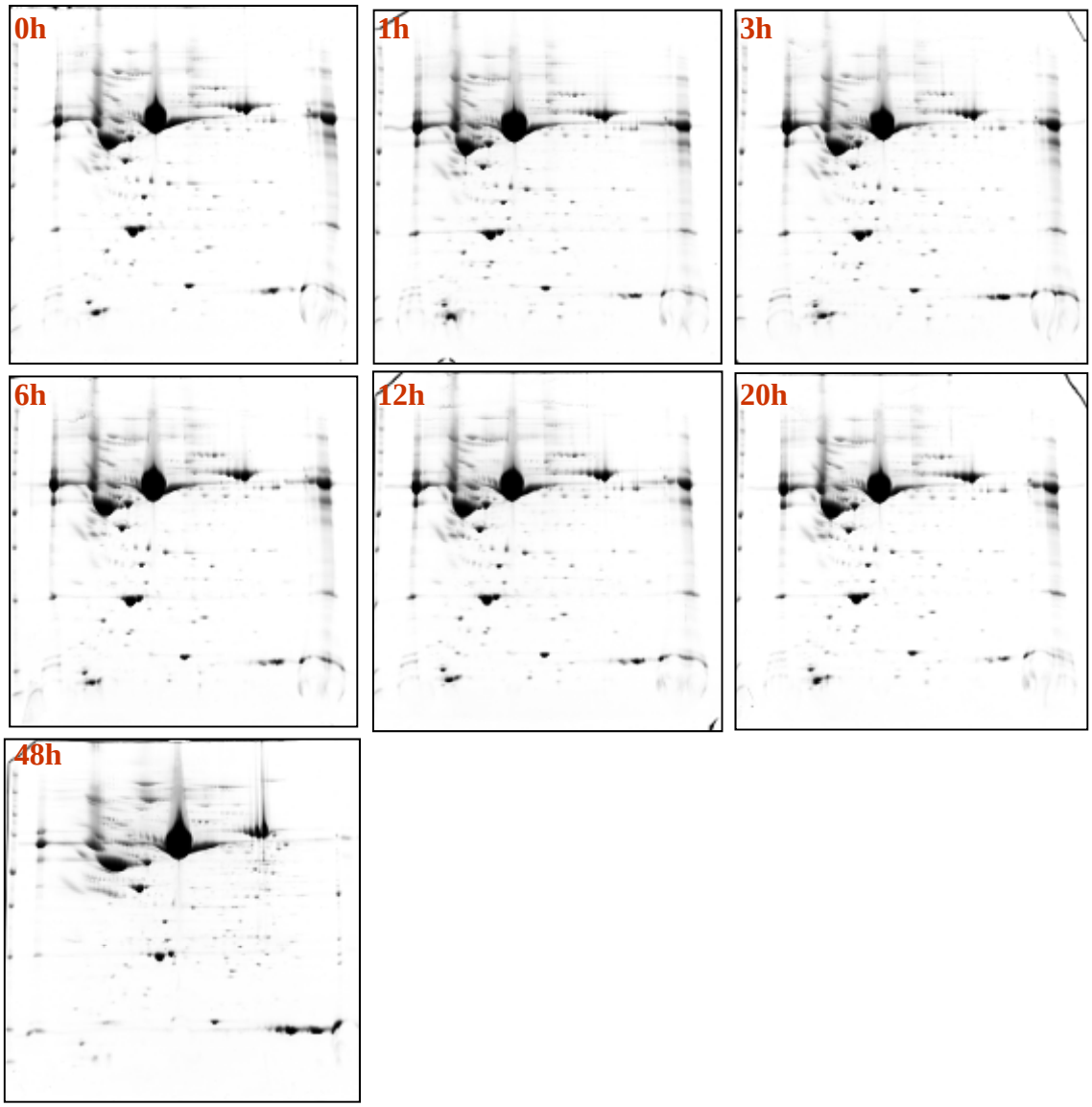

Supplementary figure 4

b)

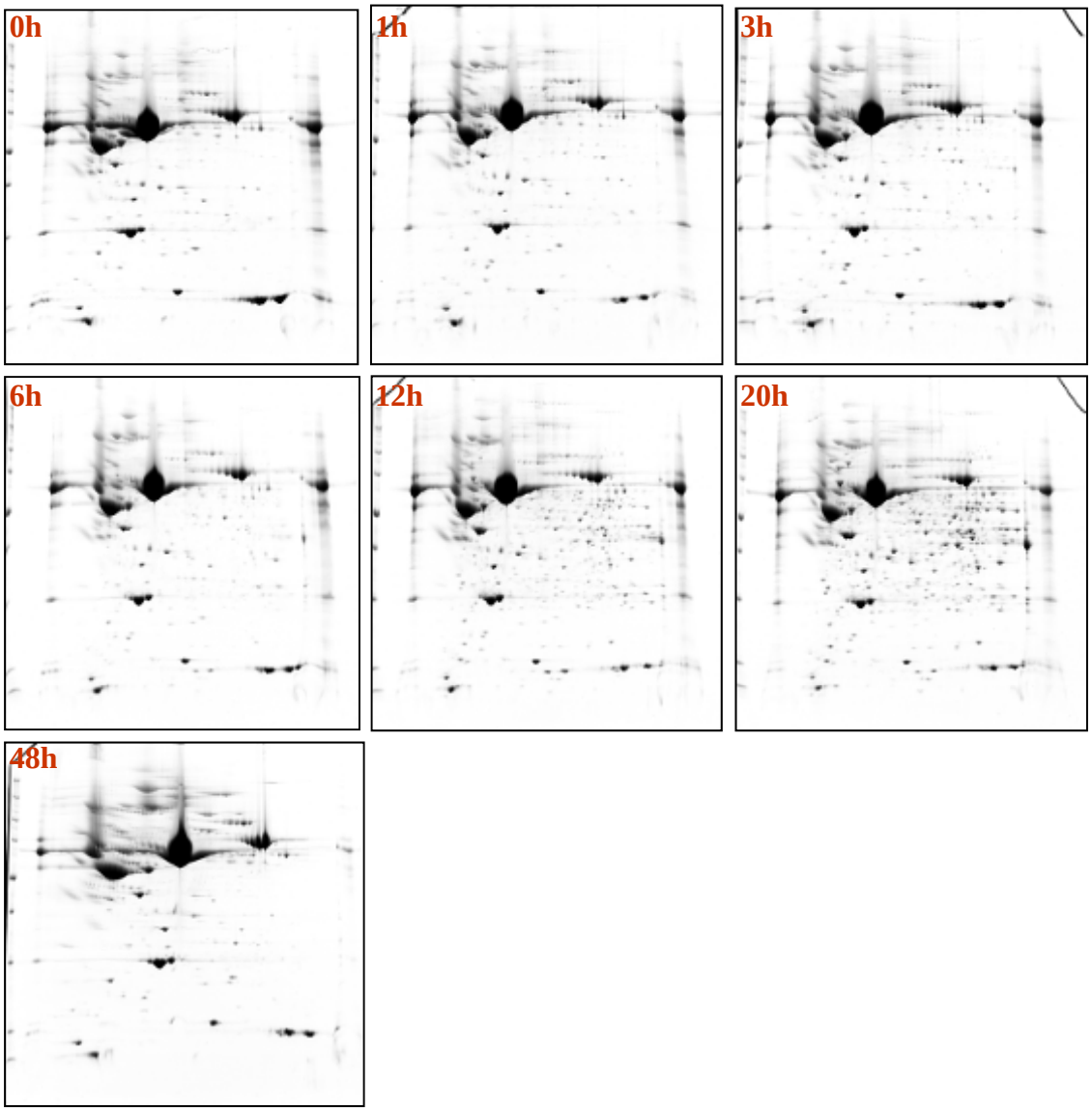

Supplementary figure 5

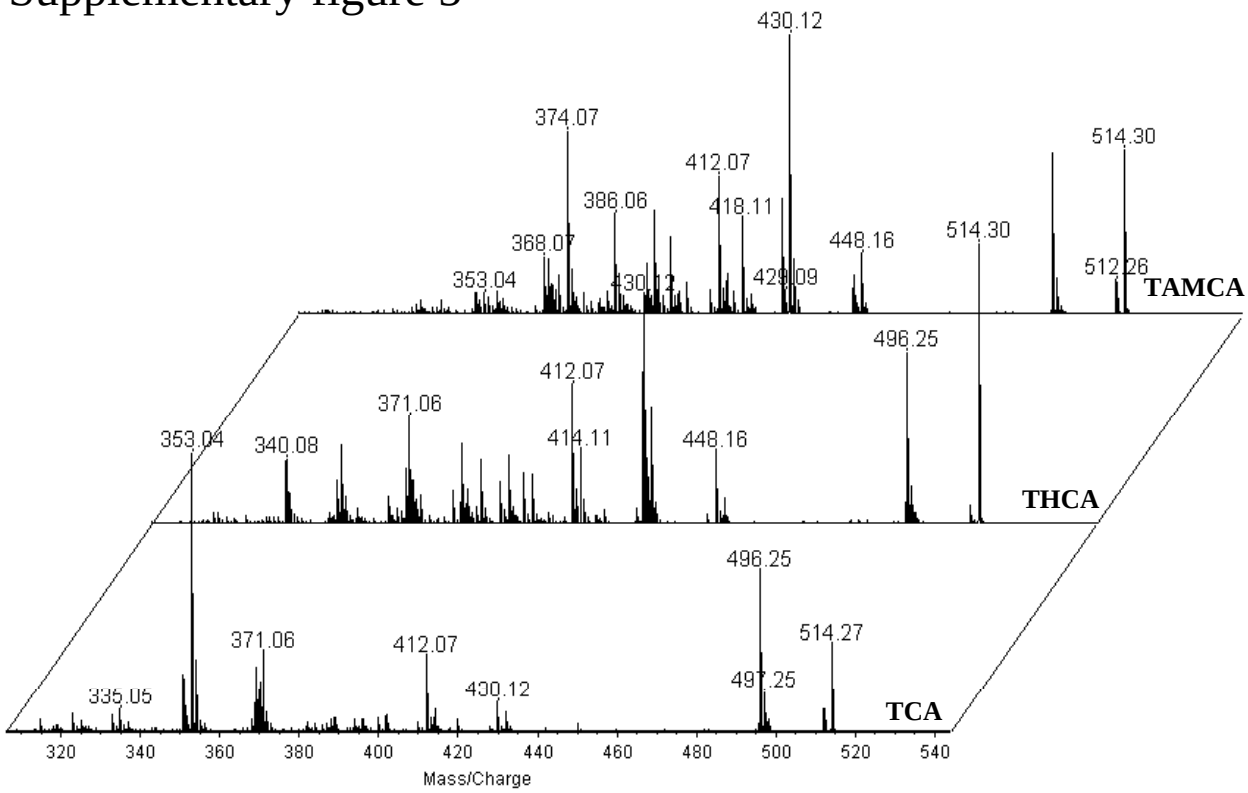

Supplementary figure 6

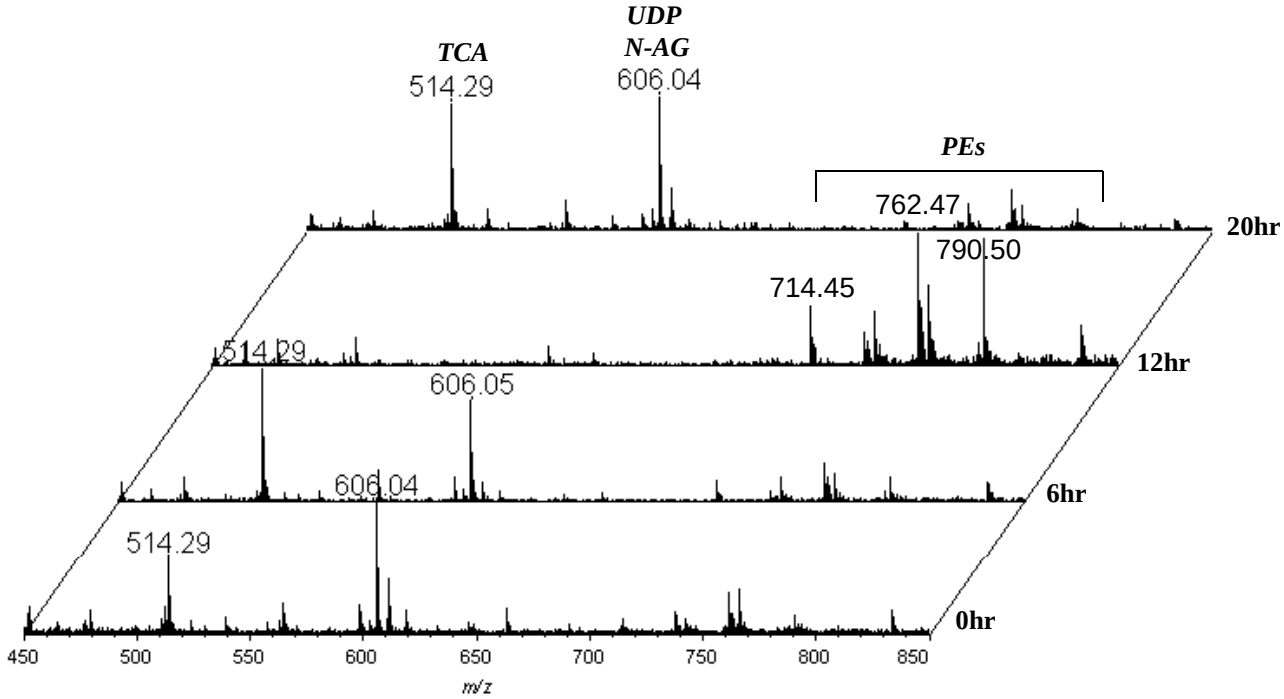

Supplementary figure 7

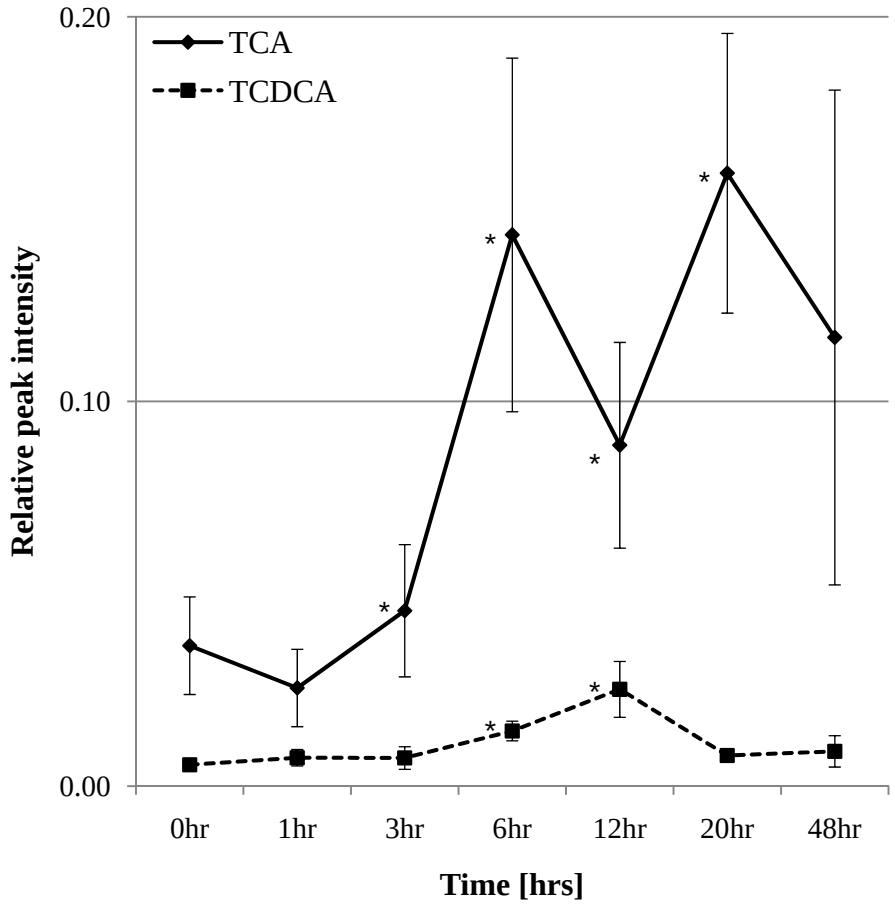

Supplementary table 1a. Identified protein list with up-regulated in serum

Lists of idenrified protein informations

Time point [hr]; comparative time point of proteome change
SSP on 2D gel; protein spot number on 2D gel assigned by PDQuest
Fold change; fold change of protein spot quantity calculated by GeneSpring GX
Gene symbol; gene symbol
Accession; accession number of UniProt database
UP ID; UniProt database ID
Protein name; common protein name
Calculated mass; molecular weight calculated by amino acid sequence
MOWSE score; MOWSE score of Mascot search results
pI on 2D gel; protein pI value calculated by PDQuest
Mr on 2D gel; mobility shift on 2D-PAGE gel calculated by PDQuest
Sequence coverage %; matched peptide sequence coverage
Matched/Searched peptides; matched peptide number / searched peptide number on Mascot search

Time point [hr]	SSP on 2D gel	Fold change	Gene symbol	Accession	UP ID	Protein name	Calculated mass	MOWSE score	pI on 2D gel	Mr on 2d gel	Sequence coverage %	Matched/ Searched peptides
([01hr] vs [00hr])	SSP 2013	5.27	OBP2A	OBP2A_HUMAN	Q9NY56	odorant binding protein Ia	17044	173	5.2	16773	74	14/50
([03hr] vs [01hr])	SSP 2506	13.65	Hspa5	GRP78_MOUSE	P20029	78 kDa glucose-regulated protein precursor	72492	323	5.1	72300	54	39/65
	SSP 3303	7.11	Fgb	FIBB_MOUSE	Q8K0E8	Fibrinogen beta chain precursor [Contains: Fibrinopeptide B]	55402	219	6.7	40984	49	29/47
	SSP 5005	10.95	Saa2	SAA2_MOUSE	P05367	Serum amyloid A-2 protein precursor [Contains: Amyloid protein A	13728	127	6.4	13518	63	10/29
	SSP 7108	5.88	Psma2	PSA2_MOUSE	P49722	Proteasome subunit alpha type-2	26023	191	8.4	24319	58	13/36
	SSP 8327	11.38	Aldoa	ALDOA_MOUSE	P05064	Fructose-bisphosphate aldolase A	39787	92	8.5	39600	40	14/71
([06hr] vs [03hr])	SSP 4207	8.92	Fbp1	F16P1_MOUSE	Q9QXD6	Fructose-1,6-bisphosphatase 1	37288	250	6.2	36443	65	25/56
	SSP 5005	20.29	Saa2	SAA2_MOUSE	P05367	Serum amyloid A-2 protein precursor [Contains: Amyloid protein A	13728	127	6.4	13518	63	10/29
	SSP 5214	10.47	Alad	HEM2_MOUSE	P10518	Delta-aminolevulinic acid dehydratase	36456	201	6.3	35400	52	24/62
	SSP 7206	4.12	Gpd1	GPDA_MOUSE	P13707	Glycerol-3-phosphate dehydrogenase [NAD+], cytoplasmic	38176	268	6.8	32375	67	28/57
	SSP 7307	7.13	Idh1	IDHC_MOUSE	O88844	Isocitrate dehydrogenase [NADP] cytoplasmic	47030	215	6.5	44280	60	27/52
	SSP 7310	5.06	Fah	FAAA_MOUSE	P35505	Fumarylacetoacetase	46416	208	6.9	41082	62	27/65
([12hr] vs [06hr])	SSP 1010	53.95	Cyb5a	CYB5_MOUSE	P56395	Cytochrome b5	15232	82	5.0	17500	52	6/37
	SSP 1103	13.39	Ywhae	1433E_MOUSE	P62259	14-3-3 protein epsilon	29326	143	4.6	29300	63	20/68
	SSP 1104	10.65	Psma5	PSA5_MOUSE	Q9Z2U1	Proteasome subunit alpha type-5	26565	151	4.7	26400	63	16/36

Time point [hr]	SSP on 2D gel	Fold change	Gene symbol	Accession	UP ID	Protein name	Calculated mass	MOWSE score	pI on 2D gel	Mr on 2d gel	Sequence coverage %	Matched/ Searched peptides
	SSP 2004	18.82	Prdx2	PRDX2_MOUSE	Q61171	Peroxiredoxin-2	21936	126	5.2	22071	51	10/73
	SSP 2106	17.13	Glo1	LGUL_MOUSE	Q9CPU0	Lactoylglutathione lyase	20967	143	5.2	23562	51	11/32
	SSP 2110	20.78	Pbld2	PBLD2_MOUSE	Q9CXN7	Phenazine biosynthesis-like domain-containing protein 2	32191	219	5.2	30491	56	20/43
	SSP 2204	21.66	Rgn	RGN_MOUSE	Q64374	Regucalcin	33899	209	5.2	33846	70	21/45
	SSP 2211	4.05	Apoe	APOE_MOUSE	P08226	Apolipoprotein E precursor	35901	135	5.6	32811	32	15/32
	SSP 2307	23.40	Hp	HPT_MOUSE	Q61646	Haptoglobin precursor [Contains: Haptoglobin alpha chain; Haptoglobin beta chain]	39241	120	5.9	39222	36	16/51
	SSP 2312	1.87	Actb	ACTB_MOUSE	P60710	Actin, cytoplasmic 1	42052	103	5.3	42800	39	14/55
	SSP 3009	5.01	Ftl1	FRIL1_MOUSE	P29391	Ferritin light chain 1	20846	196	5.7	22411	73	15/52
	SSP 3101	8.52	Gclm	GSH0_MOUSE	O09172	Glutamate--cysteine ligase regulatory subunit	30858	125	5.4	27851	40	12/30
	SSP 3105	8.00	Psme2	PSME2_MOUSE	P97372	Proteasome activator complex subunit 2	27268	151	5.5	28733	55	16/55
	SSP 3119	5.35	Psme1	PSME1_MOUSE	P97371	Proteasome activator complex subunit 1	28826	221	5.7	28445	69	21/44
	SSP 3201	14.30	Ppa1	IPYR_MOUSE	Q9D819	Inorganic pyrophosphatase	33102	149	5.4	34419	49	15/49
	SSP 3229	26.56	Khk	KHK_MOUSE	P97328	Ketohexokinase	33300	104	5.8	30972	41	10/27
	SSP 3303	7.59	Fgb	FIBB_MOUSE	Q8K0E8	Fibrinogen beta chain precursor [Contains: Fibrinopeptide B]	55402	219	6.7	40984	46	29/47
	SSP 4101	29.61	Np	PNPH_MOUSE	P23492	Purine nucleoside phosphorylase	32541	209	5.8	29264	58	26/53
	SSP 4106	6.92	Hyi	HYI_MOUSE	Q8R1F5	Putative hydroxypyruvate isomerase	30544	103	6.0	27713	53	13/63
	SSP 4113	10.24	Psmb7	PSB7_MOUSE	P70195	Proteasome subunit beta type-7 precursor	30214	131	8.1	27490	35	15/42
	SSP 4207	10.66	Fbp1	F16P1_MOUSE	Q9QXD6	Fructose-1,6-bisphosphatase 1	37288	250	6.2	36443	65	25/56
	SSP 4301	14.66	Adk	ADK_MOUSE	P55264	Adenosine kinase	40466	170	5.8	44522	50	16/43
	SSP 4313	9.37	Ttc38	TTC38_MOUSE	A3KMP2	UPF0530 protein	52703	228	5.9	47142	57	28/45
	SSP 4314	11.86	Tcn2	TCO2_MOUSE	O88968	Transcobalamin-2 precursor	48012	145	5.9	42240	45	14/47
	SSP 4407	7.98	Shpk	SHPK_MOUSE	Q9D5J6	Sedoheptulokinase	51783	211	5.8	47535	56	23/58
	SSP 4411	27.15	Selenbp1	SBP1_MOUSE	P17563	Selenium-binding protein 1	53051	240	5.9	53140	68	29/74
	SSP 4414	10.32	Gdi2	GDIB_MOUSE	Q61598	Rab GDP dissociation inhibitor beta	51018	305	5.9	47525	71	32/53
	SSP 4420	29.45	Naprt1	PNCB_MOUSE	Q8CC86	Nicotinate phosphoribosyltransferase	58799	240	6.1	54986	51	23/45
	SSP 4421	6.74	Csad	CSAD_MOUSE	Q9DBE0	Cysteine sulfinic acid decarboxylase	55737	235	6.2	51813	49	27/57
	SSP 5001	12.26	Sod1	SODC_MOUSE	P08228	Superoxide dismutase [Cu-Zn]	16104	78	6.0	17327	44	7/32

Time point [hr]	SSP on 2D gel	Fold change	Gene symbol	Accession	UP ID	Protein name	Calculated mass	MOWSE score	pI on 2D gel	Mr on 2d gel	Sequence coverage %	Matched/ Searched peptides
	SSP 5109	5.00	Prdx6	PRDX6_MOUSE	O08709	Peroxiredoxin-6	24969	229	5.7	25091	79	20/61
	SSP 5210	11.80	Qprt	NADC_MOUSE	Q91X91	Nicotinate-nucleotide pyrophosphorylase [carboxylating]	31852	180	6.2	34101	47	14/27
	SSP 5214	7.15	Alad	HEM2_MOUSE	P10518	Delta-aminolevulinic acid dehydratase	36456	201	6.3	35400	52	24/62
	SSP 5307	22.75	Ahcy	SAHH_MOUSE	P50247	Adenosylhomocysteinase	48170	287	6.1	43864	67	35/71
	SSP 5311	9.62	Arg1	ARGI1_MOUSE	Q61176	Arginase-1	34957	129	6.5	39806	58	16/52
	SSP 5401	67.38	Aldh7a1	AL7A1_MOUSE	Q9DBF1	Alpha-aminoadipic semialdehyde dehydrogenase	56066	254	6.0	52967	48	25/64
	SSP 5405	13.37	Eno1	ENOA_MOUSE	P17182	Alpha-enolase	47453	271	6.4	47679	71	30/62
	SSP 5408	100.46	Csad	CSAD_MOUSE	Q9DBE0	Cysteine sulfinic acid decarboxylase	55737	253	6.2	51636	52	32/71
	SSP 5412	16.02	Naprt1	PNCB_MOUSE	Q8CC86	Nicotinate phosphoribosyltransferase	58799	208	6.1	54912	47	21/42
	SSP 5413	35.71	Gpt	ALAT1_MOUSE	Q8QZR5	Alanine aminotransferase 1	55905	186	6.2	51137	50	27/68
	SSP 5415	9.93	Ces3	CES3_MOUSE	Q8VCT4	Carboxylesterase 3 precursor	62034	191	6.2	57863	50	26/67
	SSP 6002	49.87	Gpx1	GPX1_MOUSE	P11352	Glutathione peroxidase 1	22544	130	6.7	22950	65	11/32
	SSP 6005	12.77	Psmb2	PSB2_MOUSE	Q9R1P3	Proteasome subunit beta type-2	23063	170	6.5	22552	58	13/47
	SSP 6007	5.63	Nme1	NDKA_MOUSE	P15532	Nucleoside diphosphate kinase A	17311	161	6.8	17389	76	14/36
	SSP 6102	18.89	Gstz1	MAAI_MOUSE	Q9WVL0	Maleylacetoacetate isomerase	24431	138	7.7	24696	61	12/31
	SSP 6108	8.34	Pgam1	PGAM1_MOUSE	Q9DBJ1	Phosphoglycerate mutase 1	28928	158	6.7	26833	72	17/59
	SSP 6110	14.63	Nqo2	NQO2_MOUSE	Q9JI75	Ribosyldihydronicotinamide dehydrogenase [quinone]	26459	142	6.5	25298	62	114/49
	SSP 6112	19.62	PTPN20A	PTN20_HUMAN	Q4JDL3	protein tyrosine phosphatase, non-receptor type 20 isoform 5	26756	66	6.6	24899	34	9/38
	SSP 6116	5.60	Aspdh	ASPD_MOUSE	Q9DCQ2	Putative L-aspartate dehydrogenase	30479	221	6.5	29457	64	19/44
	SSP 6118	10.05	Gstp1	GSTP1_MOUSE	P19157	Glutathione S-transferase P 1	23765	95	7.7	23746	54	10/42
	SSP 6122	11.40	Gsta4	GSTA4_MOUSE	P24472	Glutathione S-transferase A4	25547	82	6.8	23854	47	12/47
	SSP 6202	24.30	Taldo1	TALDO_MOUSE	Q93092	Transaldolase	37534	134	6.6	37203	40	18/43
	SSP 6204	15.76	Alad	HEM2_MOUSE	P10518	Delta-aminolevulinic acid dehydratase	36456	209	6.3	35574	53	22/54
	SSP 6209	4.36	Arg1	ARGI1_MOUSE	Q61176	Arginase-1	34957	178	6.5	37714	63	18/47
	SSP 6211	4.95	Gnmt	GNMT_MOUSE	Q9QXF8	Glycine N-methyltransferase	33110	110	7.1	32520	40	10/29
	SSP 6215	32.19	Grhpr	GRHPR_MOUSE	Q91Z53	Glyoxylate reductase/hydroxypyruvate reductase	35706	210	7.6	33671	54	20/47
	SSP 6220	7.74	Ldha	LDHA_MOUSE	P06151	L-lactate dehydrogenase A chain	36817	239	7.6	33611	64	23/47
	SSP 6223	54.65	Arg1	ARGI1_MOUSE	Q61176	Arginase-1	34957	166	6.5	37513	57	18/51

Time point [hr]	SSP on 2D gel	Fold change	Gene symbol	Accession	UP ID	Protein name	Calculated mass	MOWSE score	pI on 2D gel	Mr on 2d gel	Sequence coverage %	Matched/ Searched peptides
	SSP 6301	8.59	Ahcy	SAHH_MOUSE	P50247	Adenosylhomocysteinase	48170	130	6.1	44156	45	21/71
	SSP 6303	4.64	Upb1	BUP1_MOUSE	Q8VC97	Beta-ureidopropionase	44479	218	6.3	43021	45	21/43
	SSP 6304	5.11	Idh1	IDHC_MOUSE	O88844	Isocitrate dehydrogenase [NADP] cytoplasmic	47030	184	6.5	44664	49	19/37
	SSP 6306	58.75	Sord	DHSO_MOUSE	Q64442	Sorbitol dehydrogenase	38795	172	6.6	38902	64	18/50
	SSP 6309	19.83	Upb1	BUP1_MOUSE	Q8VC97	Beta-ureidopropionase	44479	266	6.3	42686	53	24/52
	SSP 6310	9.19	Fah	FAAA_MOUSE	P35505	Fumarylacetoacetase	46416	194	6.9	41553	54	23/50
	SSP 6312	8.16	Ccbl1	KAT1_MOUSE	Q8BTY1	Kynurenine--oxoglutarate transaminase 1	47932	112	6.5	43598	35	14/45
	SSP 6314	64.35	Idh1	IDHC_MOUSE	O88844	Isocitrate dehydrogenase [NADP] cytoplasmic	47030	183	6.5	44352	55	30/78
	SSP 6315	11.60	Hpd	HPPD_MOUSE	P49429	4-hydroxyphenylpyruvate dioxygenase	45254	200	6.6	43376	55	23/61
	SSP 6316	16.65	Glul	GLNA_MOUSE	P15105	Glutamine synthetase	42834	180	6.6	43316	41	20/71
	SSP 6317	9.09	Upb1	BUP1_MOUSE	Q8VC97	Beta-ureidopropionase	44479	209	6.3	42595	48	22/58
	SSP 6402	13.05	Shmt1	GLYC_MOUSE	P50431	Serine hydroxymethyltransferase, cytosolic	53065	97	6.5	50445	34	14/44
	SSP 6403	14.14	Scp2	NLTP_MOUSE	P32020	Non-specific lipid-transfer protein	59715	75	7.2	47536	26	13/34
	SSP 6406	20.38	Asl	ARLY_MOUSE	Q91YI0	Argininosuccinate lyase	51878	166	6.5	50437	45	20/51
	SSP 6412	49.91	Asl	ARLY_MOUSE	Q91YI0	Argininosuccinate lyase	51878	235	6.5	49744	58	29/61
	SSP 6417	12.05	Asl	ARLY_MOUSE	Q91YI0	Argininosuccinate lyase	51878	138	6.5	50232	43	19/53
	SSP 6422	43.77	Hgd	HGD_MOUSE	O09173	Homogentisate 1,2-dioxygenase	50756	188	6.9	48819	54	25/63
	SSP 6504	8.21	Dak	DHAK_MOUSE	Q8VC30	Dihydroxyacetone kinase	59938	91	6.4	63010	27	9/22
	SSP 6510	16.34	Pgm1	PGM1_MOUSE	Q9D0F9	Phosphoglucomutase-1	61764	307	6.3	61980	60	31/58
	SSP 6612	7.05	Dmgdh	M2GD_MOUSE	Q9DBT9	Dimethylglycine dehydrogenase, mitochondrial precursor	97422	112	7.7	89501	29	18/55
	SSP 6704	48.88	Cps1	CPSM_MOUSE	Q8C196	Carbamoyl-phosphate synthase [ammonia], mitochondrial precursor	165711	114	6.5	160688	19	28/67
	SSP 7002	5.72	Rps27a	UBIQ_MOUSE	P62991	Ubiquitin	8560	120	6.6	9954	84	9/43
	SSP 7008	4.56	Nme2	NDKB_MOUSE	Q01768	Nucleoside diphosphate kinase B	17466	116	7.0	18017	75	13/36
	SSP 7103	92.03	Gstm2	GSTM2_MOUSE	P15626	Glutathione S-transferase Mu 2	25871	184	6.9	24837	73	21/52
	SSP 7106	7.71	Arpc2	ARPC2_MOUSE	Q9CVB6	Actin-related protein 2/3 complex subunit 2	34450	215	6.8	30769	58	18/30
	SSP 7107	10.13	Gsto1	GSTO1_MOUSE	O09131	Glutathione transferase omega-1	27708	124	6.9	28746	48	14/33
	SSP 7108	26.11	Psma2	PSA2_MOUSE	P49722	Proteasome subunit alpha type-2	26023	191	8.4	24319	58	13/36
	SSP 7109	9.68	Psma4	PSA4_MOUSE	Q9R1P0	Proteasome subunit alpha type-4	29737	145	7.6	27961	62	15/49

Time point [hr]	SSP on 2D gel	Fold change	Gene symbol	Accession	UP ID	Protein name	Calculated mass	MOWSE score	pI on 2D gel	Mr on 2d gel	Sequence coverage %	Matched/ Searched peptides
	SSP 7110	17.79	Gstm1	GSTM1_MOUSE	P10649	Glutathione S-transferase Mu 1	26067	246	7.7	25302	75	30/53
	SSP 7111	19.08	Pbld1	PBLD1_MOUSE	Q9DCG6	Phenazine biosynthesis-like domain-containing protein 1	32199	201	6.5	30293	58	18/38
	SSP 7113	4.36	Isoc1	ISOC1_MOUSE	Q91V64	Isochorismatase domain-containing protein 1	32297	178	7.0	30575	58	16/39
	SSP 7114	10.67	Isoc1	ISOC1_MOUSE	Q91V64	Isochorismatase domain-containing protein 1	32297	88	7.0	30727	48	11/52
	SSP 7115	43.07	Gstt1	GSTT1_MOUSE	Q64471	Glutathione S-transferase theta-1	27644	114	6.8	24587	39	12/34
	SSP 7118	16.66	Ca3	CAH3_MOUSE	P16015	Carbonic anhydrase 3	29633	201	6.9	26882	76	16/44
	SSP 7202	51.66	Esd	ESTD_MOUSE	Q9R0P3	S-formylglutathione hydrolase	31870	146	6.7	31619	64	15/42
	SSP 7203	19.77	Gnmt	GNMT_MOUSE	Q9QXF8	Glycine N-methyltransferase	33110	105	7.1	32438	39	11/30
	SSP 7204	4.24	Otc	OTC_MOUSE	P11725	Ornithine carbamoyltransferase, mitochondrial precursor	39854	85	8.8	36769	25	10/29
	SSP 7206	6.68	Gpd1	GPDA_MOUSE	P13707	Glycerol-3-phosphate dehydrogenase [NAD+], cytoplasmic	38176	268	6.8	32375	67	28/57
	SSP 7210	46.14	C4	CO4B_MOUSE	P01029	Complement C4-B precursor [Contains: Complement C4 beta chain; Complement C4 alpha chain; C4a anaphylatoxin; Complement C4 gamma chain]	194417	70	7.4	35905	10	18/32
	SSP 7211	44.86	Ldha	LDHA_MOUSE	P06151	L-lactate dehydrogenase A chain	36817	250	7.6	33312	69	29/55
	SSP 7212	16.24	Akr1a1	AK1A1_MOUSE	Q9JII6	Alcohol dehydrogenase [NADP+]	36792	179	6.9	37362	48	15/32
	SSP 7213	229.11	Gnmt	GNMT_MOUSE	Q9QXF8	Glycine N-methyltransferase	33110	110	7.1	32350	45	12/34
	SSP 7217	30.56	Aldh1a1	AL1A1_MOUSE	P24549	Retinal dehydrogenase 1	55060	114	7.9	31781	33	13/32
	SSP 7301	9.31	Ccbl2	KAT3_MOUSE	Q71RI9	Kynurenine--oxoglutarate transaminase 3	51663	178	8.6	46211	43	22/47
	SSP 7302	50.73	Fah	FAAA_MOUSE	P35505	Fumarylacetoacetase	46416	217	6.9	41387	65	24/58
	SSP 7304	32.85	Amdhd1	HUTI_MOUSE	Q9DBA8	Probable imidazolonepropionase	47086	226	6.5	43408	73	26/55
	SSP 7305	49.69	Hpd	HPPD_MOUSE	P49429	4-hydroxyphenylpyruvate dioxygenase	45254	245	6.6	43470	64	27/62
	SSP 7307	22.04	Idh1	IDHC_MOUSE	O88844	Isocitrate dehydrogenase [NADP] cytoplasmic	47030	215	6.5	44280	60	27/52
	SSP 7310	41.98	Fah	FAAA_MOUSE	P35505	Fumarylacetoacetase	46416	208	6.9	41082	62	27/65
	SSP 7311	19.23	Arg1	ARGI1_MOUSE	Q61176	Arginase-1	34957	129	6.5	39349	54	14/51
	SSP 7312	54.72	Hpd	HPPD_MOUSE	P49429	4-hydroxyphenylpyruvate dioxygenase	45254	295	6.6	43194	66	28/54
	SSP 7314	139.75	Adh5	ADHX_MOUSE	P28474	Alcohol dehydrogenase class-3	40320	84	7.0	39229	51	15/72
	SSP 7316	6.83	Got1	AATC_MOUSE	P05201	Aspartate aminotransferase, cytoplasmic	46488	279	6.7	40889	56	20/26
	SSP 7319	113.95	Ass1	ASSY_MOUSE	P16460	Argininosuccinate synthase	46840	125	8.4	45004	41	20/71
	SSP 7320	55.81	Acat2	THIC_MOUSE	Q8CAY6	Acetyl-CoA acetyltransferase, cytosolic	41727	161	7.2	39265	48	17/46

Time point [hr]	SSP on 2D gel	Fold change	Gene symbol	Accession	UP ID	Protein name	Calculated mass	MOWSE score	pI on 2D gel	Mr on 2d gel	Sequence coverage %	Matched/ Searched peptides
	SSP 7321	12.47	Fah	FAAA_MOUSE	P35505	Fumarylacetoacetase	46416	137	6.9	41879	52	21/47
	SSP 7401	11.76	Glud1	DHE3_MOUSE	P26443	Glutamate dehydrogenase 1, mitochondrial precursor	61640	217	7.7	53046	44	28/55
	SSP 7404	28.49	Lap3	AMPL_MOUSE	Q9CPY7	Cytosol aminopeptidase	56505	237	7.6	54841	56	33/68
	SSP 7406	24.53	Ugp2	UGPA_MOUSE	Q91ZJ5	UTP--glucose-1-phosphate uridylyltransferase	57115	218	7.2	54212	51	28/75
	SSP 7407	27.08	Hgd	HGD_MOUSE	O09173	Homogentisate 1,2-dioxygenase	50756	178	6.9	48877	54	23/63
	SSP 7408	51.23	Dnpep	DNPEP_MOUSE	Q9Z2W0	Aspartyl aminopeptidase	52704	200	6.7	50722	46	24/59
	SSP 7409	90.56	Glud1	DHE3_MOUSE	P26443	Glutamate dehydrogenase 1, mitochondrial precursor	61640	276	8.1	52888	58	33/57
	SSP 7410	56.95	Dpys	DPYS_MOUSE	Q9EQF5	Dihydropyrimidinase	57202	247	6.7	54706	47	24/42
	SSP 7411	15.82	Cat	CATA_MOUSE	P24270	Catalase	60013	237	7.7	57878	54	26/52
	SSP 7417	42.45	Ugp2	UGPA_MOUSE	Q91ZJ5	UTP--glucose-1-phosphate uridylyltransferase	57115	269	7.2	54109	57	32/68
	SSP 7418	56.68	Hgd	HGD_MOUSE	O09173	Homogentisate 1,2-dioxygenase	50756	194	6.9	48700	51	24/59
	SSP 7419	52.09	Cat	CATA_MOUSE	P24270	Catalase	60013	305	7.7	57494	57	31/61
	SSP 7420	9.70	Gsr	GSHR_MOUSE	P47791	Glutathione reductase, mitochondrial precursor	54256	138	8.2	52967	41	22/72
	SSP 7423	7.26	Fh	FUMH_MOUSE	P97807	Fumarate hydratase, mitochondrial precursor	54564	134	9.1	47263	30	18/34
	SSP 7606	11.06	Eef2	EF2_MOUSE	P58252	Elongation factor 2	96222	251	6.4	95500	48	38/73
	SSP 7608	7.24	Mthfd1	C1TC_MOUSE	Q922D8	C-1-tetrahydrofolate synthase, cytoplasmic	101876	145	6.7	105444	21	17/31
	SSP 8002	39.47	Sod2	SODM_MOUSE	P09671	Superoxide dismutase [Mn], mitochondrial precursor	24816	144	8.8	23240	55	13/48
	SSP 8007	43.14	Prdx1	PRDX1_MOUSE	P35700	Peroxiredoxin-1	22390	258	8.3	22764	78	22/51
	SSP 8025	7.24	Psmb5	PSB5_MOUSE	O55234	Proteasome subunit beta type-5 precursor	28685	126	6.5	22863	56	16/54
	SSP 8103	45.60	Gstp1	GSTP1_MOUSE	P19157	Glutathione S-transferase P 1	23765	117	7.7	23892	45	11/40
	SSP 8104	93.90	Gstm1	GSTM1_MOUSE	P10649	Glutathione S-transferase Mu 1	26067	274	7.7	25398	84	32/59
	SSP 8118	111.58	Gstm1	GSTM1_MOUSE	P10649	Glutathione S-transferase Mu 1	26067	286	7.7	25747	80	32/58
	SSP 8119	62.72	Gstp1	GSTP1_MOUSE	P19157	Glutathione S-transferase P 1	23765	120	7.7	24287	45	11/30
	SSP 8305	10.73	Amacr	AMACR_MOUSE	O09174	Alpha-methylacyl-CoA racemase	42034	116	7.0	39614	54	16/67
	SSP 8307	26.65	Bhmt	BHMT1_MOUSE	O35490	Betaine--homocysteine S-methyltransferase 1	45448	246	8.0	45259	67	24/53
	SSP 8308	10.40	Pgk1	PGK1_MOUSE	P09411	Phosphoglycerate kinase 1	44921	158	8.0	43841	48	17/39
	SSP 8310	20.37	Acaa2	THIM_MOUSE	Q8BWT1	3-ketoacyl-CoA thiolase, mitochondrial	42288	225	8.3	42882	67	26/68
	SSP 8311	199.16	Ass1	ASSY_MOUSE	P16460	Argininosuccinate synthase	46840	223	8.4	44894	61	28/65

Time point [hr]	SSP on 2D gel	Fold change	Gene symbol	Accession	UP ID	Protein name	Calculated mass	MOWSE score	pI on 2D gel	Mr on 2d gel	Sequence coverage %	Matched/ Searched peptides
	SSP 8313	27.63	Cth	CGL_MOUSE	Q8VCN5	Cystathionine gamma-lyase	44166	202	7.6	42638	58	23/56
	SSP 8316	31.30	Acat2	THIC_MOUSE	Q8CAY6	Acetyl-CoA acetyltransferase, cytosolic	41727	109	7.2	39350	45	17/75
	SSP 8317	30.98	Bhmt	BHMT1_MOUSE	O35490	Betaine--homocysteine S-methyltransferase 1	45448	260	8.0	45317	68	28/70
	SSP 8323	313.54	Bhmt	BHMT1_MOUSE	O35490	Betaine--homocysteine S-methyltransferase 1	45448	153	8.0	45400	62	24/83
	SSP 8327	13.38	Aldoa	ALDOA_MOUSE	P05064	Fructose-bisphosphate aldolase A	39787	92	8.5	39600	40	14/71
	SSP 8402	43.56	Aldh1a1	AL1A1_MOUSE	P24549	Retinal dehydrogenase 1	55060	124	7.9	53861	37	20/62
	SSP 8408	40.25	Aldh1a1	AL1A1_MOUSE	P24549	Retinal dehydrogenase 1	55060	245	7.9	53773	57	31/66
	SSP 8415	47.73	Aldh1a1	AL1A1_MOUSE	P24549	Retinal dehydrogenase 1	55060	224	7.9	54300	44	24/51
	SSP 8514	21.12	Cat	CATA_MOUSE	P24270	Catalase	60013	298	7.7	58400	59	30/63
	SSP 8605	10.07	Aco1	ACOC_MOUSE	P28271	Cytoplasmic aconitate hydratase	98744	290	7.2	98598	47	40/74
([20hr] vs [12hr])	SSP 1010	7.31	Cyb5a	CYB5_MOUSE	P56395	Cytochrome b5	15232	82	5.0	17500	52	6/37
	SSP 1103	19.58	Ywhae	1433E_MOUSE	P62259	14-3-3 protein epsilon	29326	143	4.6	29300	63	20/68
	SSP 1105	5.16	Rerg	RERG_MOUSE	Q8R367	Ras-related and estrogen-regulated growth inhibitor	22794	66	6.9	23457	37	7/32
	SSP 1106	15.13	PSMD10	PSD10_HUMAN	O75832	26S proteasome non-ATPase regulatory subunit 10	24697	62	5.7	30573	28	6/16
	SSP 2004	6.46	Prdx2	PRDX2_MOUSE	Q61171	Peroxiredoxin-2	21936	126	5.2	22071	51	10/73
	SSP 2110	7.19	Pbld2	PBLD2_MOUSE	Q9CXN7	Phenazine biosynthesis-like domain-containing protein 2	32191	219	5.2	30491	56	20/43
	SSP 2113	12.11	Apoa1	APOA1_MOUSE	Q00623	Apolipoprotein A-I precursor	30569	65	5.6	26627	33	10/45
	SSP 2203	7.82	Cope	COPE_MOUSE	O89079	Coatomer subunit epsilon	34774	102	4.9	32643	42	12/43
	SSP 2211	17.59	Apoe	APOE_MOUSE	P08226	Apolipoprotein E precursor	35901	135	5.6	32811	41	15/32
	SSP 2614	66.33	Vcp	TERA_MOUSE	Q01853	Transitional endoplasmic reticulum ATPase	89950	336	5.1	91604	56	53/98
	SSP 2805	98.24	Ftl1	FRIL1_MOUSE	P29391	Ferritin light chain 1	20847	146	5.7	347509	73	14/60
	SSP 3005	79.13	Fth1	FRIH_MOUSE	P09528	Ferritin heavy chain	21224	172	5.5	20921	69	17/45
	SSP 3009	37.01	Ftl1	FRIL1_MOUSE	P29391	Ferritin light chain 1	20846	196	5.7	22411	73	15/52
	SSP 3101	12.21	Gclm	GSH0_MOUSE	O09172	Glutamate--cysteine ligase regulatory subunit	30858	125	5.4	27851	40	12/30
	SSP 3103	41.36	Actg1	ACTG_RAT	P63259	similar to Actin, cytoplasmic 2 (Gamma-actin)	59163	90	5.7	26993	22	12/43
	SSP 3105	16.46	Psme2	PSME2_MOUSE	P97372	Proteasome activator complex subunit 2	27268	151	5.5	28733	58	16/55
	SSP 3106	12.82	Ndst1	NDST1_MOUSE	Q3UHN9	amine N-sulfotransferase	35248	146	5.4	30584	46	16/43
	SSP 3119	10.92	Psme1	PSME1_MOUSE	P97371	Proteasome activator complex subunit 1	28826	221	5.7	28445	69	21/44

Time point [hr]	SSP on 2D gel	Fold change	Gene symbol	Accession	UP ID	Protein name	Calculated mass	MOWSE score	pI on 2D gel	Mr on 2d gel	Sequence coverage %	Matched/ Searched peptides
	SSP 3125	11.79	Psma3	PSA3_MOUSE	O70435	Proteasome subunit alpha type-3	28615	101	5.3	27831	40	12/41
	SSP 3203	19.12	Acy3	ACY3_MOUSE	Q91XE4	Aspartoacylase-2	35720	99	5.3	33326	36	12/44
	SSP 3207	39.56	Fdps	FPPS_MOUSE	Q920E5	Farnesyl pyrophosphate synthetase	40898	164	5.5	38445	49	16/37
	SSP 3220	40.68	Actb	ACTB_MOUSE	P60710	Actin, cytoplasmic 1	42052	72	5.3	34579	26	7/22
	SSP 3229	8.18	Khk	KHK_MOUSE	P97328	Ketohexokinase	33300	104	5.8	30972	41	10/27
	SSP 3303	19.71	Fgb	FIBB_MOUSE	Q8K0E8	Fibrinogen beta chain precursor [Contains: Fibrinopeptide B]	55402	219	6.7	40984	49	29/47
	SSP 3304	59.10	Fgb	FIBB_MOUSE	Q8K0E8	Fibrinogen beta chain precursor [Contains: Fibrinopeptide B]	55402	154	6.7	42267	39	19/40
	SSP 4101	7.98	Np	PNPH_MOUSE	P23492	Purine nucleoside phosphorylase	32541	209	5.8	29264	58	26/53
	SSP 4107	23.02	Pgam1	PGAM1_MOUSE	Q9DBJ1	Phosphoglycerate mutase 1	28928	199	6.7	26807	76	18/49
	SSP 4111	14.10	Prdx4	PRDX4_MOUSE	O08807	Peroxiredoxin-4	31261	171	6.7	25600	63	14/36
	SSP 4113	12.03	Psmb7	PSB7_MOUSE	P70195	Proteasome subunit beta type-7 precursor	30214	131	8.1	27490	35	15/42
	SSP 4216	3.11	Mdh1	MDHC_MOUSE	P14152	Malate dehydrogenase, cytoplasmic	36659	122	6.2	33300	48	14/49
	SSP 4301	4.67	Adk	ADK_MOUSE	P55264	Adenosine kinase	40466	170	5.8	44522	50	16/43
	SSP 4304	5.63	Psmc2	PRS7_MOUSE	P46471	26S protease regulatory subunit 7	49016	144	5.7	46918	38	15/34
	SSP 4310	41.41	Adk	ADK_MOUSE	P55264	Adenosine kinase	40466	110	5.8	45638	37	11/41
	SSP 4313	8.93	Ttc38	TTC38_MOUSE	A3KMP2	UPF0530 protein	52703	228	5.9	47142	57	28/45
	SSP 4316	30.05	Fgb	FIBB_MOUSE	Q8K0E8	Fibrinogen beta chain precursor [Contains: Fibrinopeptide B]	55402	152	6.7	42067	43	23/56
	SSP 4405	20.79	Eno1	ENOA_MOUSE	P17182	Alpha-enolase	47453	145	6.4	48706	47	18/52
	SSP 4407	6.74	Shpk	SHPK_MOUSE	Q9D5J6	Sedoheptulokinase	51783	211	5.8	47535	56	23/58
	SSP 4414	6.83	Gdi2	GDIB_MOUSE	Q61598	Rab GDP dissociation inhibitor beta	51018	305	5.9	47525	71	32/53
	SSP 4416	46.59	Aldh7a1	AL7A1_MOUSE	Q9DBF1	Alpha-aminoadipic semialdehyde dehydrogenase	56066	84	6.0	53422	22	7/13
	SSP 4421	11.19	Csad	CSAD_MOUSE	Q9DBE0	Cysteine sulfinic acid decarboxylase	55737	235	6.2	51813	49	27/57
	SSP 4601	25.71	Aldh1l1	FTHFD_MOUSE	Q8R0Y6	10-formyltetrahydrofolate dehydrogenase	99502	287	5.6	97035	46	35/65
	SSP 5009	12.88	Psmb2	PSB2_MOUSE	Q9R1P3	Proteasome subunit beta type-2	23063	113	6.5	22611	50	12/50
	SSP 5216	13.88	Grhpr	GRHPR_MOUSE	Q91Z53	Glyoxylate reductase/hydroxypyruvate reductase	35706	164	7.6	33721	56	18/58
	SSP 5310	32.03	Sord	DHSO_MOUSE	Q64442	Sorbitol dehydrogenase	38795	154	6.6	39133	57	18/53
	SSP 5311	8.13	Arg1	ARGI1_MOUSE	Q61176	Arginase-1	34957	129	6.5	39806	58	16/52
	SSP 5402	12.52	Gpt	ALAT1_MOUSE	Q8QZR5	Alanine aminotransferase 1	55905	188	6.2	51040	47	21/35

Time point [hr]	SSP on 2D gel	Fold change	Gene symbol	Accession	UP ID	Protein name	Calculated mass	MOWSE score	pI on 2D gel	Mr on 2d gel	Sequence coverage %	Matched/ Searched peptides
	SSP 5412	3.05	Naprt1	PNCB_MOUSE	Q8CC86	Nicotinate phosphoribosyltransferase	58799	208	6.1	54912	47	21/42
	SSP 5415	3.63	Ces3	CES3_MOUSE	Q8VCT4	Carboxylesterase 3 precursor	62034	191	6.2	57863	50	26/67
	SSP 5416	67.97	Eno1	ENOA_MOUSE	P17182	Alpha-enolase	47453	166	6.4	48304	57	21/55
	SSP 5418	8.33	Dars	SYDC_MOUSE	Q922B2	Aspartyl-tRNA synthetase, cytoplasmic	57537	74	6.1	54692	21	9/41
	SSP 6005	5.15	Psmb2	PSB2_MOUSE	Q9R1P3	Proteasome subunit beta type-2	23063	170	6.5	22552	58	13/47
	SSP 6006	18.50	Nme1	NDKA_MOUSE	P15532	Nucleoside diphosphate kinase A	17311	198	6.8	17102	78	16/37
	SSP 6007	19.29	Nme1	NDKA_MOUSE	P15532	Nucleoside diphosphate kinase A	17311	161	6.8	17389	76	14/36
	SSP 6008	25.95	Nme2	NDKB_MOUSE	Q01768	Nucleoside diphosphate kinase B	17466	125	7.0	17936	71	11/24
	SSP 6101	27.85	Psma2	PSA2_MOUSE	P49722	Proteasome subunit alpha type-2	26023	177	8.4	24302	62	14/39
	SSP 6102	4.00	Gstz1	MAAI_MOUSE	Q9WVL0	Maleylacetoacetate isomerase	24431	138	7.7	24696	61	12/31
	SSP 6103	10.16	Pgam1	PGAM1_MOUSE	Q9DBJ1	Phosphoglycerate mutase 1	28928	134	6.7	28701	55	11/33
	SSP 6108	4.65	Pgam1	PGAM1_MOUSE	Q9DBJ1	Phosphoglycerate mutase 1	28928	158	6.7	26833	72	17/59
	SSP 6113	9.58	Nit1	NIT1_MOUSE	Q8VDK1	Nitrilase homolog 1	36413	186	8.2	27659	60	22/51
	SSP 6116	13.31	Aspdh	ASPD_MOUSE	Q9DCQ2	Putative L-aspartate dehydrogenase	30479	221	6.5	29457	64	19/44
	SSP 6118	7.61	Gstp1	GSTP1_MOUSE	P19157	Glutathione S-transferase P 1	23765	95	7.7	23746	54	10/42
	SSP 6122	5.80	Gsta4	GSTA4_MOUSE	P24472	Glutathione S-transferase A4	25547	82	6.8	23854	47	12/47
	SSP 6202	3.64	Taldo1	TALDO_MOUSE	Q93092	Transaldolase	37534	134	6.6	37203	40	18/43
	SSP 6203	10.67	Bhmt2	BHMT2_MOUSE	Q91WS4	Betaine--homocysteine S-methyltransferase 2	40416	197	6.1	38393	60	20/45
	SSP 6204	10.40	Alad	HEM2_MOUSE	P10518	Delta-aminolevulinic acid dehydratase	36456	209	6.3	35574	53	22/54
	SSP 6207	61.26	Akr7a2	ARK72_MOUSE	Q8CG76	Aflatoxin B1 aldehyde reductase member 2	41028	119	8.4	37142	43	16/53
	SSP 6209	21.43	Arg1	ARGI1_MOUSE	Q61176	Arginase-1	34957	178	6.5	37714	63	18/47
	SSP 6211	21.02	Gnmt	GNMT_MOUSE	Q9QXF8	Glycine N-methyltransferase	33110	110	7.1	32520	40	10/29
	SSP 6215	6.38	Grhpr	GRHPR_MOUSE	Q91Z53	Glyoxylate reductase/hydroxypyruvate reductase	35706	210	7.6	33671	54	20/47
	SSP 6220	13.52	Ldha	LDHA_MOUSE	P06151	L-lactate dehydrogenase A chain	36817	239	7.6	33611	64	23/47
	SSP 6223	3.93	Arg1	ARGI1_MOUSE	Q61176	Arginase-1	34957	166	6.5	37513	57	18/51
	SSP 6301	12.00	Ahcy	SAHH_MOUSE	P50247	Adenosylhomocysteinase	48170	130	6.1	44156	45	21/71
	SSP 6303	9.51	Upb1	BUP1_MOUSE	Q8VC97	Beta-ureidopropionase	44479	218	6.3	43021	45	21/43
	SSP 6304	31.41	Idh1	IDHC_MOUSE	O88844	Isocitrate dehydrogenase [NADP] cytoplasmic	47030	184	6.5	44664	49	19/37

Time point [hr]	SSP on 2D gel	Fold change	Gene symbol	Accession	UP ID	Protein name	Calculated mass	MOWSE score	pI on 2D gel	Mr on 2d gel	Sequence coverage %	Matched/ Searched peptides
	SSP 6305	17.03	Sord	DHSO_MOUSE	Q64442	Sorbitol dehydrogenase	38795	104	6.6	41555	37	9/22
	SSP 6306	5.03	Sord	DHSO_MOUSE	Q64442	Sorbitol dehydrogenase	38795	172	6.6	38902	64	18/50
	SSP 6309	10.35	Upb1	BUP1_MOUSE	Q8VC97	Beta-ureidopropionase	44479	266	6.3	42686	53	24/52
	SSP 6310	9.68	Fah	FAAA_MOUSE	P35505	Fumarylacetoacetase	46416	194	6.9	41553	54	23/50
	SSP 6312	17.69	Ccbl1	KAT1_MOUSE	Q8BTY1	Kynurenine--oxoglutarate transaminase 1	47932	112	6.5	43598	35	14/45
	SSP 6315	6.58	Hpd	HPPD_MOUSE	P49429	4-hydroxyphenylpyruvate dioxygenase	45254	200	6.6	43376	55	23/61
	SSP 6316	5.06	Glul	GLNA_MOUSE	P15105	Glutamine synthetase	42834	180	6.6	43316	41	20/71
	SSP 6402	3.60	Shmt1	GLYC_MOUSE	P50431	Serine hydroxymethyltransferase, cytosolic	53065	97	6.5	50445	34	14/44
	SSP 6403	4.09	Scp2	NLTP_MOUSE	P32020	Non-specific lipid-transfer protein	59715	75	7.2	47536	26	13/34
	SSP 6406	3.74	Asl	ARLY_MOUSE	Q91YI0	Argininosuccinate lyase	51878	166	6.5	50437	45	20/51
	SSP 6408	9.17	Gpt	ALAT1_MOUSE	Q8QZR5	Alanine aminotransferase 1	55905	176	6.2	51185	43	24/53
	SSP 6411	59.28	Hgd	HGD_MOUSE	O09173	Homogentisate 1,2-dioxygenase	50756	128	6.9	48842	35	16/43
	SSP 6417	17.84	Asl	ARLY_MOUSE	Q91YI0	Argininosuccinate lyase	51878	138	6.5	50232	43	19/53
	SSP 6422	5.24	Hgd	HGD_MOUSE	O09173	Homogentisate 1,2-dioxygenase	50756	188	6.9	48819	54	25/63
	SSP 6504	7.18	Dak	DHAK_MOUSE	Q8VC30	Dihydroxyacetone kinase	59938	91	6.4	63010	27	9/22
	SSP 6510	4.04	Pgm1	PGM1_MOUSE	Q9D0F9	Phosphoglucomutase-1	61764	307	6.3	61980	60	31/58
	SSP 6612	4.69	Dmgdh	M2GD_MOUSE	Q9DBT9	Dimethylglycine dehydrogenase, mitochondrial precursor	97422	112	7.7	89501	29	18/55
	SSP 7002	11.28	Rps27a	UBIQ_MOUSE	P62991	Ubiquitin	8560	120	6.6	9954	84	9/43
	SSP 7005	15.83	Psmb8	PSB8_MOUSE	P28063	Proteasome subunit beta type-8 precursor	30526	129	6.2	21931	49	16/39
	SSP 7008	3.74	Nme2	NDKB_MOUSE	Q01768	Nucleoside diphosphate kinase B	17466	116	7.0	18017	75	13/36
	SSP 7106	8.46	Arpc2	ARPC2_MOUSE	Q9CVB6	Actin-related protein 2/3 complex subunit 2	34450	215	6.8	30769	58	18/30
	SSP 7111	6.63	Pbld1	PBLD1_MOUSE	Q9DCG6	Phenazine biosynthesis-like domain-containing protein 1	32199	201	6.5	30293	58	18/38
	SSP 7113	12.10	Isoc1	ISOC1_MOUSE	Q91V64	Isochorismatase domain-containing protein 1	32297	178	7.0	30575	58	16/39
	SSP 7114	12.26	Isoc1	ISOC1_MOUSE	Q91V64	Isochorismatase domain-containing protein 1	32297	88	7.0	30727	48	11/52
	SSP 7115	2.61	Gstt1	GSTT1_MOUSE	Q64471	Glutathione S-transferase theta-1	27644	114	6.8	24587	39	12/34
	SSP 7202	2.94	Esd	ESTD_MOUSE	Q9R0P3	S-formylglutathione hydrolase	31870	146	6.7	31619	64	15/42
	SSP 7203	11.61	Gnmt	GNMT_MOUSE	Q9QXF8	Glycine N-methyltransferase	33110	105	7.1	32438	39	11/30
	SSP 7204	4.23	Otc	OTC_MOUSE	P11725	Ornithine carbamoyltransferase, mitochondrial precursor	39854	85	8.8	36769	25	10/29

Time point [hr]	SSP on 2D gel	Fold change	Gene symbol	Accession	UP ID	Protein name	Calculated mass	MOWSE score	pI on 2D gel	Mr on 2d gel	Sequence coverage %	Matched/ Searched peptides
	SSP 7206	6.66	Gpd1	GPDA_MOUSE	P13707	Glycerol-3-phosphate dehydrogenase [NAD+], cytoplasmic	38176	268	6.8	32375	67	28/57
	SSP 7211	4.72	Ldha	LDHA_MOUSE	P06151	L-lactate dehydrogenase A chain	36817	250	7.6	33312	69	29/55
	SSP 7213	4.03	Gnmt	GNMT_MOUSE	Q9QXF8	Glycine N-methyltransferase	33110	110	7.1	32350	45	12/34
	SSP 7217	4.49	Aldh1a1	AL1A1_MOUSE	P24549	Retinal dehydrogenase 1	55060	114	7.9	31781	33	13/32
	SSP 7301	9.26	Ccbl2	KAT3_MOUSE	Q71RI9	Kynurenine--oxoglutarate transaminase 3	51663	178	8.6	46211	43	22/47
	SSP 7302	4.61	Fah	FAAA_MOUSE	P35505	Fumarylacetoacetase	46416	217	6.9	41387	65	24/58
	SSP 7304	8.72	Amdhd1	HUTI_MOUSE	Q9DBA8	Probable imidazolonepropionase	47086	226	6.5	43408	73	26/55
	SSP 7305	4.46	Hpd	HPPD_MOUSE	P49429	4-hydroxyphenylpyruvate dioxygenase	45254	245	6.6	43470	64	27/62
	SSP 7311	13.93	Arg1	ARGI1_MOUSE	Q61176	Arginase-1	34957	129	6.5	39349	54	14/51
	SSP 7314	3.76	Adh5	ADHX_MOUSE	P28474	Alcohol dehydrogenase class-3	40320	84	7.0	39229	51	15/72
	SSP 7316	6.69	Got1	AATC_MOUSE	P05201	Aspartate aminotransferase, cytoplasmic	46488	279	6.7	40889	56	20/26
	SSP 7319	3.35	Ass1	ASSY_MOUSE	P16460	Argininosuccinate synthase	46840	125	8.4	45004	41	20/71
	SSP 7320	4.29	Acat2	THIC_MOUSE	Q8CAY6	Acetyl-CoA acetyltransferase, cytosolic	41727	161	7.2	39265	48	17/46
	SSP 7321	5.69	Fah	FAAA_MOUSE	P35505	Fumarylacetoacetase	46416	137	6.9	41879	52	21/47
	SSP 7406	8.29	Ugp2	UGPA_MOUSE	Q91ZJ5	UTP--glucose-1-phosphate uridylyltransferase	57115	218	7.2	54212	51	28/75
	SSP 7407	6.76	Hgd	HGD_MOUSE	O09173	Homogentisate 1,2-dioxygenase	50756	178	6.9	48877	54	23/63
	SSP 7411	7.20	Cat	CATA_MOUSE	P24270	Catalase	60013	237	7.7	57878	54	26/52
	SSP 7422	6.57	Cap1	CAP1_MOUSE	P40124	Adenylyl cyclase-associated protein 1	51885	197	7.2	55669	52	22/59
	SSP 7423	6.04	Fh	FUMH_MOUSE	P97807	Fumarate hydratase, mitochondrial precursor	54564	134	9.1	47263	30	18/34
	SSP 7608	7.12	Mthfd1	C1TC_MOUSE	Q922D8	C-1-tetrahydrofolate synthase, cytoplasmic	101876	145	6.7	105444	21	17/31
	SSP 8007	4.23	Prdx1	PRDX1_MOUSE	P35700	Peroxiredoxin-1	22390	258	8.3	22764	78	22/51
	SSP 8025	17.18	Psmb5	PSB5_MOUSE	O55234	Proteasome subunit beta type-5 precursor	28685	126	6.5	22863	56	16/54
	SSP 8113	62.58	Psmb1	PSB1_MOUSE	O09061	Proteasome subunit beta type-1 precursor	26583	190	7.7	24174	77	18/52
	SSP 8305	26.83	Amacr	AMACR_MOUSE	O09174	Alpha-methylacyl-CoA racemase	42034	116	7.0	39614	54	16/67
	SSP 8307	7.97	Bhmt	BHMT1_MOUSE	O35490	Betaine--homocysteine S-methyltransferase 1	45448	246	8.0	45259	67	24/53
	SSP 8312	11.51	Fh	FUMH_MOUSE	P97807	Fumarate hydratase, mitochondrial precursor	54564	183	9.1	47205	41	28/59
	SSP 8406	16.99	Aldh8a1	AL8A1_MOUSE	Q8BH00	Aldehyde dehydrogenase family 8 member A1	54371	263	7.5	55376	66	29/66
	SSP 8408	4.65	Aldh1a1	AL1A1_MOUSE	P24549	Retinal dehydrogenase 1	55060	245	7.9	53773	57	31/66

Time point [hr]	SSP on 2D gel	Fold change	Gene symbol	Accession	UP ID	Protein name	Calculated mass	MOWSE score	pI on 2D gel	Mr on 2d gel	Sequence coverage %	Matched/ Searched peptides
	SSP 8514	7.11	Cat	CATA_MOUSE	P24270	Catalase	60013	298	7.7	58400	59	30/63
	SSP 8605	19.24	Aco1	ACOC_MOUSE	P28271	Cytoplasmic aconitate hydratase	98744	290	7.2	98598	47	40/74
([48hr] vs [20hr])	SSP 2313	85.84	Apoa4	APOA4_MOUSE	P06728	Apolipoprotein A-IV precursor	45001	98	5.4	40238	44	14/50
	SSP 5007	6.60	Rbp4	RET4_MOUSE	Q00724	Plasma retinol-binding protein precursor	23533	155	5.7	21212	69	14/57
	SSP 5105	58.71	A2m	A2M_MOUSE	Q61838	Alpha-2-macroglobulin precursor	167144	67	6.2	28306	11	14/52
	SSP 5415	4.27	Ces3	CES3_MOUSE	Q8VCT4	Carboxylesterase 3 precursor	62034	191	6.2	57863	50	26/67
	SSP 7804	43.74	APOB	APOB_HUMAN	P04114	apolipoprotein B precursor	510481	268	6.4	250973	19	81/108
([96hr] vs [48hr])	SSP 1004	3.22	NUDT6	NUDT6_HUMAN	P53370	Nucleoside diphosphate-linked moiety X motif 6	35998	77	8.2	9938	30	9/34
	SSP 2010	1.48	Ttr	TTHY_MOUSE	P07309	Transthyretin precursor	15880	139	5.8	18493	55	10/35
([1week] vs [96hr])	SSP 1004	1.78	NUDT6	NUDT6_HUMAN	P53370	Nucleoside diphosphate-linked moiety X motif 6	35998	77	8.2	9938	30	9/34

Supplementary table 1b. Identified protein list with down-regulated in serum

Time point [hr]	SSP on 2D gel	Fold change	Gene symbol	Accession	UP ID	Protein name	Calculated mass	MOWSE score	pI on 2D gel	Mr on 2d gel	Sequence coverage %	Matched/ Searched peptides
([03hr] vs [01hr])	SSP 4607	7.68	Gsn	GELS_MOUSE	P13020	Gelsolin precursor	86287	166	5.8	89700	43	27/83
([06hr] vs [03hr])	SSP 3303	7.83	Fgb	FIBB_MOUSE	Q8K0E8	Fibrinogen beta chain precursor [Contains: Fibrinopeptide B]	55402	219	6.7	40984	49	29/47
	SSP 7108	12.82	Psma2	PSA2_MOUSE	P49722	Proteasome subunit alpha type-2	26023	191	8.4	24319	58	13/36
([20hr] vs [12hr])	SSP 2103	1.74	Mbl2	MBL2_MOUSE	P41317	Mannose-binding protein C precursor	26340	160	5.0	27629	55	14/47
	SSP 5007	2.12	Rbp4	RET4_MOUSE	Q00724	Plasma retinol-binding protein precursor	23533	155	5.7	21212	69	14/57
([48hr] vs [20hr])	SSP 1004	3.24	NUDT6	NUDT6_HUMAN	P53370	Nucleoside diphosphate-linked moiety X motif 6	35998	77	8.2	9938	30	9/34
	SSP 1010	15.76	Cyb5a	CYB5_MOUSE	P56395	Cytochrome b5	15232	82	5.0	17500	52	6/37
	SSP 1103	488.31	Ywhae	1433E_MOUSE	P62259	14-3-3 protein epsilon	29326	143	4.6	29300	63	20/68
	SSP 1104	328.32	Psma5	PSA5_MOUSE	Q9Z2U1	Proteasome subunit alpha type-5	26565	151	4.7	26400	63	16/36
	SSP 1105	5.78	Rerg	RERG_MOUSE	Q8R367	Ras-related and estrogen-regulated growth inhibitor	22794	66	6.9	23457	37	7/32
	SSP 1106	16.95	PSMD10	PSD10_HUMAN	O75832	26S proteasome non-ATPase regulatory subunit 10	24697	62	5.7	30573	28	6/16
	SSP 2013	335.05	OBP2A	OBP2A_HUMAN	Q9NY56	odorant binding protein Ia	17044	173	5.2	16773	74	14/50
	SSP 2103	114.95	Mbl2	MBL2_MOUSE	P41317	Mannose-binding protein C precursor	26340	160	5.0	27629	55	14/47
	SSP 2106	270.74	Glo1	LGUL_MOUSE	Q9CPU0	Lactoylglutathione lyase	20967	143	5.2	23562	51	11/32
	SSP 2110	177.60	Pbld2	PBLD2_MOUSE	Q9CXN7	Phenazine biosynthesis-like domain-containing protein 2	32191	219	5.2	30491	56	20/43
	SSP 2113	13.56	Apoa1	APOA1_MOUSE	Q00623	Apolipoprotein A-I precursor	30569	65	5.6	26627	33	10/45
	SSP 2203	29.09	Cope	COPE_MOUSE	O89079	Coatomer subunit epsilon	34774	102	4.9	32643	42	12/43
	SSP 2204	234.67	Rgn	RGN_MOUSE	Q64374	Regucalcin	33899	209	5.2	33846	70	21/45
	SSP 2211	84.61	Apoe	APOE_MOUSE	P08226	Apolipoprotein E precursor	35901	135	5.6	32811	32	15/32
	SSP 2304	551.41	Hp	HPT_MOUSE	Q61646	Haptoglobin precursor [Contains: Haptoglobin alpha chain; Haptoglobin beta chain]	39241	155	5.9	39558	39	20/48
	SSP 2312	2.13	Actb	ACTB_MOUSE	P60710	Actin, cytoplasmic 1	42052	103	5.3	42800	39	14/55
	SSP 2506	2394.28	Hspa5	GRP78_MOUSE	P20029	78 kDa glucose-regulated protein precursor	72492	323	5.1	72300	54	39/65
	SSP 2601	138.43	Hsp90b1	ENPL_MOUSE	P08113	Endoplasmin precursor	92703	288	4.7	97405	48	44/77
	SSP 2614	230.93	Vcp	TERA_MOUSE	Q01853	Transitional endoplasmic reticulum ATPase	89950	336	5.1	91604	56	53/98
	SSP 2805	216.91	Ftl1	FRIL1_MOUSE	P29391	Ferritin light chain 1	20847	146	5.7	347509	73	14/60
	SSP 3005	122.99	Fth1	FRIH_MOUSE	P09528	Ferritin heavy chain	21224	172	5.5	20921	69	17/45

Time point [hr]	SSP on 2D gel	Fold change	Gene symbol	Accession	UP ID	Protein name	Calculated mass	MOWSE score	pI on 2D gel	Mr on 2d gel	Sequence coverage %	Matched/ Searched peptides
	SSP 3009	220.04	Ftl1	FRIL1_MOUSE	P29391	Ferritin light chain 1	20846	196	5.7	22411	73	15/52
	SSP 3101	11.65	Gclm	GSH0_MOUSE	O09172	Glutamate--cysteine ligase regulatory subunit	30858	125	5.4	27851	40	12/30
	SSP 3105	156.47	Psme2	PSME2_MOUSE	P97372	Proteasome activator complex subunit 2	27268	151	5.5	28733	58	16/55
	SSP 3106	32.76	Ndst1	NDST1_MOUSE	Q3UHN9	amine N-sulfotransferase	35248	146	5.4	30584	46	16/43
	SSP 3119	107.07	Psme1	PSME1_MOUSE	P97371	Proteasome activator complex subunit 1	28826	221	5.7	28445	69	21/44
	SSP 3125	13.20	Psma3	PSA3_MOUSE	O70435	Proteasome subunit alpha type-3	28615	101	5.3	27831	40	12/41
	SSP 3201	125.96	Ppa1	IPYR_MOUSE	Q9D819	Inorganic pyrophosphatase	33102	149	5.4	34419	49	15/49
	SSP 3203	21.42	Acy3	ACY3_MOUSE	Q91XE4	Aspartoacylase-2	35720	99	5.3	33326	36	12/44
	SSP 3207	44.30	Fdps	FPPS_MOUSE	Q920E5	Farnesyl pyrophosphate synthetase	40898	164	5.5	38445	49	16/37
	SSP 3220	8.07	Actb	ACTB_MOUSE	P60710	Actin, cytoplasmic 1	42052	72	5.3	34579	26	7/22
	SSP 3229	258.01	Khk	KHK_MOUSE	P97328	Ketohexokinase	33300	104	5.8	30972	41	10/27
	SSP 3303	177.75	Fgb	FIBB_MOUSE	Q8K0E8	Fibrinogen beta chain precursor [Contains: Fibrinopeptide B]	55402	219	6.7	40984	49	29/47
	SSP 3304	66.18	Fgb	FIBB_MOUSE	Q8K0E8	Fibrinogen beta chain precursor [Contains: Fibrinopeptide B]	55402	154	6.7	42267	39	19/40
	SSP 4002	61.37	Apom	APOM_MOUSE	Q9Z1R3	Apolipoprotein M	21602	159	6.1	20361	44	17/53
	SSP 4008	56.81	Apoa2	APOA2_MOUSE	P09813	Apolipoprotein A-II precursor	11369	78	6.6	10087	47	9/35
	SSP 4101	280.53	Np	PNPH_MOUSE	P23492	Purine nucleoside phosphorylase	32541	209	5.8	29264	58	26/53
	SSP 4106	37.64	Hyi	HYI_MOUSE	Q8R1F5	Putative hydroxypyruvate isomerase	30544	103	6.0	27713	53	13/63
	SSP 4107	66.60	Pgam1	PGAM1_MOUSE	Q9DBJ1	Phosphoglycerate mutase 1	28928	199	6.7	26807	76	18/49
	SSP 4207	67.45	Fbp1	F16P1_MOUSE	Q9QXD6	Fructose-1,6-bisphosphatase 1	37288	250	6.2	36443	65	25/56
	SSP 4216	9.64	Mdh1	MDHC_MOUSE	P14152	Malate dehydrogenase, cytoplasmic	36659	122	6.2	33300	48	14/49
	SSP 4301	81.34	Adk	ADK_MOUSE	P55264	Adenosine kinase	40466	170	5.8	44522	50	16/43
	SSP 4304	6.30	Psmc2	PRS7_MOUSE	P46471	26S protease regulatory subunit 7	49016	144	5.7	46918	38	15/34
	SSP 4310	46.37	Adk	ADK_MOUSE	P55264	Adenosine kinase	40466	110	5.8	45638	37	11/41
	SSP 4312	92.14	Acy1	ACY1_MOUSE	Q99JW2	Aminoacylase-1	45980	262	5.9	42286	59	23/35
	SSP 4313	16.85	Ttc38	TTC38_MOUSE	A3KMP2	UPF0530 protein	52703	228	5.9	47142	57	28/45
	SSP 4314	82.56	Tcn2	TCO2_MOUSE	O88968	Transcobalamin-2 precursor	48012	145	5.9	42240	45	14/47
	SSP 4316	53.43	Fgb	FIBB_MOUSE	Q8K0E8	Fibrinogen beta chain precursor [Contains: Fibrinopeptide B]	55402	152	6.7	42067	43	23/56
	SSP 4405	23.28	Eno1	ENOA_MOUSE	P17182	Alpha-enolase	47453	145	6.4	48706	47	18/52

Time point [hr]	SSP on 2D gel	Fold change	Gene symbol	Accession	UP ID	Protein name	Calculated mass	MOWSE score	pI on 2D gel	Mr on 2d gel	Sequence coverage %	Matched/ Searched peptides
	SSP 4407	63.84	Shpk	SHPK_MOUSE	Q9D5J6	Sedoheptulokinase	51783	211	5.8	47535	56	23/58
	SSP 4411	99.87	Selenbp1	SBP1_MOUSE	P17563	Selenium-binding protein 1	53051	240	5.9	53140	68	19/74
	SSP 4414	83.70	Gdi2	GDIB_MOUSE	Q61598	Rab GDP dissociation inhibitor beta	51018	305	5.9	47525	71	32/53
	SSP 4416	52.18	Aldh7a1	AL7A1_MOUSE	Q9DBF1	Alpha-aminoadipic semialdehyde dehydrogenase	56066	84	6.0	53422	22	7/13
	SSP 4420	25.43	Naprt1	PNCB_MOUSE	Q8CC86	Nicotinate phosphoribosyltransferase	58799	240	6.1	54986	51	23/45
	SSP 4421	89.62	Csad	CSAD_MOUSE	Q9DBE0	Cysteine sulfinic acid decarboxylase	55737	235	6.2	51813	49	27/57
	SSP 4601	40.96	Aldh1l1	FTHFD_MOUSE	Q8R0Y6	10-formyltetrahydrofolate dehydrogenase	99502	287	5.6	97035	46	35/65
	SSP 4607	413.17	Gsn	GELS_MOUSE	P13020	Gelsolin precursor	86287	166	5.8	89700	43	27/83
	SSP 4718	8.54	Vcl	VINC_MOUSE	Q64727	Vinculin	117215	151	5.8	124173	26	24/52
	SSP 5001	10.91	Sod1	SODC_MOUSE	P08228	Superoxide dismutase [Cu-Zn]	16104	78	6.0	17327	44	7/32
	SSP 5003	61.11	Apom	APOM_MOUSE	Q9Z1R3	Apolipoprotein M	21602	175	6.1	20607	44	17/45
	SSP 5008	359.04	Pcbd1	PHS_MOUSE	P61458	Pterin-4-alpha-carbinolamine dehydratase	12035	138	6.3	11955	69	11/40
	SSP 5009	14.42	Psmb2	PSB2_MOUSE	Q9R1P3	Proteasome subunit beta type-2	23063	113	6.5	22611	50	12/50
	SSP 5010	11.46	Saa1	SAA1_MOUSE	P05366	Serum amyloid A-1 protein precursor	13876	86	6.5	13676	54	8/38
	SSP 5103	205.71	Psmb3	PSB3_MOUSE	Q9R1P1	Proteasome subunit beta type-3	23234	139	6.2	23796	52	19/53
	SSP 5109	364.58	Prdx6	PRDX6_MOUSE	O08709	Peroxiredoxin-6	24969	229	5.7	25091	79	20/61
	SSP 5216	15.55	Grhpr	GRHPR_MOUSE	Q91Z53	Glyoxylate reductase/hydroxypyruvate reductase	35706	164	7.6	33721	56	18/58
	SSP 5307	126.83	Ahcy	SAHH_MOUSE	P50247	Adenosylhomocysteinase	48170	287	6.1	43864	67	35/71
	SSP 5311	92.89	Arg1	ARGI1_MOUSE	Q61176	Arginase-1	34957	129	6.5	39806	58	16/52
	SSP 5401	162.13	Aldh7a1	AL7A1_MOUSE	Q9DBF1	Alpha-aminoadipic semialdehyde dehydrogenase	56066	254	6.0	52967	48	25/64
	SSP 5402	58.61	Gpt	ALAT1_MOUSE	Q8QZR5	Alanine aminotransferase 1	55905	188	6.2	51040	47	21/35
	SSP 5405	96.78	Eno1	ENOA_MOUSE	P17182	Alpha-enolase	47453	271	6.4	47679	71	30/62
	SSP 5408	480.58	Csad	CSAD_MOUSE	Q9DBE0	Cysteine sulfinic acid decarboxylase	55737	253	6.2	51636	52	32/71
	SSP 5412	58.02	Naprt1	PNCB_MOUSE	Q8CC86	Nicotinate phosphoribosyltransferase	58799	208	6.1	54912	47	21/42
	SSP 5413	179.60	Gpt	ALAT1_MOUSE	Q8QZR5	Alanine aminotransferase 1	55905	186	6.2	51137	50	27/68
	SSP 5416	148.48	Eno1	ENOA_MOUSE	P17182	Alpha-enolase	47453	166	6.4	48304	57	21/55
	SSP 5418	9.32	Dars	SYDC_MOUSE	Q922B2	Aspartyl-tRNA synthetase, cytoplasmic	57537	74	6.1	54692	21	9/41
	SSP 6002	471.79	Gpx1	GPX1_MOUSE	P11352	Glutathione peroxidase 1	22544	130	6.7	22950	65	11/32

Time point [hr]	SSP on 2D gel	Fold change	Gene symbol	Accession	UP ID	Protein name	Calculated mass	MOWSE score	pI on 2D gel	Mr on 2d gel	Sequence coverage %	Matched/ Searched peptides
	SSP 6006	85.81	Nme1	NDKA_MOUSE	P15532	Nucleoside diphosphate kinase A	17311	198	6.8	17102	78	16/37
	SSP 6007	128.93	Nme1	NDKA_MOUSE	P15532	Nucleoside diphosphate kinase A	17311	161	6.8	17389	76	14/36
	SSP 6008	29.06	Nme2	NDKB_MOUSE	Q01768	Nucleoside diphosphate kinase B	17466	125	7.0	17936	71	11/24
	SSP 6101	48.27	Psma2	PSA2_MOUSE	P49722	Proteasome subunit alpha type-2	26023	177	8.4	24302	62	14/39
	SSP 6102	89.85	Gstz1	MAAI_MOUSE	Q9WVL0	Maleylacetoacetate isomerase	24431	138	7.7	24696	61	12/31
	SSP 6103	11.38	Pgam1	PGAM1_MOUSE	Q9DBJ1	Phosphoglycerate mutase 1	28928	134	6.7	28701	55	11/33
	SSP 6108	78.15	Pgam1	PGAM1_MOUSE	Q9DBJ1	Phosphoglycerate mutase 1	28928	158	6.7	26833	72	17/59
	SSP 6110	227.08	Nqo2	NQO2_MOUSE	Q9JI75	Ribosyldihydronicotinamide dehydrogenase [quinone]	26459	142	6.5	25298	62	114/49
	SSP 6112	73.18	PTPN20A	PTN20_HUMAN	Q4JDL3	protein tyrosine phosphatase, non-receptor type 20 isoform 5	26756	66	6.6	24899	34	9/38
	SSP 6113	89.31	Nit1	NIT1_MOUSE	Q8VDK1	Nitrilase homolog 1	36413	186	8.2	27659	60	22/51
	SSP 6116	88.48	Aspdh	ASPD_MOUSE	Q9DCQ2	Putative L-aspartate dehydrogenase	30479	221	6.5	29457	64	19/44
	SSP 6118	90.85	Gstp1	GSTP1_MOUSE	P19157	Glutathione S-transferase P 1	23765	95	7.7	23746	54	10/42
	SSP 6122	78.09	Gsta4	GSTA4_MOUSE	P24472	Glutathione S-transferase A4	25547	82	6.8	23854	47	12/47
	SSP 6202	105.02	Taldo1	TALDO_MOUSE	Q93092	Transaldolase	37534	134	6.6	37203	40	18/43
	SSP 6203	19.29	Bhmt2	BHMT2_MOUSE	Q91WS4	Betaine--homocysteine S-methyltransferase 2	40416	197	6.1	38393	60	20/45
	SSP 6204	4.92	Alad	HEM2_MOUSE	P10518	Delta-aminolevulinic acid dehydratase	36456	209	6.3	35574	53	22/54
	SSP 6207	68.60	Akr7a2	ARK72_MOUSE	Q8CG76	Aflatoxin B1 aldehyde reductase member 2	41028	119	8.4	37142	43	16/53
	SSP 6209	110.99	Arg1	ARGI1_MOUSE	Q61176	Arginase-1	34957	178	6.5	37714	63	18/47
	SSP 6211	123.52	Gnmt	GNMT_MOUSE	Q9QXF8	Glycine N-methyltransferase	33110	110	7.1	32520	40	10/29
	SSP 6215	244.05	Grhpr	GRHPR_MOUSE	Q91Z53	Glyoxylate reductase/hydroxypyruvate reductase	35706	210	7.6	33671	54	20/47
	SSP 6220	124.30	Ldha	LDHA_MOUSE	P06151	L-lactate dehydrogenase A chain	36817	239	7.6	33611	64	23/47
	SSP 6223	24.58	Arg1	ARGI1_MOUSE	Q61176	Arginase-1	34957	166	6.5	37513	57	18/51
	SSP 6301	13.19	Ahcy	SAHH_MOUSE	P50247	Adenosylhomocysteinase	48170	130	6.1	44156	45	21/71
	SSP 6303	52.44	Upb1	BUP1_MOUSE	Q8VC97	Beta-ureidopropionase	44479	218	6.3	43021	45	21/43
	SSP 6304	5.76	Idh1	IDHC_MOUSE	O88844	Isocitrate dehydrogenase [NADP] cytoplasmic	47030	184	6.5	44664	49	19/37
	SSP 6305	19.08	Sord	DHSO_MOUSE	Q64442	Sorbitol dehydrogenase	38795	104	6.6	41555	37	9/22
	SSP 6306	5.15	Sord	DHSO_MOUSE	Q64442	Sorbitol dehydrogenase	38795	172	6.6	38902	64	18/50
	SSP 6309	243.82	Upb1	BUP1_MOUSE	Q8VC97	Beta-ureidopropionase	44479	266	6.3	42686	53	24/52

Time point [hr]	SSP on 2D gel	Fold change	Gene symbol	Accession	UP ID	Protein name	Calculated mass	MOWSE score	pI on 2D gel	Mr on 2d gel	Sequence coverage %	Matched/ Searched peptides
	SSP 6310	105.59	Fah	FAAA_MOUSE	P35505	Fumarylacetoacetase	46416	194	6.9	41553	54	23/50
	SSP 6312	171.44	Ccbl1	KAT1_MOUSE	Q8BTY1	Kynurenine--oxoglutarate transaminase 1	47932	112	6.5	43598	35	14/45
	SSP 6314	389.40	Idh1	IDHC_MOUSE	O88844	Isocitrate dehydrogenase [NADP] cytoplasmic	47030	183	6.5	44352	55	30/78
	SSP 6315	90.72	Hpd	HPPD_MOUSE	P49429	4-hydroxyphenylpyruvate dioxygenase	45254	200	6.6	43376	55	23/61
	SSP 6316	183.69	Glul	GLNA_MOUSE	P15105	Glutamine synthetase	42834	180	6.6	43316	41	20/71
	SSP 6317	37.71	Upb1	BUP1_MOUSE	Q8VC97	Beta-ureidopropionase	44479	209	6.3	42595	48	22/58
	SSP 6402	55.80	Shmt1	GLYC_MOUSE	P50431	Serine hydroxymethyltransferase, cytosolic	53065	97	6.5	50445	34	14/44
	SSP 6403	68.63	Scp2	NLTP_MOUSE	P32020	Non-specific lipid-transfer protein	59715	75	7.2	47536	26	13/34
	SSP 6406	90.63	Asl	ARLY_MOUSE	Q91YI0	Argininosuccinate lyase	51878	166	6.5	50437	45	20/51
	SSP 6408	82.29	Gpt	ALAT1_MOUSE	Q8QZR5	Alanine aminotransferase 1	55905	176	6.2	51185	43	24/53
	SSP 6412	996.97	Asl	ARLY_MOUSE	Q91YI0	Argininosuccinate lyase	51878	235	6.5	49744	58	29/61
	SSP 6417	559.85	Asl	ARLY_MOUSE	Q91YI0	Argininosuccinate lyase	51878	138	6.5	50232	43	19/53
	SSP 6504	134.90	Dak	DHAK_MOUSE	Q8VC30	Dihydroxyacetone kinase	59938	91	6.4	63010	27	9/22
	SSP 6510	158.12	Pgm1	PGM1_MOUSE	Q9D0F9	Phosphoglucomutase-1	61764	307	6.3	61980	60	31/58
	SSP 6612	39.26	Dmgdh	M2GD_MOUSE	Q9DBT9	Dimethylglycine dehydrogenase, mitochondrial precursor	97422	112	7.7	89501	29	18/55
	SSP 6704	132.69	Cps1	CPSM_MOUSE	Q8C196	Carbamoyl-phosphate synthase [ammonia], mitochondrial precursor	165711	114	6.5	160688	19	28/67
	SSP 7002	76.65	Rps27a	UBIQ_MOUSE	P62991	Ubiquitin	8560	120	6.6	9954	84	9/43
	SSP 7005	17.73	Psmb8	PSB8_MOUSE	P28063	Proteasome subunit beta type-8 precursor	30526	129	6.2	21931	49	16/39
	SSP 7008	17.08	Nme2	NDKB_MOUSE	Q01768	Nucleoside diphosphate kinase B	17466	116	7.0	18017	75	13/36
	SSP 7106	77.55	Arpc2	ARPC2_MOUSE	Q9CVB6	Actin-related protein 2/3 complex subunit 2	34450	215	6.8	30769	58	18/30
	SSP 7107	82.34	Gsto1	GSTO1_MOUSE	O09131	Glutathione transferase omega-1	27708	124	6.9	28746	48	14/33
	SSP 7110	325.46	Gstm1	GSTM1_MOUSE	P10649	Glutathione S-transferase Mu 1	26067	246	7.7	25302	75	30/53
	SSP 7111	150.25	Pbld1	PBLD1_MOUSE	Q9DCG6	Phenazine biosynthesis-like domain-containing protein 1	32199	201	6.5	30293	58	18/38
	SSP 7112	15.03	Ca3	CAH3_MOUSE	P16015	Carbonic anhydrase 3	29633	152	6.9	26915	63	13/46
	SSP 7113	62.60	Isoc1	ISOC1_MOUSE	Q91V64	Isochorismatase domain-containing protein 1	32297	178	7.0	30575	58	16/39
	SSP 7114	155.37	Isoc1	ISOC1_MOUSE	Q91V64	Isochorismatase domain-containing protein 1	32297	88	7.0	30727	48	11/52
	SSP 7115	133.42	Gstt1	GSTT1_MOUSE	Q64471	Glutathione S-transferase theta-1	27644	114	6.8	24587	39	12/34
	SSP 7118	169.74	Ca3	CAH3_MOUSE	P16015	Carbonic anhydrase 3	29633	201	6.9	26882	76	16/44

Time point [hr]	SSP on 2D gel	Fold change	Gene symbol	Accession	UP ID	Protein name	Calculated mass	MOWSE score	pI on 2D gel	Mr on 2d gel	Sequence coverage %	Matched/ Searched peptides
	SSP 7202	180.58	Esd	ESTD_MOUSE	Q9R0P3	S-formylglutathione hydrolase	31870	146	6.7	31619	64	15/42
	SSP 7203	272.52	Gnmt	GNMT_MOUSE	Q9QXF8	Glycine N-methyltransferase	33110	105	7.1	32438	39	11/30
	SSP 7204	21.30	Otc	OTC_MOUSE	P11725	Ornithine carbamoyltransferase, mitochondrial precursor	39854	85	8.8	36769	25	10/29
	SSP 7206	411.25	Gpd1	GPDA_MOUSE	P13707	Glycerol-3-phosphate dehydrogenase [NAD+], cytoplasmic	38176	268	6.8	32375	67	28/57
	SSP 7211	234.74	Ldha	LDHA_MOUSE	P06151	L-lactate dehydrogenase A chain	36817	250	7.6	33312	69	29/55
	SSP 7212	44.18	Akr1a1	AK1A1_MOUSE	Q9JII6	Alcohol dehydrogenase [NADP+]	36792	179	6.9	37362	48	15/32
	SSP 7213	1780.52	Gnmt	GNMT_MOUSE	Q9QXF8	Glycine N-methyltransferase	33110	110	7.1	32350	45	12/34
	SSP 7217	162.92	Aldh1a1	AL1A1_MOUSE	P24549	Retinal dehydrogenase 1	55060	114	7.9	31781	33	13/32
	SSP 7301	102.44	Ccbl2	KAT3_MOUSE	Q71RI9	Kynurenine--oxoglutarate transaminase 3	51663	178	8.6	46211	43	22/47
	SSP 7302	3.68	Fah	FAAA_MOUSE	P35505	Fumarylacetoacetase	46416	217	6.9	41387	65	24/58
	SSP 7304	340.46	Amdhd1	HUTI_MOUSE	Q9DBA8	Probable imidazolonepropionase	47086	226	6.5	43408	73	26/55
	SSP 7305	31.28	Hpd	HPPD_MOUSE	P49429	4-hydroxyphenylpyruvate dioxygenase	45254	245	6.6	43470	64	27/62
	SSP 7307	82.77	Idh1	IDHC_MOUSE	O88844	Isocitrate dehydrogenase [NADP] cytoplasmic	47030	215	6.5	44280	60	27/52
	SSP 7311	318.23	Arg1	ARGI1_MOUSE	Q61176	Arginase-1	34957	129	6.5	39349	54	14/51
	SSP 7312	684.79	Hpd	HPPD_MOUSE	P49429	4-hydroxyphenylpyruvate dioxygenase	45254	295	6.6	43194	66	28/54
	SSP 7314	72.21	Adh5	ADHX_MOUSE	P28474	Alcohol dehydrogenase class-3	40320	84	7.0	39229	51	15/72
	SSP 7316	119.87	Got1	AATC_MOUSE	P05201	Aspartate aminotransferase, cytoplasmic	46488	279	6.7	40889	56	20/26
	SSP 7319	35.53	Ass1	ASSY_MOUSE	P16460	Argininosuccinate synthase	46840	125	8.4	45004	41	20/71
	SSP 7320	172.19	Acat2	THIC_MOUSE	Q8CAY6	Acetyl-CoA acetyltransferase, cytosolic	41727	161	7.2	39265	48	17/46
	SSP 7321	84.26	Fah	FAAA_MOUSE	P35505	Fumarylacetoacetase	46416	137	6.9	41879	52	21/47
	SSP 7406	400.81	Ugp2	UGPA_MOUSE	Q91ZJ5	UTP--glucose-1-phosphate uridylyltransferase	57115	218	7.2	54212	51	28/75
	SSP 7408	82.10	Dnpep	DNPEP_MOUSE	Q9Z2W0	Aspartyl aminopeptidase	52704	200	6.7	50722	46	24/59
	SSP 7410	10.17	Dpys	DPYS_MOUSE	Q9EQF5	Dihydropyrimidinase	57202	247	6.7	54706	47	24/42
	SSP 7411	10.81	Cat	CATA_MOUSE	P24270	Catalase	60013	237	7.7	57878	54	26/52
	SSP 7417	9.25	Ugp2	UGPA_MOUSE	Q91ZJ5	UTP--glucose-1-phosphate uridylyltransferase	57115	269	7.2	54109	57	32/68
	SSP 7419	12.80	Cat	CATA_MOUSE	P24270	Catalase	60013	305	7.7	57494	57	31/61
	SSP 7422	55.91	Cap1	CAP1_MOUSE	P40124	Adenylyl cyclase-associated protein 1	51885	197	7.2	55669	52	22/59
	SSP 7423	89.11	Fh	FUMH_MOUSE	P97807	Fumarate hydratase, mitochondrial precursor	54564	134	9.1	47263	30	18/34

Time point [hr]	SSP on 2D gel	Fold change	Gene symbol	Accession	UP ID	Protein name	Calculated mass	MOWSE score	pI on 2D gel	Mr on 2d gel	Sequence coverage %	Matched/ Searched peptides
	SSP 7606	330.23	Eef2	EF2_MOUSE	P58252	Elongation factor 2	96222	251	6.4	95500	48	38/73
	SSP 7608	61.23	Mthfd1	C1TC_MOUSE	Q922D8	C-1-tetrahydrofolate synthase, cytoplasmic	101876	145	6.7	105444	21	17/31
	SSP 8002	69.99	Sod2	SODM_MOUSE	P09671	Superoxide dismutase [Mn], mitochondrial precursor	24816	144	8.8	23240	55	13/48
	SSP 8007	360.58	Prdx1	PRDX1_MOUSE	P35700	Peroxiredoxin-1	22390	258	8.3	22764	78	22/51
	SSP 8103	141.26	Gstp1	GSTP1_MOUSE	P19157	Glutathione S-transferase P 1	23765	117	7.7	23892	45	11/40
	SSP 8104	798.50	Gstm1	GSTM1_MOUSE	P10649	Glutathione S-transferase Mu 1	26067	274	7.7	25398	84	32/59
	SSP 8113	117.24	Psmb1	PSB1_MOUSE	O09061	Proteasome subunit beta type-1 precursor	26583	190	7.7	24174	77	18/52
	SSP 8118	668.02	Gstm1	GSTM1_MOUSE	P10649	Glutathione S-transferase Mu 1	26067	286	7.7	25747	80	32/58
	SSP 8119	83.03	Gstp1	GSTP1_MOUSE	P19157	Glutathione S-transferase P 1	23765	120	7.7	24287	45	11/30
	SSP 8123	15.62	Gsta3	GSTA3_MOUSE	P30115	Glutathione S-transferase A3	25401	160	8.8	25353	55	22/51
	SSP 8305	341.93	Amacr	AMACR_MOUSE	O09174	Alpha-methylacyl-CoA racemase	42034	116	7.0	39614	54	16/67
	SSP 8307	577.60	Bhmt	BHMT1_MOUSE	O35490	Betaine--homocysteine S-methyltransferase 1	45448	246	8.0	45259	67	24/53
	SSP 8310	42.48	Acaa2	THIM_MOUSE	Q8BWT1	3-ketoacyl-CoA thiolase, mitochondrial	42288	225	8.3	42882	67	26/68
	SSP 8311	27.82	Ass1	ASSY_MOUSE	P16460	Argininosuccinate synthase	46840	223	8.4	44894	61	28/65
	SSP 8312	69.32	Fh	FUMH_MOUSE	P97807	Fumarate hydratase, mitochondrial precursor	54564	183	9.1	47205	41	28/59
	SSP 8313	143.75	Cth	CGL_MOUSE	Q8VCN5	Cystathionine gamma-lyase	44166	202	7.6	42638	58	23/56
	SSP 8317	601.20	Bhmt	BHMT1_MOUSE	O35490	Betaine--homocysteine S-methyltransferase 1	45448	260	8.0	45317	68	28/70
	SSP 8323	2253.91	Bhmt	BHMT1_MOUSE	O35490	Betaine--homocysteine S-methyltransferase 1	45448	153	8.0	45400	62	24/83
	SSP 8327	11.26	Aldoa	ALDOA_MOUSE	P05064	Fructose-bisphosphate aldolase A	39787	92	8.5	39600	40	14/71
	SSP 8402	31.62	Aldh1a1	AL1A1_MOUSE	P24549	Retinal dehydrogenase 1	55060	124	7.9	53861	37	20/62
	SSP 8406	209.26	Aldh8a1	AL8A1_MOUSE	Q8BH00	Aldehyde dehydrogenase family 8 member A1	54371	263	7.5	55376	66	29/66
	SSP 8408	260.78	Aldh1a1	AL1A1_MOUSE	P24549	Retinal dehydrogenase 1	55060	245	7.9	53773	57	31/66
	SSP 8415	368.86	Aldh1a1	AL1A1_MOUSE	P24549	Retinal dehydrogenase 1	55060	224	7.9	54300	44	24/51
	SSP 8514	254.41	Cat	CATA_MOUSE	P24270	Catalase	60013	298	7.7	58400	59	30/63
	SSP 8605	230.26	Aco1	ACOC_MOUSE	P28271	Cytoplasmic aconitate hydratase	98744	290	7.2	98598	47	40/74
([96hr] vs [48hr])	SSP 1010	43.88	Cyb5a	CYB5_MOUSE	P56395	Cytochrome b5	15232	82	5.0	17500	52	6/37
	SSP 3101	9.93	Gclm	GSH0_MOUSE	O09172	Glutamate--cysteine ligase regulatory subunit	30858	125	5.4	27851	40	12/30
	SSP 3103	47.13	Actg1	ACTG_RAT	P63259	similar to Actin, cytoplasmic 2 (Gamma-actin)	59163	90	5.7	26993	22	12/43

Time point [hr]	SSP on 2D gel	Fold change	Gene symbol	Accession	UP ID	Protein name	Calculated mass	MOWSE score	pI on 2D gel	Mr on 2d gel	Sequence coverage %	Matched/ Searched peptides
	SSP 3220	5.28	Actb	ACTB_MOUSE	P60710	Actin, cytoplasmic 1	42052	72	5.3	34579	26	7/22
	SSP 3414	17.87	Gss	GSHB_MOUSE	P51855	Glutathione synthetase	52442	224	5.6	51742	49	25/56
	SSP 4111	45.97	Prdx4	PRDX4_MOUSE	O08807	Peroxiredoxin-4	31261	171	6.7	25600	63	14/36
	SSP 4113	5.22	Psmb7	PSB7_MOUSE	P70195	Proteasome subunit beta type-7 precursor	30214	131	8.1	27490	35	15/42
	SSP 4420	3.45	Naprt1	PNCB_MOUSE	Q8CC86	Nicotinate phosphoribosyltransferase	58799	240	6.1	54986	51	23/45
	SSP 5001	11.07	Sod1	SODC_MOUSE	P08228	Superoxide dismutase [Cu-Zn]	16104	78	6.0	17327	44	7/32
	SSP 5214	145.83	Alad	HEM2_MOUSE	P10518	Delta-aminolevulinic acid dehydratase	36456	201	6.3	35400	52	24/62
	SSP 5310	54.05	Sord	DHSO_MOUSE	Q64442	Sorbitol dehydrogenase	38795	154	6.6	39133	57	18/53
	SSP 5405	9.51	Eno1	ENOA_MOUSE	P17182	Alpha-enolase	47453	271	6.4	47679	71	30/62
	SSP 5415	310.83	Ces3	CES3_MOUSE	Q8VCT4	Carboxylesterase 3 precursor	62034	191	6.2	57863	50	26/67
	SSP 6005	6.04	Psmb2	PSB2_MOUSE	Q9R1P3	Proteasome subunit beta type-2	23063	170	6.5	22552	58	13/47
	SSP 6217	313.47	Sord	DHSO_MOUSE	Q64442	Sorbitol dehydrogenase	38795	165	6.6	38705	64	22/65
	SSP 6223	21.04	Arg1	ARGI1_MOUSE	Q61176	Arginase-1	34957	166	6.5	37513	57	18/51
	SSP 6304	30.99	Idh1	IDHC_MOUSE	O88844	Isocitrate dehydrogenase [NADP] cytoplasmic	47030	184	6.5	44664	49	19/37
	SSP 6306	165.95	Sord	DHSO_MOUSE	Q64442	Sorbitol dehydrogenase	38795	172	6.6	38902	64	18/50
	SSP 6411	93.95	Hgd	HGD_MOUSE	O09173	Homogentisate 1,2-dioxygenase	50756	128	6.9	48842	35	16/43
	SSP 6416	54.29	Lap3	AMPL_MOUSE	Q9CPY7	Cytosol aminopeptidase	56505	244	7.6	55251	42	18/21
	SSP 6422	366.32	Hgd	HGD_MOUSE	O09173	Homogentisate 1,2-dioxygenase	50756	188	6.9	48819	54	25/63
	SSP 6424	143.76	Lap3	AMPL_MOUSE	Q9CPY7	Cytosol aminopeptidase	56505	160	7.6	55279	44	21/56
	SSP 7210	45.99	C4	CO4B_MOUSE	P01029	Complement C4-B precursor [Contains: Complement C4 beta chain; Complement C4 alpha chain; C4a anaphylatoxin; Complement C4 gamma chain]	194417	70	7.4	35905	10	18/32
	SSP 7302	54.30	Fah	FAAA_MOUSE	P35505	Fumarylacetoacetase	46416	217	6.9	41387	65	24/58
	SSP 7305	14.86	Hpd	HPPD_MOUSE	P49429	4-hydroxyphenylpyruvate dioxygenase	45254	245	6.6	43470	64	27/62
	SSP 7307	13.87	Idh1	IDHC_MOUSE	O88844	Isocitrate dehydrogenase [NADP] cytoplasmic	47030	215	6.5	44280	60	27/52
	SSP 7310	303.01	Fah	FAAA_MOUSE	P35505	Fumarylacetoacetase	46416	208	6.9	41082	62	27/65
	SSP 7314	8.08	Adh5	ADHX_MOUSE	P28474	Alcohol dehydrogenase class-3	40320	84	7.0	39229	51	15/72
	SSP 7319	11.93	Ass1	ASSY_MOUSE	P16460	Argininosuccinate synthase	46840	125	8.4	45004	41	20/71
	SSP 7401	97.87	Glud1	DHE3_MOUSE	P26443	Glutamate dehydrogenase 1, mitochondrial precursor	61640	217	7.7	53046	44	28/55

Time point [hr]	SSP on 2D gel	Fold change	Gene symbol	Accession	UP ID	Protein name	Calculated mass	MOWSE score	pI on 2D gel	Mr on 2d gel	Sequence coverage %	Matched/ Searched peptides
	SSP 7404	375.33	Lap3	AMPL_MOUSE	Q9CPY7	Cytosol aminopeptidase	56505	237	7.6	54841	56	33/68
	SSP 7407	80.06	Hgd	HGD_MOUSE	O09173	Homogentisate 1,2-dioxygenase	50756	178	6.9	48877	54	23/63
	SSP 7409	27.93	Glud1	DHE3_MOUSE	P26443	Glutamate dehydrogenase 1, mitochondrial precursor	61640	276	8.1	52888	58	33/57
	SSP 7410	43.47	Dpys	DPYS_MOUSE	Q9EQF5	Dihydropyrimidinase	57202	247	6.7	54706	47	24/42
	SSP 7411	15.95	Cat	CATA_MOUSE	P24270	Catalase	60013	237	7.7	57878	54	26/52
	SSP 7417	19.84	Ugp2	UGPA_MOUSE	Q91ZJ5	UTP--glucose-1-phosphate uridylyltransferase	57115	269	7.2	54109	57	32/68
	SSP 7418	242.25	Hgd	HGD_MOUSE	O09173	Homogentisate 1,2-dioxygenase	50756	194	6.9	48700	51	24/59
	SSP 7419	32.26	Cat	CATA_MOUSE	P24270	Catalase	60013	305	7.7	57494	57	31/61
	SSP 7420	17.43	Gsr	GSHR_MOUSE	P47791	Glutathione reductase, mitochondrial precursor	54256	138	8.2	52967	41	22/72
	SSP 8108	29.45	Psma4	PSA4_MOUSE	Q9R1P0	Proteasome subunit alpha type-4	29737	94	7.6	28218	54	12/58
	SSP 8204	21.72	Ldha	LDHA_MOUSE	P06151	L-lactate dehydrogenase A chain	36817	245	7.6	33200	61	31/63
	SSP 8308	13.74	Pgk1	PGK1_MOUSE	P09411	Phosphoglycerate kinase 1	44921	158	8.0	43841	48	17/39
	SSP 8311	10.05	Ass1	ASSY_MOUSE	P16460	Argininosuccinate synthase	46840	223	8.4	44894	61	28/65
	SSP 8316	54.20	Acat2	THIC_MOUSE	Q8CAY6	Acetyl-CoA acetyltransferase, cytosolic	41727	109	7.2	39350	45	17/75
	SSP 8327	230.69	Aldoa	ALDOA_MOUSI	P05064	Fructose-bisphosphate aldolase A	39787	92	8.5	39600	40	14/71
	SSP 8402	29.23	Aldh1a1	AL1A1_MOUSE	P24549	Retinal dehydrogenase 1	55060	124	7.9	53861	37	20/62
([1week] vs [96hr])	SSP 2004	24.16	Prdx2	PRDX2_MOUSE	Q61171	Peroxiredoxin-2	21936	126	5.2	22071	51	10/73
	SSP 2313	8.24	Apoa4	APOA4_MOUSE	P06728	Apolipoprotein A-IV precursor	45001	98	5.4	40238	44	14/50
	SSP 4113	52.22	Psmb7	PSB7_MOUSE	P70195	Proteasome subunit beta type-7 precursor	30214	131	8.1	27490	35	15/42
	SSP 5110	19.49	Pgam1	PGAM1_MOUSI	Q9DBJ1	Phosphoglycerate mutase 1	28928	177	6.7	26703	65	19/58
	SSP 6005	59.97	Psmb2	PSB2_MOUSE	Q9R1P3	Proteasome subunit beta type-2	23063	170	6.5	22552	58	13/47
	SSP 6204	50.06	Alad	HEM2_MOUSE	P10518	Delta-aminolevulinic acid dehydratase	36456	209	6.3	35574	53	22/54
	SSP 7103	67.90	Gstm2	GSTM2_MOUSI	P15626	Glutathione S-transferase Mu 2	25871	184	6.9	24837	73	21/52
	SSP 7108	65.93	Psma2	PSA2_MOUSE	P49722	Proteasome subunit alpha type-2	26023	191	8.4	24319	58	13/36
	SSP 7109	83.91	Psma4	PSA4_MOUSE	Q9R1P0	Proteasome subunit alpha type-4	29737	145	7.6	27961	62	15/49
	SSP 7409	9.99	Glud1	DHE3_MOUSE	P26443	Glutamate dehydrogenase 1, mitochondrial precursor	61640	276	8.1	52888	58	33/57
	SSP 8025	36.41	Psmb5	PSB5_MOUSE	O55234	Proteasome subunit beta type-5 precursor	28685	126	6.5	22863	56	16/54

Chapter IV:

Concluding remarks

In this study, I focused on ‘from omics to multi-omics’ for a new mass spectrometry-based biomarker discovery to be definite the output: basic or clinical output. The quality of large-scale dataset derived from proteomic studies is one of the most important concepts that directly influence the success of the following functional analysis. So, I propose essential solution for data mining method for proteomic research. 1) Appropriate protein extraction, tryptic digestion and peptide recovery for each analytical platform. 2) Reproducible and quantitative dataset of possible confirmation by another experimental method. 3) Accurate protein identification by mass spectrometric method (peptide mass fingerprinting, MS/MS analysis and precise criteria of database search results or verification of protein physicochemical properties and post-translational modifications). 4) Contain many important proteins in the dataset as expected for objective research field. 5) Statistically quantitative cutoff with appropriate number of dataset (100 to 2000 data, not low or high). 6) Time-dependent quantitative dataset. 7) Biologically over-representation by up- or down-regulated protein expression. By this concept, it came to understand an important biological event at each time point with statistically significant change using gene ontology annotated proteomic dataset, and the researcher became possible to know to which event focus had to be done. I will propose one of the essential solutions for serum proteomic research.

Next, this proteomic dataset only is insufficient for the development of clinical biomarker. Clinical biomarkers have of at least 3 potential to diagnose criteria:[46] First, reference limits are generated with the use of cross-sectional analyses of a reference sample with an arbitrary percentile cut-points. Second, discrimination limits are also used to indicate abnormal biomarker values with evaluating the degree of overlap between patients with and without disease in cross-sectional studies. And third, risk

threshold is to define “undesirable” biomarker levels on follow-up by relating values to the incidence of disease and seeking a threshold beyond which risk escalates.

Especially, for informative biomarker in the field of hepatic disease, it is necessary to identify the molecules that are directly relationship on the liver pathobiology. I consistently used the same serum sample from acute to regenerative phase, and focused on serum bile acid metabolome. In this biomarker strategy, I was carried out three new concept and technology: 1) serum proteomic dataset as supporting information of disease organ pathobiology, 2) development of MS-based simple and high-throughput quantification method for serum bile acid, and 3) imaging mass spectrometry as cross-validation of serum biomarker on the disease tissue. In this approach, I demonstrated that serum bile acid profile can be a diagnostic marker for liver injury/regeneration in the CCl_4-induced mouse model. And this strategy is indicated by integrating time and spatial distribution of bile acids in circulation.

Acknowledgment

I would like to express my deep gratitude to all those who provided me guidance, support and encouragement during the preparation of this dissertation.

Most of all, I would like to express my sincere thanks to Professor Akiyoshi Fukamizu for useful discussions and encouragements throughout my research work.

I would like to thank Dr. Jun Yanagisawa, Dr. Keiji Tanimoto and Dr. Koichiro Kako for valuable comments and discussions.

I would like to express sincere thanks to Dr. Masaya Ikegawa (Genomic Medical Sciences, Kyoto Prefectural University of Medicine), especially for directing my bile acid research work into refined and exciting discussions in terms of its clinical significance.

Dr. Kenya Yamanaka (Department of Surgery, Division of Hepato-pancreato-billiary Surgery and Transplantation, Kyoto University) helped me by giving useful comments on liver histopathology.

I am deeply thanks to Shimadzu Corporation and Dr. Taka-Aki Sato for authorization my society doctoral program of the University of Tsukuba.

I am deeply indebted to Drs. Satoru and Mitsue Tokutomi (University of Osaka Prefecture and National Institute of Agrobiological Sciences), and Drs. Kotoku and Sumiko Kurachi (Kyushu University) for useful discussions and encouragements.

Finally, I appreciate greatly the support of my family, Maho, Rio and Ryuto.

Reference

1. Hofmann, A. F.; Hagey, L. R., Bile acids: chemistry, pathochemistry, biology, pathobiology, and therapeutics. *Cell Mol Life Sci* **2008,** 65, (16), 2461-83.

2. Alnouti, Y., Bile Acid sulfation: a pathway of bile acid elimination and detoxification. *Toxicol Sci* **2009,** 108, (2), 225-46.

3. Lefebvre, P.; Cariou, B.; Lien, F.; Kuipers, F.; Staels, B., Role of bile acids and bile acid receptors in metabolic regulation. *Physiol Rev* **2009,** 89, (1), 147-91.

4. Hylemon, P. B.; Zhou, H.; Pandak, W. M.; Ren, S.; Gil, G.; Dent, P., Bile acids as regulatory molecules. *J Lipid Res* **2009,** 50, (8), 1509-20.

5. Thomas, C.; Pellicciari, R.; Pruzanski, M.; Auwerx, J.; Schoonjans, K., Targeting bile-acid signalling for metabolic diseases. *Nat Rev Drug Discov* **2008,** 7, (8), 678-93.

6. Houten, S. M.; Watanabe, M.; Auwerx, J., Endocrine functions of bile acids. *Embo J* **2006,** 25, (7), 1419-25.

7. Huang, W.; Ma, K.; Zhang, J.; Qatanani, M.; Cuvillier, J.; Liu, J.; Dong, B.; Huang, X.; Moore, D. D., Nuclear receptor-dependent bile acid signaling is required for normal liver regeneration. *Science* **2006,** 312, (5771), 233-6.

8. Claudel, T.; Staels, B.; Kuipers, F., The Farnesoid X receptor: a molecular link between bile acid and lipid and glucose metabolism. *Arterioscler Thromb Vasc Biol* **2005,** 25, (10), 2020-30.

9. Anderson, N. L.; Anderson, N. G., The human plasma proteome: history, character, and diagnostic prospects. *Mol Cell Proteomics* **2002,** 1, (11), 845-67.

10. Schiess, R.; Wollscheid, B.; Aebersold, R., Targeted proteomic strategy for

clinical biomarker discovery. *Mol Oncol* **2009,** 3, (1), 33-44.

11. Rifai, N.; Gillette, M. A.; Carr, S. A., Protein biomarker discovery and validation: the long and uncertain path to clinical utility. *Nat Biotechnol* **2006,** 24, (8), 971-83.

12. Hanash, S. M.; Pitteri, S. J.; Faca, V. M., Mining the plasma proteome for cancer biomarkers. *Nature* **2008,** 452, (7187), 571-9.

13. Huang da, W.; Sherman, B. T.; Lempicki, R. A., Systematic and integrative analysis of large gene lists using DAVID bioinformatics resources. *Nat Protoc* **2009,** 4, (1), 44-57.

14. Camon, E.; Magrane, M.; Barrell, D.; Lee, V.; Dimmer, E.; Maslen, J.; Binns, D.; Harte, N.; Lopez, R.; Apweiler, R., The Gene Ontology Annotation (GOA) Database: sharing knowledge in Uniprot with Gene Ontology. *Nucleic Acids Res* **2004,** 32, (Database issue), D262-6.

15. Shaham, O.; Wei, R.; Wang, T. J.; Ricciardi, C.; Lewis, G. D.; Vasan, R. S.; Carr, S. A.; Thadhani, R.; Gerszten, R. E.; Mootha, V. K., Metabolic profiling of the human response to a glucose challenge reveals distinct axes of insulin sensitivity. *Mol Syst Biol* **2008,** 4, 214.

16. Martin, F. P.; Dumas, M. E.; Wang, Y.; Legido-Quigley, C.; Yap, I. K.; Tang, H.; Zirah, S.; Murphy, G. M.; Cloarec, O.; Lindon, J. C.; Sprenger, N.; Fay, L. B.; Kochhar, S.; van Bladeren, P.; Holmes, E.; Nicholson, J. K., A top-down systems biology view of microbiome-mammalian metabolic interactions in a mouse model. *Mol Syst Biol* **2007,** 3, 112.

17. Nguyen, A.; Bouscarel, B., Bile acids and signal transduction: role in glucose homeostasis. *Cell Signal* **2008,** 20, (12), 2180-97.

18. Lai, K. K.; Kolippakkam, D.; Beretta, L., Comprehensive and quantitative proteome profiling of the mouse liver and plasma. *Hepatology* **2008,** 47, (3), 1043-51.

19. Parent, R.; Beretta, L., Proteomics in the study of liver pathology. *J Hepatol* **2005,** 43, (1), 177-83.

20. Amacher, D. E.; Adler, R.; Herath, A.; Townsend, R. R., Use of proteomic methods to identify serum biomarkers associated with rat liver toxicity or hypertrophy. *Clin Chem* **2005,** 51, (10), 1796-803.

21. Craig, A.; Sidaway, J.; Holmes, E.; Orton, T.; Jackson, D.; Rowlinson, R.; Nickson, J.; Tonge, R.; Wilson, I.; Nicholson, J., Systems toxicology: integrated genomic, proteomic and metabonomic analysis of methapyrilene induced hepatotoxicity in the rat. *J Proteome Res* **2006,** 5, (7), 1586-601.

22. Merrick, B. A.; Bruno, M. E.; Madenspacher, J. H.; Wetmore, B. A.; Foley, J.; Pieper, R.; Zhao, M.; Makusky, A. J.; McGrath, A. M.; Zhou, J. X.; Taylor, J.; Tomer, K. B., Alterations in the rat serum proteome during liver injury from acetaminophen exposure. *J Pharmacol Exp Ther* **2006,** 318, (2), 792-802.

23. Minami, K.; Saito, T.; Narahara, M.; Tomita, H.; Kato, H.; Sugiyama, H.; Katoh, M.; Nakajima, M.; Yokoi, T., Relationship between hepatic gene expression profiles and hepatotoxicity in five typical hepatotoxicant-administered rats. *Toxicol Sci* **2005,** 87, (1), 296-305.

24. Ozer, J.; Ratner, M.; Shaw, M.; Bailey, W.; Schomaker, S., The current state of serum biomarkers of hepatotoxicity. *Toxicology* **2008,** 245, (3), 194-205.

25. Bollard, M. E.; Contel, N. R.; Ebbels, T. M.; Smith, L.; Beckonert, O.; Cantor, G. H.; Lehman-McKeeman, L.; Holmes, E. C.; Lindon, J. C.; Nicholson, J. K.; Keun, H. C., NMR-based metabolic profiling identifies biomarkers of liver regeneration

following partial hepatectomy in the rat. *J Proteome Res* **2010,** 9, (1), 59-69.

26. Fannin, R. D.; Russo, M.; O'Connell, T. M.; Gerrish, K.; Winnike, J. H.; Macdonald, J.; Newton, J.; Malik, S.; Sieber, S. O.; Parker, J.; Shah, R.; Zhou, T.; Watkins, P. B.; Paules, R. S., Acetaminophen dosing of humans results in blood transcriptome and metabolome changes consistent with impaired oxidative phosphorylation. *Hepatology* **2010,** 51, (1), 227-36.

27. Shinoda, K.; Sugimoto, M.; Tomita, M.; Ishihama, Y., Informatics for peptide retention properties in proteomic LC-MS. *Proteomics* **2008,** 8, (4), 787-98.

28. Burkard, I.; von Eckardstein, A.; Rentsch, K. M., Differentiated quantification of human bile acids in serum by high-performance liquid chromatography-tandem mass spectrometry. *J Chromatogr B Analyt Technol Biomed Life Sci* **2005,** 826, (1-2), 147-59.

29. Mims, D.; Hercules, D., Quantification of bile acids directly from urine by MALDI-TOF-MS. *Anal Bioanal Chem* **2003,** 375, (5), 609-16.

30. Caldwell, R. L.; Caprioli, R. M., Tissue profiling by mass spectrometry: a review of methodology and applications. *Mol Cell Proteomics* **2005,** 4, (4), 394-401.

31. Murphy, R. C.; Hankin, J. A.; Barkley, R. M., Imaging of lipid species by MALDI mass spectrometry. *J Lipid Res* **2009,** 50 Suppl, S317-22.

32. Quadroni, M.; James, P., Proteomics and automation. *Electrophoresis* **1999,** 20, (4-5), 664-77.

33. Brunt, E. M., Grading and staging the histopathological lesions of chronic hepatitis: the Knodell histology activity index and beyond. *Hepatology* **2000,** 31, (1), 241-6.

34. LeSage, G. D.; Benedetti, A.; Glaser, S.; Marucci, L.; Tretjak, Z.; Caligiuri, A.; Rodgers, R.; Phinizy, J. L.; Baiocchi, L.; Francis, H.; Lasater, J.; Ugili, L.; Alpini, G.,

Acute carbon tetrachloride feeding selectively damages large, but not small, cholangiocytes from normal rat liver. *Hepatology* **1999,** 29, (2), 307-19.

35. Suhler, E.; Lin, W.; Yin, H. L.; Lee, W. M., Decreased plasma gelsolin concentrations in acute liver failure, myocardial infarction, septic shock, and myonecrosis. *Crit Care Med* **1997,** 25, (4), 594-8.

36. Uhlar, C. M.; Whitehead, A. S., Serum amyloid A, the major vertebrate acute-phase reactant. *Eur J Biochem* **1999,** 265, (2), 501-23.

37. Tegoni, M.; Pelosi, P.; Vincent, F.; Spinelli, S.; Campanacci, V.; Grolli, S.; Ramoni, R.; Cambillau, C., Mammalian odorant binding proteins. *Biochim Biophys Acta* **2000,** 1482, (1-2), 229-40.

38. Graham, T. E.; Yang, Q.; Bluher, M.; Hammarstedt, A.; Ciaraldi, T. P.; Henry, R. R.; Wason, C. J.; Oberbach, A.; Jansson, P. A.; Smith, U.; Kahn, B. B., Retinol-binding protein 4 and insulin resistance in lean, obese, and diabetic subjects. *N Engl J Med* **2006,** 354, (24), 2552-63.

39. Jungermann, K.; Kietzmann, T., Zonation of parenchymal and nonparenchymal metabolism in liver. *Annu Rev Nutr* **1996,** 16, 179-203.

40. Jones, A. L.; Hradek, G. T.; Renston, R. H.; Wong, K. Y.; Karlaganis, G.; Paumgartner, G., Autoradiographic evidence for hepatic lobular concentration gradient of bile acid derivative. *Am J Physiol* **1980,** 238, (3), G233-7.

41. Angelin, B.; Bjorkhem, I.; Einarsson, K.; Ewerth, S., Hepatic uptake of bile acids in man. Fasting and postprandial concentrations of individual bile acids in portal venous and systemic blood serum. *J Clin Invest* **1982,** 70, (4), 724-31.

42. Zhang, Y.; Edwards, P. A., FXR signaling in metabolic disease. *FEBS Lett* **2008,** 582, (1), 10-8.

43. Yamagata, K.; Daitoku, H.; Shimamoto, Y.; Matsuzaki, H.; Hirota, K.; Ishida, J.; Fukamizu, A., Bile acids regulate gluconeogenic gene expression via small heterodimer partner-mediated repression of hepatocyte nuclear factor 4 and Foxo1. *J Biol Chem* **2004,** 279, (22), 23158-65.

44. Matsuzaki, Y.; Bouscarel, B.; Ikegami, T.; Honda, A.; Doy, M.; Ceryak, S.; Fukushima, S.; Yoshida, S.; Shoda, J.; Tanaka, N., Selective inhibition of CYP27A1 and of chenodeoxycholic acid synthesis in cholestatic hamster liver. *Biochim Biophys Acta* **2002,** 1588, (2), 139-48.

45. Falany, C. N.; Fortinberry, H.; Leiter, E. H.; Barnes, S., Cloning, expression, and chromosomal localization of mouse liver bile acid CoA:amino acid N-acyltransferase. *J Lipid Res* **1997,** 38, (6), 1139-48.

46. Vasan, R. S., Biomarkers of cardiovascular disease: molecular basis and practical considerations. *Circulation* **2006,** 113, (19), 2335-62.